UNIVERSIDADE FEDERAL DE SANTA CATARINA
CAMPUS TRINDADE
PROGRAMA DE PÓS-GRADUAÇÃO EM ENGENHARIA MECÂNICA

Thaís Doll Luz

SUPERCRITICAL CARBON DIOXIDE AS THERMAL ENERGY STORAGE MEDIUM FROM EXPERIMENTAL AND NUMERICAL STANDPOINTS

Florianópolis - Brasil
2020

Thaís Doll Luz

SUPERCRITICAL CARBON DIOXIDE AS THERMAL ENERGY STORAGE MEDIUM FROM EXPERIMENTAL AND NUMERICAL STANDPOINTS

Dissertação submetida ao Programa de Pós-Graduação em Engenharia Mecânica da Universidade Federal de Santa Catarina para a obtenção do título de Mestre em Engenharia Mecânica com ênfase em Engenharia e Ciências Térmicas.
Orientador: Prof. Alexandre Kupka da Silva, Ph.D.

Florianópolis - Brasil
2020

Ficha de identificação da obra elaborada pelo autor,
através do Programa de Geração Automática da Biblioteca Universitária da UFSC.

Doll Luz, Thaís
SUPERCRITICAL CARBON DIOXIDE AS THERMAL ENERGY STORAGE MEDIUM FROM EXPERIMENTAL AND NUMERICAL STANDPOINTS / Thaís Doll Luz ; orientador, Alexandre Kupka da Silva, 2020.
118 p.

Dissertação (mestrado) - Universidade Federal de Santa Catarina, Centro Tecnológico, Programa de Pós-Graduação em Engenharia Mecânica, Florianópolis, 2020.

Inclui referências.

1. Engenharia Mecânica. 2. Armazenamento Térmico. 3. Dióxido de Carbono. 4. Fluido Supercrítico. I. Kupka da Silva, Alexandre. II. Universidade Federal de Santa Catarina. Programa de Pós-Graduação em Engenharia Mecânica. III. Título.

Thaís Doll Luz

SUPERCRITICAL CARBON DIOXIDE AS THERMAL ENERGY STORAGE MEDIUM FROM EXPERIMENTAL AND NUMERICAL STANDPOINTS

O presente trabalho em nível de Mestrado foi avaliado e aprovado por banca examinadora composta pelos seguintes membros:

Prof. Jader Riso Barbosa Jr, Ph.D.
Universidade Federal de Santa Catarina

Profa. Cíntia Soares, Dra Eng.
Universidade Federal de Santa Catarina

Prof. Marcelo Lanza, Dr.
Universidade Federal de Santa Catarina

Certificamos que esta é a **versão original e final** do trabalho de conclusão que foi julgado adequado para obtenção do título de Mestre em Engenharia Mecânica com ênfase em Engenharia e Ciências Térmicas.

Documento assinado digitalmente
Jonny Carlos da Silva
Data: 15/05/2020 15:28:06-0300
CPF: 514.515.064-49

Prof. Jonny Carlos da Silva, Dr.
Coordenador do Programa

Documento assinado digitalmente
Alexandre Kupka da Silva
Data: 14/05/2020 14:15:17-0300
CPF: 000.190.189-32

Prof. Alexandre Kupka da Silva, Ph.D.
Orientador

Documento assinado digitalmente
Thais Doll Luz
Data: 14/05/2020 11:42:07-0300
CPF: 016.975.110-40

Thaís Doll Luz, Eng.

Florianópolis - Brasil, 31 de Março de 2020.

This work is dedicated to my mom Adriana, who taught
me to always put a smile on my face and to never give up.

AGRADECIMENTOS

Primeiramente, agradeço à minha mãe, Adriana, pessoa fundamental na minha vida. Mãe, obrigada por todo o apoio e incentivo que sempre me deste para perseguir os meus sonhos e atingir os meus objetivos. És a minha maior inspiração, hoje e sempre.

Ao Renatto, muito obrigada por ter aguentado as minhas mudanças de humor quando as coisas não estavam indo de acordo ao planejado. Por ter levado comida para mim nos dias e noites em que eu não podia sair de perto da bancada enquanto rodava testes e por todo o apoio, carinho e compreensão ao longo deste processo.

Ao meu orientador, Prof. Alexandre Kupka da Silva, agradeço a oportunidade de participar deste projeto. Pelo incentivo nos momentos de dificuldades com a bancada, pela confiança que demonstrou depositar em mim quando parecia que esta não ia funcionar e pela liberdade que me deu para desenvolver a pesquisa.

Ao insubstituível Júlio N. Scussel, por toda a ajuda com a parte experimental do trabalho, por tirar as minhas dúvidas sempre que eu me sentia insegura em implementar algo na bancada e pelas conversas e descontrações.

À queridíssima Rosângela, por ter me ajudado a encaminhar todos os pedidos de compra para a bancada e por manter em ordem toda a burocracia do laboratório.

A todos os amigos e colegas do Lepten/Labsolar pelo apoio, conversas e ideias trocadas, em especial ao Felipe G. Battisti, obrigada por todas as discussões a respeito do trabalho e por me ajudar a direcionar a pesquisa em momentos em que estive um pouco sem rumo. Ao Ramon, agradeço por toda a ajuda durante a construção da bancada. Ao Alex Sant'Ana, Olívia da Rosa, Bruno Emmerick, Ruan Commeli, Paulo Galeano, Adriano Hissanaga, Giovanni Delsoto, Daniela Rodrigues, Victor Dutra, obrigada por fazerem meus dias no laboratório mais alegres. Aos amigos que já não fazem parte do Lepten ou que são de outros laboratórios mas que sempre se fazem presentes, Arthur Veiga, Ianto Oliveira, Vinícius Kramer, Luigi Passos, Eduardo Alves, Marcus Vinícius, Leonardo Casagrande, Arthur Cleyton muito obrigada!

À Petrobrás/ANEEL pelo suporte através do Projeto PD-00553-0042/2016.

Ao POSMEC e à UFSC, pela oportunidade e infraestrutura disponíveis para que eu desenvolvesse um mestrado de qualidade nesta instituição.

Por fim, para todos aqueles que de não foram mencionados, muito obrigada!

Let the future tell the truth,
and evaluate each one according
to his work and accomplishments.
The present is theirs; the future,
for which I have really worked,
is mine." (Nikolas Tesla)

RESUMO

O advento da industrialização faz com que haja um aumento na demanda de energia mundial. Devido a isto e à crescente preocupação com o meio ambiente, há um interesse em substituir combustíveis fósseis por fontes de geração de energia renováveis. Contudo, tais fontes possuem certas características que limitam a sua aplicação. Uma destas limitações é o fato de serem intermitentes, fazendo com que a geração de energia dependa da disponibilidade da fonte. Um exemplo disto é o caso da energia solar, em que há desencontro entre as horas de geração, durante o dia, e as horas em que há uma maior demanda, à noite. Assim, sistemas de armazenamento de energia térmica (*Thermal Energy Storage – TES*) são uma opção viável para mitigar os efeitos de intermitência, permitindo que a energia térmica seja utilizada quando a fonte não está mais disponível. Todavia, as tecnologias de TES atuais possuem certas restrições, principalmente no que concerne às limitadas taxas de transferência de calor e densidade de energia armazenada, e à corrosividade dos materiais utilizados. Deste modo, devido à intensa variação de propriedades termofísicas perto do ponto crítico, fluidos supercríticos parecem ser uma opção viável como meios de TES, apresentando elevados coeficientes de transferência de calor e densidade de energia. Baseado no que foi discutido, uma bancada experimental operando a volume constante foi construída para estudar o coeficiente de convecção natural em fios aquecidos com dióxido de carbono supercrítico (s-CO_2) e a densidade de energia armazenada neste fluido. Resultados de transferência de calor foram obtidos mediante simulação numérica para complementar os resultados experimentais e avaliar condições de operação aquém das testadas experimentalmente. Da mesma maneira, análises termodinâmicas foram realizadas para expandir os resultados experimentais de densidade de energia armazenada para outras condições de temperatura e pressão de operação. Condições ótimas de operação para maximizar a taxa de transferência de calor foram observadas as quais estão diretamente relacionadas ao comportamento das propriedades termofísicas do fluido. A densidade de energia armazenada também apresenta condições de temperatura e pressão que maximizam o armazenamento térmico. A obtenção de resultados de transferência de calor e densidade de energia térmica armazenada para condições além das testadas permite avaliar o desempenho do s-CO_2 em condições de operação mais próximas daquelas necessárias em aplicações de geração de energia. Deste modo, os resultados teóricos para s-CO_2 são comparados com ar, nitrogênio e hélio, fluidos que também são estudados para aplicação em sistemas de geração de energia solar térmica, uma das aplicações de TES. Os resultados de tal análise mostram que o s-CO_2 apresenta coeficiente de transferência de calor menor apenas do que o hélio e densidade de armazenamento superior a todos os fluidos avaliados, indicando assim que o dióxido de carbono supercrítico pode ser um meio de armazenamento térmico até para condições muito acima do ponto crítico, onde as propriedades termofísicas não apresentam variações elevadas.

Palavras-chave: Supercrítico. Armazenamento Térmico. Dióxido de carbono.

RESUMO EXPANDIDO

Introdução

Atualmente, uma maior demanda energética juntamente a uma crescente preocupação ambiental faz com que se deseje aumentar o uso de fontes renováveis para a geração de eletricidade. No entanto, tais fontes apresentam limitações, como por exemplo o caso da energia solar que depende da presença da luz do sol para a geração de eletricidade. Esta intermitência causa um desencontro entre as horas de geração de energia, durante o dia, e as horas de pico de demanda, geralmente à noite. Sistemas de armazenamento térmico permitem que a energia térmica seja guardada para ser utilizada posteriormente e, no caso das usinas solares térmicas, diminua estes efeitos de intermitência da fonte, justificando a importância de tais sistemas.

Deseja-se que, dentre outras caracteríticas, os sistemas de TES apresentem alta densidade de energia armazenada e alta taxa de transferência de calor entre o meio de armazenamento e o fluido de trabalho. Neste contexto, duas tecnologias de armazenamento térmico são atualmente consideradas na indústria: armazenamento por calor sensível e por calor latente. Os materiais de armazenamento por calor sensível, cujo armazenamento está relacionado à variação de temperatura do material, apesar de apresentarem baixo custo possuem como desvantagem o fato de apresentarem baixa densidade de energia, necessitando de grandes volumes de material para o armazenamento. Por outro lado, os materiais de mudança de fase usados no armazenamento por calor latente, onde se aproveita a elevada entalpia de mudança de fase do material para armazenar a energia térmica, apresentam alta densidade de energia, sendo limitados, contudo, pela baixa taxa de transferência de calor entre eles e o fluido de trabalho.

Os fluidos supercríticos surgem como alternativa de meio de armazenamento, tirando-se vantagem da intensa variação de propriedades termofísicas destes em condições próximas ao ponto crítico para elevar a taxa de transferência de calor e a densidade de energia térmica armazenada nestas condições. Apesar de uma sequência de trabalhos numéricos mostrarem a vantagem, até em aspectos econômicos, de tais fluidos como meios de armazenamento, faltam trabalhos experimentais na literatura que estudem estes fluidos para a aplicação de armazenamento térmico. O dióxido de carbono supercrítico, ou s-CO_2, por apresentar ponto crítico em condições amenas de temperatura e médias de pressão, dentre outras caracteríticas vantajosas, é um fluido interessante para se trabalhar experimentalmente em escala laboratorial, sendo o fluido escolhido para o desenvolvimento deste trabalho. Além disto também é um fluido que está sendo estudado para aplicação em sistemas de potência em usinas solares térmicas, uma das aplicações possíveis dos sistemas de TES.

Objetivos

No contexto apresentado, o objetivo principal deste trabalho é estudar e avaliar o dióxido de carbono supercrítico como meio de armazenamento térmico, operando em condições de volume constante.

Para atingir este objetivo principal, vários objetivos específicos tiveram de ser alcançados durante o desenvolvimento deste trabalho:

- Compreender as vantagens dos fluidos supercríticos como meios de armazenamento térmico através de revisão bibliográfica;
- Estudar os mecanismos de transferência de calor agindo no dióxido de carbono em condições supercríticas;
- Verificar experimentalmente o comportamento do coeficiente de transferência de calor e da densidade de energia do dióxido de carbono em condições supercríticas operando a volume constante;
- Utilizar um modelo numérico validado para estudar o coeficiente de transferência de calor e a densidade de energia em condições de temperatura e pressão não atingidas nos experimentos;
- Contribuir para o entendimento a respeito do potencial de fluidos supercríticos como meios de TES.

Metodologia

A metodologia seguida ao longo deste trabalho consiste na mistura de uma abordagem experimental e numérica para avaliar o s-CO_2 como meio de armazenamento. Uma bancada experimental capaz de medir o coeficiente de transferência de calor por convecção natural ao redor de um fio aquecido no CO_2 em diferentes condições de operação foi construída. A bancada consiste, resumidamente, em um vaso de pressão contendo CO_2 com um fio em seu interior dissipando potência. Este vaso de pressão está envolto por uma camisa de PVC contendo água e conectada a um banho termostático, que regula a temperatura do CO_2 no interior do vaso de pressão. As condições de temperatura e pressão de operação do s-CO_2 eram medidas, possibilitando que o calor armazenado no CO_2 fosse estimado através de análise termodinânica, verificando as condições iniciais e finais dos testes.

Os resultados experimentais de transferência de calor foram expandidos para outras condições de operação através do desenvolvimento de um modelo numérico, validado com resultados da literatura. Já os resultados de densidade de energia térmica armazenada

foram expandidos para outras condições com a mesma análise termodinâmica. Expandir tais resultados para condições além daquelas testadas experimentalmente permitiu comparar o desempenho do s-CO_2 como meio de armazenamento em condições nas quais este fluido seria utilizado em ciclos de potência para aplicações em usinas solares térmicas. Estas análises teóricas do coeficiente de transferência de calor do s-CO_2 e da sua densidade de energia foram comparadas com os resultados de outros três fluidos também estudados para aplicações em sistemas de potência: hélio, nitrogênio e ar.

Resultados e Discussão

Os resultados mostram que mantendo-se a temperatura do fluido fixa, picos de coeficiente de transferência de calor são observados para as suas pressões pseudocríticas, ou seja, as pressões para cada temperatura onde o calor específico do fluido atinge seu valor máximo. Além disto, estes picos observados são mais intensos para temperaturas mais próximas da temperatura crítica do CO_2. Comportamentos diferentes do coeficiente de transferência de calor foram observados dependendo da diferença de temperatura entre o fio e o fluido, resultando em condições ótimas de temperatura, pressão e diferença de temperatura entre o fio e o fluido para maximizar a taxa de transferência de calor. Além disto, comparou-se os resultados de coeficiente de transferência de calor das simulações com correlações de convecção natural ao redor de cilindros aquecidos, uma fazendo uso da integração de propriedades entre as temperaturas do fluido e do fio, proposta em diversos artigos experimentais da revisão bibliográfica deste trabalho, e outra utilizando propriedades avaliadas na temperatura bulk do fluido. Observou-se que o uso da integração de propriedades está relacionado com o comportamento do coeficiente de expansão isobárica do fluido, propriedade relevante no fenômeno de convecção natural.

Com relação à densidade de energia armazenada, os resultados experimentais mostram que, para tal estudo de armazenamento térmico, a bancada experimental ainda precisa ser melhorada. Isto pois um balanço de energia no sistema mostra que a maior parte da energia fornecida pelo fio foi perdida pelo CO_2 para a água que envolve o vaso de pressão. Porém, as análises termodinâmicas mostram que, para operação à volume constante, a densidade de energia armazenada é maior para pressões de operação maiores, uma vez que isto significa maior densidade de fluido para armazenar energia térmica. Porém, para uma dada temperatura bulk do fluido, parece haver uma condição ótima de pressão para maximizar a densidade de energia armazenada também.

Os resultados do coeficiente de transferência de calor e da densidade de energia armazenada do s-CO_2 em condições próximas ao seu ponto crítico parecem mostrar uma elevada densidade de energia armazenada e densidade de armazenamento térmico. Avaliou-se

então estes resultados do s-CO_2 para condições de temperatura e pressão muito além do ponto crítico, onde as propriedades termofísicas não variam mais tão intensamente, e que são condições interessantes para aplicações do s-CO_2 em ciclos de potência, que seria uma das aplicações plausíveis de sistemas de armazenamento térmico. Comparou-se então o s-CO_2 nestas condições com outros três fluidos, hélio, ar e nitrogênio, cada fluido nas condições de operação que melhoram o desempenho de seus respectivos ciclos de potência. Tal análise mostra que o s-CO_2 apresenta coeficiente de transferência de calor menor apenas do que o hélio, apresentando, contudo, densidade de energia armazenada superior a todos os fluidos analisados. Deste modo, verifica-se que o s-CO_2 pode ser um meio de armazenamento térmico interessante mesmo para condições de operação muito além do seu ponto crítico.

Considerações Finais

Os resultados deste trabalho mostram que o s-CO_2 parece ser um meio de armazenamento promissor, uma vez que apresenta elevadas taxas de transferência de calor e densidade de energia térmica armazenada superior a alguns outros fluidos que podem ser considerados para aplicação em ciclos de potência. Além disto, condições ótimas de operação para maximizar tanto a transferência de calor quanto a energia armazenada são observadas. Contudo, os resultados experimentais de densidade de energia deixam a desejar, de modo que algumas modificações na bancada experimental são sugeridas para os trabalhos futuros, conseguindo-se assim avaliar tal parâmetro de maneira mais eficiente.

Palavras-chave: Supercrítico. Armazenamento Térmico. Dióxido de carbono.

ABSTRACT

The advent of industrialization causes an increase on energy demand around the world. Because of this and to the increasing concern about the environment, there is an interest in replacing fossil fuels for renewable energy. However, such energy sources present certain characteristics that limit their usage. One of these limitations is the fact that they are intermittent, which makes the energy generation dependent on the availability of the source. One example of this is solar energy, in which there is a mismatch between the generation hours, during daytime, and the hours in which the demand is greater, at nighttime. Thus, Thermal Energy Storage (TES) systems are a viable option to diminish these intermittency effects, making it possible for thermal energy to be used when the source is not available anymore. Nonetheless, current TES technologies possess certain restrictions, mostly concerning the limited heat transfer rates and stored energy density, and to the fact that these materials present high corrosion. Hence, given the intense thermophysical properties variation near the critical point, supercritical fluids seem to be a viable option as TES medium, presenting elevated heat transfer coefficients and energy density. Based on what was discussed, an experimental apparatus operating at constant volume was built to study the convective heat transfer coefficient for natural convection in heated wires with Supercritical Carbon Dioxide (s-CO_2) and its stored energy density. Heat transfer results were obtained through numerical simulation to aggregate the experimental results and evaluate operational conditions beyond the ones tested experimentally. Similarly, thermodynamical analyses were made to expand the experimental results about stored thermal energy density for other conditions of temperature and pressure. Optimal operational conditions to maximize the heat transfer rate were observed, which are directly related to the behaviour of the fluid's thermophysical properties. The stored energy density also presents temperature and pressure conditions that maximize the TES. Obtaining heat transfer and TES density results for operational conditions beyond the ones tested allows the evaluation of the performance of s-CO_2 as TES medium in conditions closer to the ones required for power generation application. Hence, the theoretical results of s-CO_2 are compared with air, nitrogen and helium, fluids that have also been studied for thermal solar power, one of the applications of TES. The results of this analysis shows that the s-CO_2 presents heat transfer coefficient smaller only than helium, and thermal energy density higher than all other fluids evaluated, implying that supercritical carbon dioxide can be a TES medium even for operational conditions much above its critical point, where the thermophysical properties do not present elevated variations.

Keywords: Supercritical. Thermal energy storage. Carbon dioxide.

LIST OF FIGURES

LIST OF TABLES

LIST OF ABBREVIATIONS AND ACRONYMS

CPTES	Constant Pressure Thermal Energy Storage
CSP	Concentrated Solar Power
CVTES	Constant Volume Thermal Energy Storage
DAQ	Data Aquisition System
FEM	Finite Element Method
GWP	Global Warming Potential
HTF	Heat Transfer Fluid
ODP	Ozone Depleting Potential
PCM	Phase Change Material
s-CO_2	Supercritical Carbon Dioxide
s-TES	Supercritical Thermal Energy Storage
TES	Thermal Energy Storage

LIST OF SYMBOLS

c_v	Specific heat at constant volume [J/kg/K]
Nu_{D}	Nusselt Number
D	Circunference diameter[mm]
k	Thermal conductivity [W/m/K]
J	Property evaluated
T_{wire}	Wire temperature [°C]
T_{bulk}	Bulk temperature [°C]
Gr_{D}	Grashof Number
Pr	Prandlt Number
g	Gravity acceleration [m/s]
D_{wire}	Wire diameter [mm^2]
ν	Cinematic viscosity [m^2/s]
ρ	Density [kg/m^3]
μ	Dynamic viscosity [Pa]
i	Specific entalphy [J/kg]
Ra_{D}	Rayleigh Number
β	Isobaric thermal expansion coefficient [1/K]
α	Thermal diffusivity [m^2/s]
P	Pressure [MPa]
P_{c}	Critical Pressure [MPa]
T_{pc}	Pseudocritical Temperature [°C]
T_{c}	Critical Temperature [°C]
i_{wire}	Specific entalphy at wire temperature [J/kg]
i_{c}	Specific entalphy at critical temperature [J/kg]
i_{pc}	Specific entalphy at pseudocritical temeprature [J/kg]
i_{bulk}	Specific entalphy at bulk temperature [J/kg]
Ga_{c}	Galilei number
q	Heat transfer rate [W]
$\dot{m}$	Mass flow rate [m/s]
c_p	Specific heat at constant pressure [J/kg/K]
ΔT	Temperature difference [°C]
m	Mass [kg]
La	Latent heat [J/kg]
I	Current [A]
V	Voltage [V]
R	Resistance [Ω]
h	Convective heat transfer coefficient [W/m^2/K]
A_{s}	Superficial Area [m^2]

Q	Energy density [J/m^3]
Δt	Time [s]
V_o	Volume [m^3]
e	Internal Energy [J/kg]
h_{average}	Effective convective heat transfer coefficient [W/m^2/K]
L	Length [m]
$\mathbf{u}$	Velocity field [m/s]
$\mathbf{F}$	Tensional forces vector [N]
v	Velocity in the y direction [m/s]
u	Velocity in the x direction [m/s]
P_o	Operational Pressure [MPa]
γ	Ratio between specific heats

CONTENTS

1 INTRODUCTION

1.1 CONTEXTUALIZATION

Due to the population increase and to industrialization there is a dramatic growth on energy demand. This, coupled with more developed environmental consciousness concerning the emission of greenhouse gases, has pushed the replacement of fossil fuels with non-polluting energy generation processes, such as wind, biomass, geothermal and solar. However, power generation with renewable resources presents several limitations such as, for example in the case of solar power systems, its intermittence, which causes a mismatch between production and demand hours. TES systems are often used to mitigate these intermittence effects, increasing the capability of Concentrated Solar Power (CSP) plants to hours where there is no sunlight available and making it possible to enhance their annual capacity factor, which can be increased from 25% to 70% with TES systems. These aspects explain why after 2014, over than 80% of the power plants in construction possessed an integrated TES system, when before this year only half of the CSP potential used this technology (GANAPATHI; WIRZ, 2012; LIU et al., 2016).

As already mentioned, a practical example of the use of TES systems is for CSP application, which is represented in Figure 1.1. In this usage, the TES system interacts with the solar field during its charging cycle, when the TES fluid absorbs thermal energy. The reverse loop occurs when the TES medium releases energy, usually to a Heat Transfer Fluid (HTF) that goes through the power block for power generation. In some cases, the TES system can store the same fluid that goes through the turbine in the power block, without the necessity of a heat exchanger. The importance and relevancy of the TES system is in the fact that thermal energy is stored to be used when the heat source is not available or is malfunctioning. In this case, for CSP application, the TES saves thermal energy to generate electricity at nighttime, when there is no sunlight available to heat the working fluid (GIL et al., 2010; TSE et al., 2013; LAKEH et al., 2013; TSE et al., 2015; LIU et al., 2019).

In this context, the most desirable characteristics of a TES system are: a high energy density and a satisfactory heat transfer rate during charging and discharging. It is also possible to mention chemical stability, environmental compatibility, low levels of corrosion and economic viability. Generally speaking, there are two main types of thermal storage: sensible and latent TES. The materials used in these types of TES usually present low thermal conductivity, limiting the heat transfer processes dominated by diffusion and restricting the potential of sensible and latent TES. Besides, other aspects that can be pointed as restraining characteristics of commonly used materials for TES applications is the low thermal energy density of solid mediums, such as concrete and bed-rocks, and the intense corrosion promoted by liquid mediums, for example molten salts and liquid metals. (GIL et al., 2010; GANAPATHI; WIRZ, 2012; LIU et al., 2016)

Figure 1.1 – Scheme of thermal energy storage system in concentrated solar application. Adapted from (GIL et al., 2010; TSE et al., 2013; LAKEH et al., 2013; TSE et al., 2015)

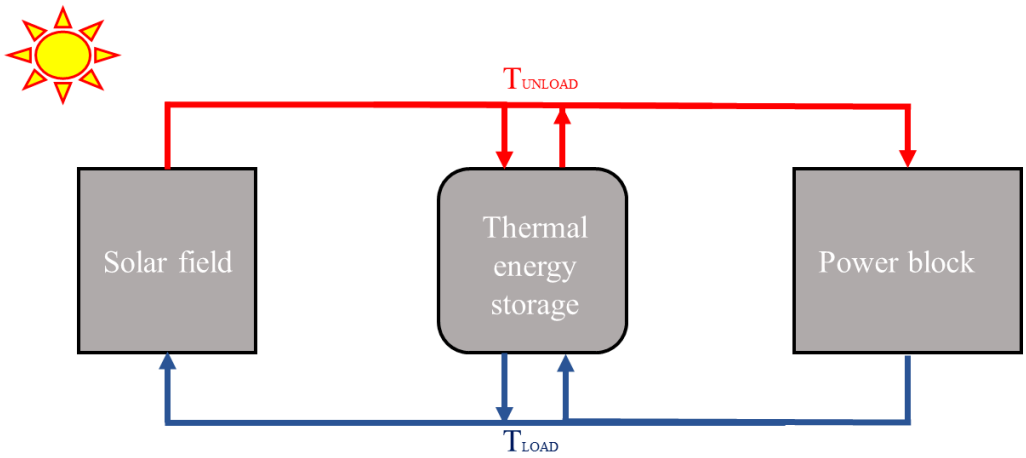

In order to mitigate some of the disadvantages discussed, supercritical fluids seem to be a viable option as storage materials, presenting an intense variation of thermophysical properties in a manner that can enhance the heat transfer and the energy density, mainly near the fluid's critical point. Several fluids conventionally used in engineering applications present good performances when working at high temperatures. Because of this, the operational conditions can define which fluid to be used as TES medium, choosing fluids with critical points closer to the desirable temperature and pressure (GIL et al., 2010; GANAPATHI; WIRZ, 2012; LIU et al., 2016; HOBOLD; da Silva, 2017). In numerical studies, it seems to present favorable energy density accordingly to Hobold & da Silva (2017). Experimental studies with carbon dioxide also show an enhancement of the heat transfer coefficient near the critical point for natural convection, which is an important phenomena for TES (DUBROVINA; SKRIPOV, 1965). There is, however, a lack of experimental studies that actually confirm the advantages on using supercritical fluids for thermal energy storage, as it will be shown in the Literature Review chapter of this dissertation, which is the gap this work aims to feel. Although presenting low critical temperature, carbon dioxide has been considered as a working fluid for power generation application in CSP Dostal et al. (2004). Besides, the results observed with carbon dioxide in near-critical conditions are expected to occur with other fluids near their critical points, which justify the usage of CO_2 in the present work (FURST et al., 2013).

Given the background discussed, this dissertation aims to evaluate supercritical carbon dioxide as a TES medium, concerning both the density of energy stored as the heat transfer mechanism. An experimental apparatus was built and validated in order

to evaluate the before mentioned parameters experimentally. A numerical model was developed and validated with experimental results from the literature to expand the heat transfer studies to conditions of temperature and pressure much above the critical point. For such conditions, the density of energy stored was studied through thermodynamical analysis.

1.2 OBJECTIVES

In the context presented, the main objective of this work is to study and evaluate carbon dioxide as a TES medium at supercritical conditions, at constant volume operation.

In order to reach this main objective, several specific objectives had to be achieved during the development of this research:

- Understand the advantages of supercritical fluids as thermal energy storage mediums through literature review
- Study the heat transfer mechanisms acting on carbon dioxide at supercritical conditions;
- Investigate experimentally the behavior of the heat transfer coefficient and of the energy density of carbon dioxide at supercritical conditions operating at constant volume;
- Use a validated numerical model to study the heat transfer coefficient and energy density at conditions of temperature and pressure not reached experimentally
- Contribute to the understanding regarding the potential of supercritical fluids as TES mediums.

1.3 DOCUMENT OUTLINE

This dissertation is divided into six chapters, whose content is described hereafter.

Chapter 2 presents a Literature Review about the characteristics of supercritical fluids and how their thermophysical properties influence on the convective heat trasnfer coefficient. The state of the art of the works about thermal energy storage developed until the time this dissertation was written is also shown, discussing experimental works with sensible and latent TES systems, followed by an explanation about the numerical works using supercritical fluids for TES.

Chapter 3 describes the concept of the Experimental Setup built during the execution of this dissertation. The construction and operation of the experimental apparatus are detailed. The apparatus was validated using air as working fluid, having the experimental results compared with results of correlations for natural convection around horizontal heated cylinders.

Chapter 4 presents the Numerical Model developed on *Multiphysics*®, (COMSOL Inc, 2017), followed by the mesh independence study and the validation of the model. The use of correlations and thermodynamic analysis to evaluate carbon dioxide as a TES medium, comparing it with other fluids, are also described in this chapter.

Chapter 5 contains the Results and Discussion of the findings with the experimental and numerical work, described in Chapters 3 and 4 respectively.

The Conclusions of this dissertation and the suggestions for future works are exhibited in Chapter 6.

2 LITERATURE REVIEW

A literature review is presented in this Chapter. Section 2.1 explains about supercritical fluids and their characteristics. Section 2.2 presents the experimental works developed to study natural convection with supercritical fluids using supercritical carbon dioxide. Finally, in Section 2.3, the technologies used for TES systems are presented, discussing their limitations and the interest in working with supercritical fluids for this application.

2.1 SUPERCRITICAL FLUIDS

Bejan (1988) describes the critical-point phenomena as a condition in which when a fluid is above its critical temperature (T_c) and critical pressure (P_c), it is impossible to separate it into two different phases. Hall (1971) simplified this concept defining the near critical region as the temperature and pressure conditions where boiling and convection phenomena converge. Hence, a supercritical fluid can be characterized as a fluid that presents pressure and temperature above its critical point, and that exhibits thermophysical properties of liquid and gas at the same time. The intense variation of properties near the critical point brings an interest in using supercritical fluids for heat transfer applications.

Rowlinson (1967) studied the singularities existent in the thermodynamic and transport properties at the critical point. The author shows that the specific heat at constant pressure, c_p, goes to infinity at the critical point, as the specific heat at constant volume, c_v. Nonetheless, Hall (1971) discusses that this infinity of c_v is much weaker than the one of c_p. Other thermophysical properties present interesting behaviors at critical conditions, for example, the density of the fluid, ρ, presents a sharp increase with the increase of the pressure after the critical point. The same happens with the thermal conductivity, k, however peaking at the critical point and diminishing its value the further the conditions of temperature and pressure are from T_c and P_c.

Figure 2.1 presents the four thermodynamic and transport properties commented, c_p, c_v, k and ρ for carbon dioxide at supercritical conditions, evaluated at temperatures slightly above T_c, 31.05 °C. The temperatures are (i) $1.05 \times T_c$, which is 32.60 °C, (ii) $1.10 \times T_c$, which is 34.20 °C, (iii)$1.25 \times T_c$, corresponding to 38.88 °C and (iv) $1.5 \times T_c$, that is 46.65 °C. The critical pressure for carbon dioxide, P_c, is highlighted in each graph. These properties were evaluated using the properties library Coolprop, (BELL et al., 2014). The interesting and important fact in Figure 2.1 is how intensely the properties vary the nearest the conditions for temperature and pressure are from the critical point, becoming more constant the further they are from this condition.

Another important aspect when discussing the thermophysical properties of supercritical fluids is the fact that they present the same behavior near the critical point for

Figure 2.1 – Supercritical carbon dioxide thermophysical properties for temperatures slightly above T_c

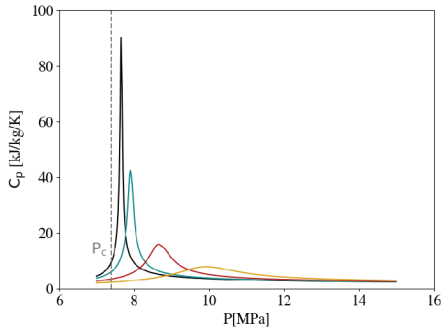

(a) Specific heat capacity at constant pressure, c_p

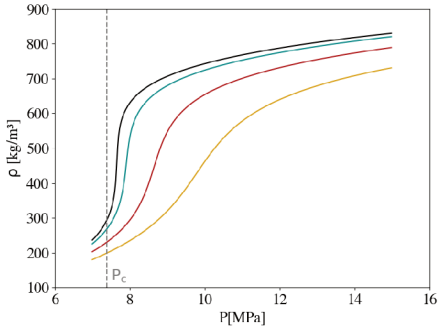

(b) Density, ρ

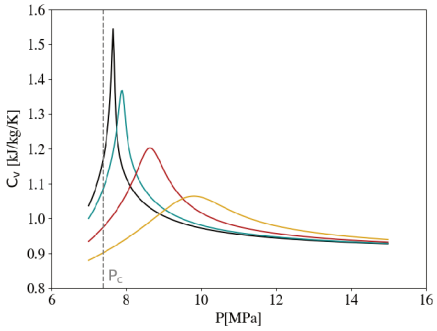

(c) Specific heat capacity at constant volume, c_v

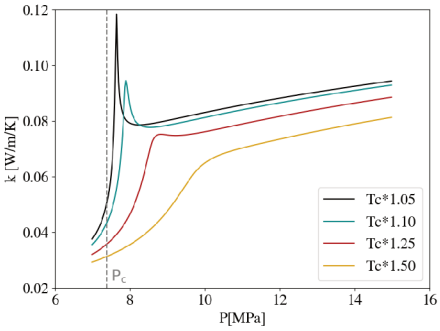

(d) Conductivity, k

all fluids (HALL, 1971). Figure 2.2 presents the four thermophysical properties shown on Figure 2.1 for s-CO_2, but now for water, which supercritical point is $T_c = 374.14$ °C and $P_c = 22.09$ MPa. As it can be seen, the behaviour of the thermophysical properties is the same for both fluids. Furst et al. (2013) already emphasized that the trends in the results observed using a supercritical fluid should be expected to occur using other fluids at supercritical conditions, because of this similar behaviour of thermophysical properties. In this context, since there is a wide range of critical points depending on the fluid, for example for CO_2 it is $T_c = 31.05$ °C and $P_c = 73.8$ MPa, supercritical fluids can be used for a wide range of applications depending on the desired operational conditions of pressure and temperature (HOBOLD; da Silva, 2017).

Carbon dioxide has been considered a working fluid for heat transfer applications. The appeal of CO_2 is in the fact that its Ozone Depleting Potential (ODP) is 0, which is an important environmental aspect showing that its presence in the atmosphere does not damage the ozone layer. Besides, CO_2's Global Warming Potential (GWP), a property that evaluates the fluid's impact as greenhouse gas, which for values closer to 0 means less impact, is 1. As well as not being very damaging to the environment, as previously inferred, the critical point of CO_2 occurs at mild conditions, mostly mild temperature

Figure 2.2 – Supercritical water thermophysical properties for temperatures slightly above T_c

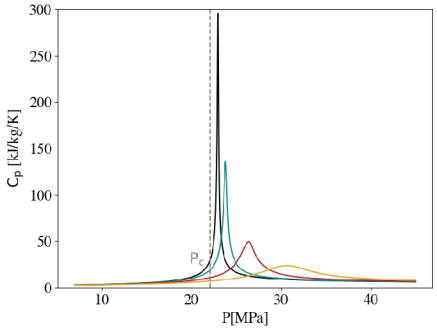

(a) Specific heat capacity at constant pressure, c_p

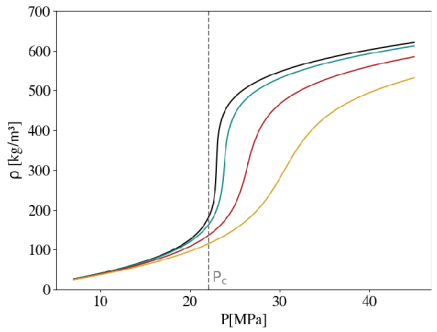

(b) Density, ρ

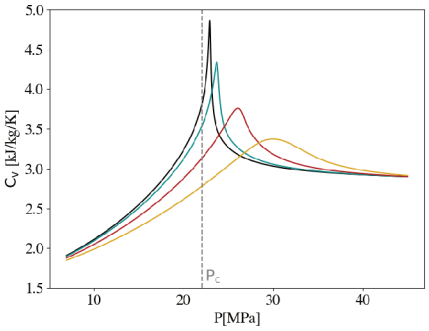

(c) Specific heat capacity at constant volume, c_v

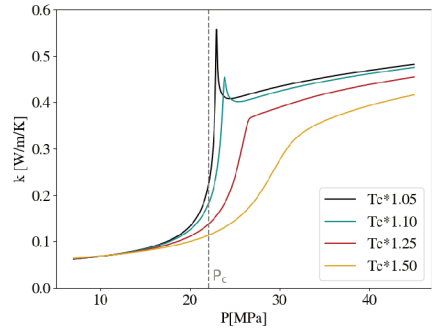

(d) Conductivity, k

conditions, which makes it an attractive fluid to experiment on in supercritical conditions (CECCINATO; CORRADI, 2011; PéREZ-GARCíA et al., 2013; PIGANI et al., 2016).

In this context, studies about heat transfer phenomena with s-CO_2 have been made since the 60's. More specifically, Hall (1971) discusses the experimental results found by Dubrovina & Skripov (1965) for natural convection on s-CO_2 around a heated wire and a vertical plate, expecting such trends to be observed in other supercritical fluids. Studies about natural convection are relevant because it is an important heat transfer phenomena for TES systems, since it is expected to be the main heat transfer phenomena observed in the storage fluid when it is in a tank trespassed by tubes containing the HTF (LAKEH et al., 2013). Dubrovina & Skripov (1965) found the same trends for the convective heat transfer coefficient both in horizontal and vertical configurations. Figure 2.3 presents the results for the convective heat transfer coefficient, h, around the horizontal wire, for temperatures of 31.5 °C, 32.0 °C and 34.0 °C, using a wire of 0.029 mm. It can be noticed that h can reach values in the order 10^4 [$W/m^2/K$] for natural convection. Furthermore, the curves of the convective heat transfer seem to present optimal conditions to enhance the heat transfer, showing more elevated values with temperatures closer to the critical point, and the peak at pressures closer to the pseudocritical pressure of each temperature,

which is the pressure for a temperature in which c_p is maximized. In fact, comparing the curves of h presented by Dubrovina & Skripov (1965) with the c_p curves in Figure 2.1, similar behaviors are observed.

Figure 2.3 – Convective heat transfer coefficient for s-CO_2. Adapted from Dubrovina & Skripov (1965)

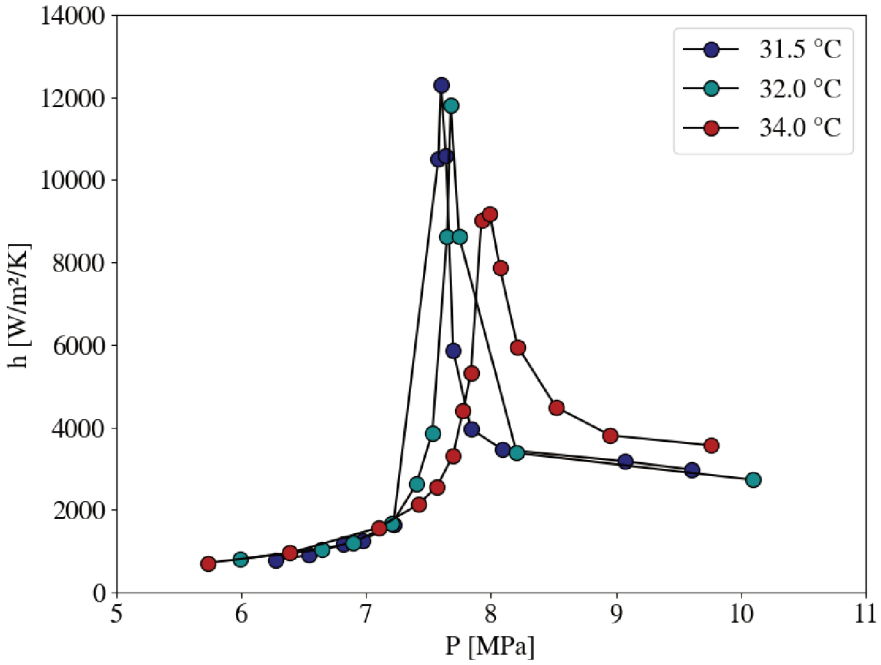

2.2 NATURAL CONVECTION WITH SUPERCRITICAL FLUIDS

As already mentioned, experimental studies with carbon dioxide have been developed since the decade of 1960. The study and the results found by Dubrovina & Skripov (1965) were already presented in the previous section, however in this section the experimental apparatus used in this and in studies developed by other researchers with s-CO_2 will be described. Besides, the correlations for natural convection with supercritical fluids developed and compared with the experimental results are also presented.

Dubrovina & Skripov (1965) performed an experiment where two pressure vessels of stainless steel containing carbon dioxide at supercritical pressures were sunken into a water chamber with controlled temperature that would also control the bulk temperature of the carbon dioxide. An scheme of the experimental apparatus is shown in Figure 2.4. In one of the pressure vessels, a horizontal wire with diameter of 29 μm connected between two electrodes dissipated power, and in the other vessel a vertical wire did the same. The temperature of the heated wire was determined by measuring the change on its electrical

resistance. Visual observations were made through a self-sealing glass window to study the occurrence of bubbles during the transition of the fluid to the supercritical condition. Another objective of this experiment was to evaluate the convective heat transfer coefficient for different bulk temperatures, different temperature differences between the fluid and the wire, and pressures, ranging from 5.92 to 10.10 MPa, as already mentioned. 29 micrometer platinum wires were used for both horizontal and vertical studies.

Figure 2.4 – Experimental apparatus developed by Dubrovina & Skripov (1965). Adapted from Dubrovina & Skripov (1965)

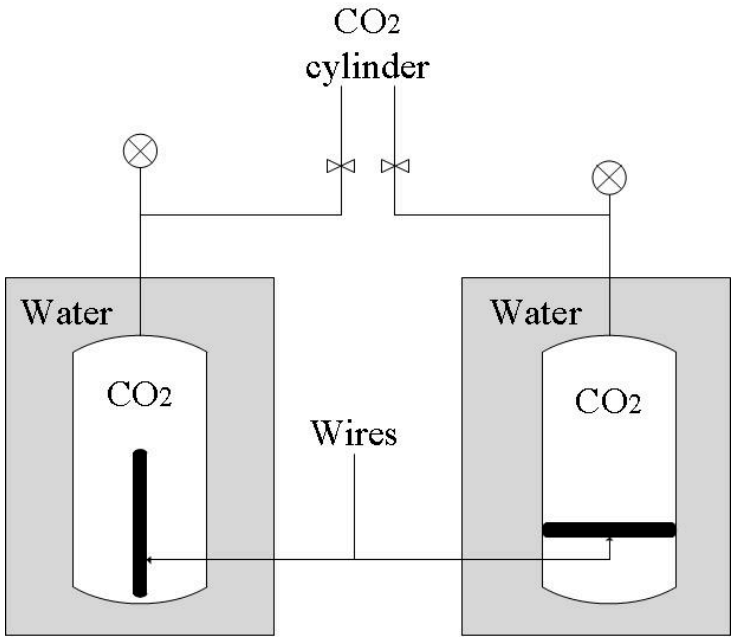

Besides the findings that the heat transfer coefficient peaks near the critical point, presented in Figure 2.3, for the visual observation it was noticed that for the same ΔT between the wire and the fluid, increasing the pressure above 62 kg/cm^2 would cause the appearance of streams along the vertical wire. The flow became turbulent when closer to the maximum power dissipated. On the horizontal wire, convective flows were observed only near the maximum heat transfer coefficient, not presenting visible streams for other conditions.

Knapp & Sabersky (1966) also performed experimental studies to investigate the heat transfer coefficient for carbon dioxide around a heated wire near the critical point, using an experimental apparatus and methodology similar to Dubrovina & Skripov (1965). The pressure in the chamber was controlled using a hydraulic accumulator driven by nitrogen gas. A Wheatstone bridge circuit was made to measure the resistance in the wire and therefore evaluate its temperature. The bulk temperature was measured with the aid of a thermocouple. Nichrome wires of 0.254 mm were used for the experiment.

Three different flow patterns were observed, the regular laminar free convection flow, a highly turbulent stream with aggregates of fluid that were similar to bubbles, and a

flow that would vary from the usual free convection flow and "bubble-like" pattern. What seems to determine the type of flow observed in the experiment was the temperature difference between the wire and the fluid, associated with the heat transfer curve observed for different operational conditions.

The Nusselt Number is an important heat transfer parameter and it is calculated using Equation 2.1, where $\overline{Nu_{\mathrm{D}}}$ is the average Nusselt number with the diameter of the cylinder as characteristic length, $\overline{h}$ is the average convective heat transfer coefficient and k_{f} is the fluid's thermal conductivity. (BERGMAN et al., 2016)

$$\overline{Nu_{\mathrm{D}}} = \frac{\overline{h}D}{k_{\mathrm{fluid}}} \tag{2.1}$$

To try and evaluate the Nusselt number for natural convection with supercritical fluids, Kato et al. (1968) proposed a reference value of the thermal properties of a fluid at supercritical conditions as an integral of the property between the surface temperature and the bulk temperature, as shown in Equation 2.2, where $\overline{J}$ is the reference thermal property, T_{wire} is the wire temperature and T_{bulk} is the fluid's bulk temperature.

$$\overline{J} = \frac{1}{T_{\mathrm{wire}} - T_{\mathrm{bulk}}} \int_{T_{\mathrm{bulk}}}^{T_{\mathrm{wire}}} J(T)dT \tag{2.2}$$

Kato et al. (1968) then proposes Equation 2.3 as a correlation for natural convection around a heated cylinder, using the integrated mean properties.

$$\overline{Nu_{\mathrm{D}}} = 0.53(\bar{Gr}_{\mathrm{D}}\bar{Pr})^{1/4} \tag{2.3}$$

The Grashof's number Gr_{D} is calculated using Equation 2.4 and the Pandtl, Pr, is given by Equation 2.5, where i is the enthalpy of the fluid at the evaluated temperature.

$$\overline{Gr_{\mathrm{D}}} = \frac{g{D_{\mathrm{wire}}}^3}{\overline{\nu}}.2\frac{\rho_{\mathrm{bulk}} - \overline{\rho}}{\overline{\mu}} \tag{2.4}$$

$$\overline{Pr} = \frac{\overline{\mu}}{k}\frac{i_{\mathrm{wire}} - i_{\mathrm{bulk}}}{T_{\mathrm{wire}} - T_{\mathrm{bulk}}} \tag{2.5}$$

The experimental results presented by Kato et al. (1968) fitted well when compared with the correlation proposed, both for the horizontal wire and for vertical plate, changing the characteristic length from the wire's diameter for the plate length in this case.

Neumannt & Hahne (1980) also performed similar experiments, however controlling the pressure inside the vessel through the temperature variation of the fluid or using a piston pump. A similar behavior of the heat transfer coefficient as in the other experimental approaches was found. They discussed the properties integrated mean value used in Equation 2.2 (NEUMANNT; HAHNE, 1980 apud NUSSELT, 1915). However they compare their results with the experimental correlation given by Equation 2.6 (NEUMANNT; HAHNE, 1980 apud ZIJNEN, 1963), finding a good fit between the experimental results

and the correlation and discussing that the deviations between Equation 2.6 and the experimental results found were smaller when increasing the wire diameter.

$$Nu_{\mathrm{D}} = 0.35 + 0.25{Ra_{\mathrm{D}}}^{1/8} + 0.45Ra_{\mathrm{D}}^{1/4} \tag{2.6}$$

The Rayleigh number Ra_{D} is given by multiplying the Grasshof and the Prandtl numbers, as shown in Equation 2.7, where α is the thermal diffusivity, given by $\alpha = k/\rho c_p$.

$$Ra_{\mathrm{D}} = Gr_{\mathrm{D}}Pr = \frac{g\beta}{\nu\alpha}(T_{\mathrm{wire}} - T_{\mathrm{bulk}})D_{\mathrm{wire}}^3 \tag{2.7}$$

More recently, Rousselet et al. (2011) performed similar experiments observing nucleate boiling at pressures under P_{c}, film boiling at higher pressures, but still under P_{c}, and natural convection at pressures above P_{c}. They compare their experimental results with correlations for the conditions (a) P $< P_{\mathrm{c}}$; (b) $P > P_{\mathrm{c}}$ and $T_{\mathrm{wire}} < T_{\mathrm{pc}}$ and (c) P $> P_{\mathrm{c}}$ and $T_{\mathrm{wire}} > T_{\mathrm{c}}$. For supercritical condition, where both the pressure and the temperature were above the critical point, it was found a good relation between the experimental results and the correlation presented in Equation 2.3.

Rousselet et al. (2013a) performed the same type of experiments, still discussing the use of the correlations for natural convection heat transfer for supercritical fluids to try to reach a conclusion about the temperature in which the fluid's properties must be evaluated, and how the property variations are to be considered. They suggest for the conditions where P $> P_{\mathrm{c}}$ and $T_{\mathrm{wire}} > T_{\mathrm{pc}}$ the use of Equation 2.8, being applicable for $1.9 \times 10^1 \leq Ra_{\mathrm{D}} \leq 1.3 \times 10^4$. The Galileo number, Ga is defined as $Ga = gD^3/\nu^2$ and all the properties are evaluated at the critical point, P_{c} and T_{c}. In their comparisons, the correlation proposed by Kato et al. (1968), Equation 2.3, presents a good fit with the experimental results found.

$$Nu_{\mathrm{D}} = 0.46Ra_{\mathrm{D}}^{-0.3}\left(\frac{i_{\mathrm{wire}}}{i_{\mathrm{c}}}\right)^{-1.2}\left(\frac{i_{\mathrm{c}}}{i_{\mathrm{pc}} - i_{\mathrm{bulk}}}\right)^{0.79}{Ga_{\mathrm{c}}}^{0.467} \tag{2.8}$$

In the second part of this work, Rousselet et al. (2013b) developed a numerical model to study the natural convection heat transfer phenomena. They used the SIMPLEC method to solve the governing equations of momentum and energy, obtaining the CO_2 properties values from REFPROP libraries. The simulation results were validated with their experimental results. They found that both for subcritical and supercritical pressures, the heat transfer coefficient h is always strongly dependant of the temperature. They have also found that the behaviour presented by h with different wire diameters does not change, being the only modification on the results the value of h. The convective heat transfer coefficient always decreases with the increase of the diameter.

Table 2.1 presents a summary of the experimental studies of natural convection with carbon dioxide at supercritical or near-critical conditions, showing the material of the wires used, the wire diameters and the configuration of the studies in therms of horizontal

wire, vertical plate or strap. The trends of h seen in Figure 2.3 were observed in all of the experiments when carbon dioxide was on supercritical conditions, presenting nonetheless different values because of the variation of wire diameters used. It is worth mentioning that Cabeza et al. (2017) developed a review of heat transfer coefficients of supercritical carbon dioxide flowing in heat exchangers. They also discuss the use of CO_2 in several different heat transfer applications.

Table 2.1 – Summary of experimental studies for natural convection around small heated cylinders with supercritical carbon dioxide. Source: Developed by the author

Authors	**Wire material**	**Wire diameter (mm)**	**Wire configuration**
Dubrovina & Skripov (1965)	Platinum	0.029	Horizontal and Vertical wires
Knapp & Sabersky (1966)	Nichrome	0.254	Horizontal wire
Kato et al. (1968)	Not mentioned	2.000	Horizontal wire Vertical plate Circular pipe
Goldstein & Aung (1968)	Platinum	0.381	Horizontal
Neumannt & Hahne (1980)	Platinum	0.050 0.100 0.300 Strip of 0.0125 mm thickness and 5 mm height	Horizontal wire and
Rousselet et al. (2011)	Platinum Nichrome 60/20	0.254 0.762 0.1 0.1016 (NiCr)	Horizontal wires
Rousselet et al. (2013a)	Platinum Nichrome 60/20	0.254 0.762 0.1 0.1016 (NiCr)	Horizontal wires

2.3 THERMAL ENERGY STORAGE SYSTEMS

As already discussed, energy storage systems are often used to minimize the mismatch problem between the generation and demand hours of intermittent powered systems. In accordance with Ganapathi & Wirz (2012), the main desirable characteristics of a TES system are:

- high energy density of the storage medium often evaluated as J/m^3 or kWh/m^3;
- high convective heat transfer coefficient between the storage medium and the working fluid;
- chemical and mechanical stability of the storage material;
- chemical compatibility between the working fluid, the heat exchanger (if used), and the storage medium;
- thermal reversibility for a high number of loading and unloading thermal cycles;
- low thermal losses;

Generally speaking, there are two main types of TES storage: sensible and latent heat storage. The first consists in storing energy through the temperature increase or decrease of a substance. TES of latent heat dwells on storing the amount of energy needed to change the phase of a substance, usually solid to liquid, taking advantage of the high internal enthalpy of fusion or boiling of these materials, known as phase change materials. There is also a new technology of heat storage in research, known as thermochemical heat storage. In this case, a determined endothermic chemical reaction occurs to absorb thermal energy. The reverse exothermic reaction takes place to extract thermal energy from the storage unit (LIU et al., 2012; GIL et al., 2010). Sensible and latent TES will be further discussed in the following subsections.

2.3.1 Sensible Thermal Energy Storage

TES through sensible heat consists on storing energy over the temperature variation of the storage medium. El-Kaddadi et al. (2017) performed an experimental work to verify the sensible heat stored in a mixture of water and a nanofluid, titanium dioxide. Figure 2.5 shows an scheme of the experimental apparatus described in the paper. It consisted on a pipe with water as HTF crossing an insulated vessel containing the storage fluid. Nine thermocouples were used to measure the temperature of the storage fluid. Two thermocouples measured the inlet and outlet temperatures of the HTF. With this, the measurement of its mass flow rate and assuming the heat loss was negligible, the heat flux is calculated using Equation 2.9, where q_{HTF} is the heat transfer rate from the HTF, $\dot{m}$ is the mass flow rate, c_p is the specific heat at constant pressure and ΔT is the temperature difference between the inlet and outlet of the HTF.

$$q_{\mathrm{HTF}} = \dot{m} c_p \Delta T \tag{2.9}$$

It was found that during the charging period the mass flow rate only affects the heat transfer in the later part of the charging cycle, increasing its effect with the increase

Figure 2.5 – Experimental apparatus developed by El-Kaddadi et al. (2017). Adapted from El-Kaddadi et al. (2017)

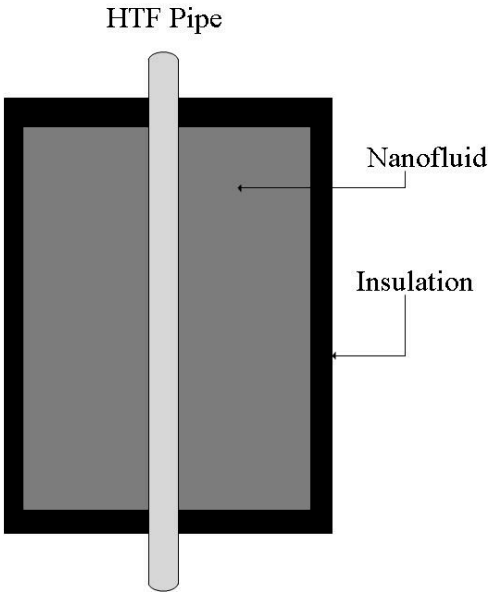

of the mass flow rate by this moment and having its effect negligible in the beginning of the cycle. With a higher flow rate, there is an increase in the heat transfer between the HTF and the storage fluid. Also, there seems to be an optimal concentration of nanoparticles to promote an increased heat transfer between the fluids.

Nordbeck et al. (2019) developed an experimental study using cement as sensible TES medium, building a prototype that consisted on a helical heat exchanger enclosed in a container filled with cement. Figure 2.6 shows an ilustrated representation of the experimental apparatus. The maximum energy density was found to occur at the maximum operational temperature of 80 °C and was 52 kWh/m^3. Lugolole et al. (2019) also performed experimental studies with solid sensible TES mediums. It consisted on using two sunflower oil in rock-bed TES tanks showing that the performance of the TES sytem during the discharging cycle depended greatly on the HTF flow rate.

Bataineh & Gharaibeh (2018) executed a numerical study evaluating dead sea salt and basalt rock as TES mediums and comparing them with concrete. The parameters evaluated were the charging efficiency of the materials and energy stored in each step of the system's cycle. The dead sea salt presented a higher charging efficiency compared to the other two materials, which is justified by the authors by the fact that this material presents a higher thermal conductivity than the other materials. Parametric studies were made to optimize the design of the storage tank, finding that for a given mass flow rate of the HTF there was an optimal charging tube diameter and an optimal number of tubes in the heat exchanger.

Another numerical study developed was the one made by Alaptekin & Ezan (2020), who modelled a sensible packed-bed heat exchanger as TES tank, coupled with a flat plate

Figure 2.6 – Experimental apparatus developed by Nordbeck et al. (2019). Adapted from Nordbeck et al. (2019)

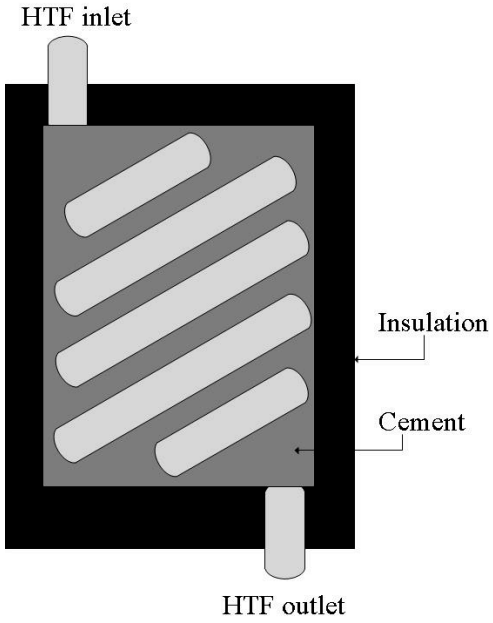

solar collector, as shown in Figure 2.7. The authors used weather data for the months of November, December, January and February in the simulation. The working fluid was SYLTHERM 800 and the TES medium was Quartzite-rock. Again, the mass flow rate influences greatly in the performance of the TES system. If by one hand increasing it reduces the charging time and boosts the mean temperature of the TES system and its exergy efficiency, it also increases the outlet temperature of the tank, reducing the solar collector's efficiency.

Figure 2.7 – Numerical model developed by Alaptekin & Ezan (2020). Adapted from Alaptekin & Ezan (2020)

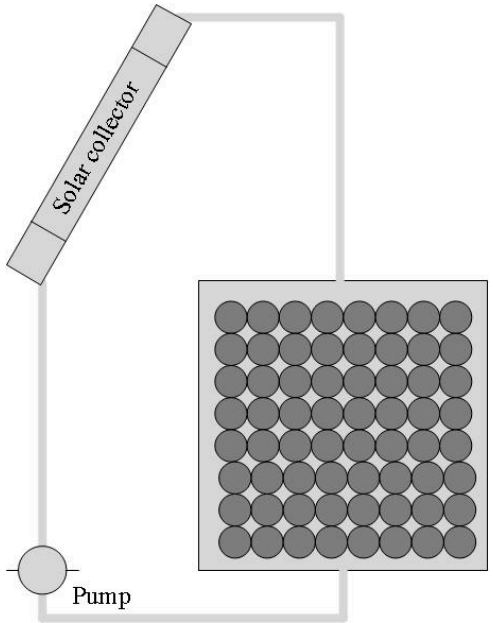

Li (2016) makes a study using as sensible TES mediums water, rock and brick and oil as HTF. The author compares these materials with latent TES using hydrate salts and organic materials, highlighting that one of the main advantages of solid mediums is in their low price, good thermal diffusivity and the fact that they are easy to manufacture. However, when comparing sensible with latent TES, they present low energy density and increased heat loss to the environment. On the other hand, the materials used for latent TES are highly corrosive. This type of TES will be further discussed in the following subsection.

2.3.2 Latent Thermal Energy Storage

There seems to be an extensive amount of experimental works using different types of Phase Change Material (PCM)s to store thermal energy. In these papers, the charging time could be defined both as the time to melt the PCM at solid state, in which case the discharging time was considered as the time to solidify it again, or as the time taken to reach a certain temperature above the melting temperature, where the thermal energy would be stored as latent heat added with the sensible heat. Table 2.2 presents a summary of some relevant experiments evaluating different PCMs for TES.

Table 2.2 – Summary of experimental studies of the heat transfer mechanisms in PCMs as TES. Source: Developed by the author

Authors	PCM	HTF	Heat Exchanger
Liu & Groulx (2014)	Dodecanoic acid	Water	Cylindrical tube containing the PCM trespassed in its center by a copper pipe with HTF
Dinker et al. (2017)	Beeswax	Water	A rectangular vessel with PCM was crossed over by a helicoidal tube with PCM
Palomba et al. (2017)	Blend of paraffin	Water	Fin-and-tube heat exchanger
Kabbara et al. (2016)	Dodecanoic acid	Water	A cylindrical tank filled with PCM. Four copper tubes in series used as heat exchanger with HTF
Liu et al. (2006)	Paraffin	Distilled water	Heat pipe heat exchanger
Avci & Yazici (2016)	Paraffin	Water	Tube-in-shell heat exchanger used as TES system
Wang et al. (2019)	Sodium acetate trihydrate mixed with nucleating agent	Water	PCM in tube of a shell- and-tube heat exchanger
Zondag et al. (2017)	Rubitherm paraffin RT70	Water	PCM in the shell of a shell-and-tube heat exchanger

In general these experimental works consisted on using a heat exchanger where the PCM would change heat with a HTF, both during the charging and discharging cycle. It was a common method to evaluate the heat flux retrieved from the HTF by measuring its inlet and outlet temperatures and its mass flow rate, then using Equation 2.9 to calculate the rate of heat transfer, since the specific heat of water is well known and all these studies used water as HTF. Also, it is common to insulate the storage media to minimize the thermal losses to the environment. Some of these authors use the integral of this instantaneous power during the duration of the charging/discharging cycle as the amount of energy absorbed/given during the cycle (DINKER et al., 2017; PALOMBA et al., 2017; KABBARA et al., 2016; LIU et al., 2006; AVCI; YAZICI, 2016; ZONDAG et al., 2017).

Another approach is to consider the sensible heat stored in the temperature variation of the PCM when it is in solid or liquid state, and add it with the latent heat of the phase change of the material, considering no loss to the environment, as shown by Equation 2.10, where q_{PCM} is the heat transfer rate, m_{PCM} is the mass of PCM, $c_{\text{p.solid}}$ is the specific heat at constant pressure of the material in solid state, ΔT_{solid} is the temperature difference the material suffers as solid, before reaching its fusion temperature and La is the material's latent heat of phase change. $c_{\text{p.liquid}}$ and ΔT_{liquid} are the specific heat and the temperature variation of the material at liquid state (DINKER et al., 2017; LIU et al., 2006; AVCI; YAZICI, 2016; ZONDAG et al., 2017).

$$q_{\text{PCM}} = \quad m_{\text{PCM}} \left[c_{\text{p.solid}} \Delta T_{\text{solid}} + La + c_{\text{p.liquid}} \Delta T_{\text{liquid}} \right] \tag{2.10}$$

A common result in these experiments (LIU; GROULX, 2014; DINKER et al., 2017; PALOMBA et al., 2017; KABBARA et al., 2016; LIU et al., 2006; AVCI; YAZICI, 2016; ZONDAG et al., 2017) is that in the beginning of the charging cycle, because the PCM is still solid, the heat transfer mechanism is conduction. This is the main heat transfer mechanism during the whole phase change, since convection starts to be slowly observed after the PCM starts melting. Because of this, a slow rise in the energy slope occurs. This happens because the heat rate is small given the reduced thermal conductivity of the PCM and of the limited heat transfer efficiency. The inlet temperature of the HTF has a high impact on the charging time. The flow rates affect forced convection heat transfer, not influencing much the charging time dominated by conduction and impacting more in the discharging time. Liu et al. (2006) comment that they observed a smaller phase change rate during the discharging cycle when comparing it to the charging cycle.

Further limitations are discussed by Li (2016) in the traditional TES systems that make use of solids or of molten salts for latent and sensible heat storage. The solid materials, both for sensible as for latent heat, present low thermal conductivity, reflecting in a low power density transferred to the heat transfer fluid. Besides, molten salts present the complication of being highly corrosive, resulting in maintenance obstacles for the storage tanks. Also, Liu et al. (2012) comment they present a high fusion temperature,

enabling a solidification of the storage material if the heat source is not enough to keep the medium's temperature above the melting point. Anti-freezing systems are used to work around this complication, presenting, though, high costs. Even if the thermo-chemical storage exhibits a high volumetric energy density, values from five to ten times higher than systems with sensible and latent heat storage, respectively, these systems are still in experimental phase, not being consolidated in industrial level.

Given the presented limitations and the increasing interest in TES integrated with renewable energy systems, developments are being sought in this research field to improve the performance of TES systems. Liu et al. (2016) discusses some of these developments, such as the use of ionic liquids, which possess lower fusion temperature than the conventionally used molten salts, and the use of nanoparticles in these ionic fluids or in molten salts to increase their thermal capacity. There is also interest in reducing the thermal resistance between the storage fluid and the working fluid, as discussed by Liu et al. (2012). It is possible to use encapsulated PCMs or use heat tubes in the heat exchanger to increase the superficial area of the heat transfer. It is also possible to use a configuration with several PCMs with different fusion temperatures to increase the heat flux transferred to the working fluid. However, this will elevate the cost of the system. Another option to increase the heat transfer between the PCM and the working fluid is the one proposed by Fleming et al. (2015), who investigated the use of aluminium foam in a shell-and-tube heat exchanger. The authors found that the foam increased the heat transfer coefficient both in the solidification as in the melting processes, presenting larger enhancement for the second process.

A still different approach considered nowadays for TES systems is the use of supercritical fluids as TES medium. Figure 2.8 shows the results found by Hobold & da Silva (2017) for several thermal energy storage mediums. The interesting aspect is that the energy density of commercial sensible TES materials can be outgrown by supercritical water (sH_2O) at 400 bar. Besides, supercritical fluids show enhanced heat transfer coefficients compared to all studied materials. Ultimately, Figure 2.8 shows the potential of supercritical fluids for TES systems in therms of heat transfer rate and of energy density. TES with supercritical fluids will be further discussed in the following Subsection.

2.3.3 Thermal Energy Storage with Supercritical Fluids

A few numerical studies have been developed with the intent of comparing conventional TES systems with systems using supercritical fluids as storage medium. Tse et al. (2014) used a numerical model to compare the performance of a single tank system with supercritical fluids with a two tanks storage system using molten salt. The two fluids evaluated are naphtalene and para-xylene. The TES system was connected to a steam generator in order to evaluate the influence it had on the power output of the turbine. The one-tank system evaluated reduces the complexity of the TES system, its cost, but also

Figure 2.8 – Heat transfer coefficient and energy density of several evaluated fluids for a temperature variations of 50 °C. Reprinted from (HOBOLD; da Silva, 2017) with permission from Elsevier.

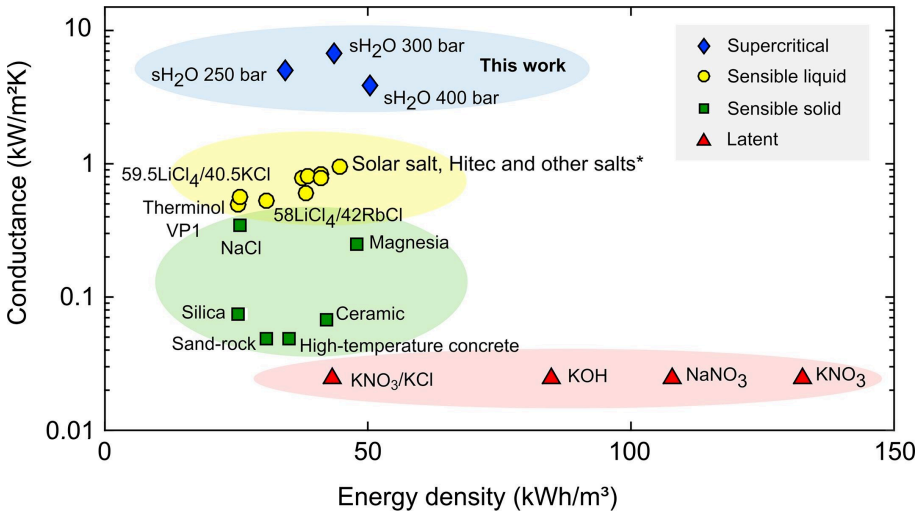

the output power of the turbine because of the temperature decay of the storage fluid with time during the discharge cycle when compared to two tanks systems using molten salts. The authors also emphasize that when working with supercritical fluids, the thickness of the tank wall must be taken into consideration, deducing that there is an optimal average density of fluid that produces a given optimal output power in the turbine at the same time minimizing the costs with the tank wall.

Furst et al. (2013) used a thermodynamic analysis of the properties of R-134a at supercritical conditions to evaluate the TES in isobaric and isocoric systems, also known as Constant Pressure Thermal Energy Storage (CPTES) and Constant Volume Thermal Energy Storage (CVTES), respectively. These storage systems were studied in subcritical and supercritical conditions. It was found out that supercritical CPTES explore a large isobaric thermal capacity near the critical point, being the critical pressure of R134a 4.06 MPa. Nonetheless in the isocoric process near the supercritical point, the specific heat does not vary much with the density of fluid and temperature. It was observed substantial benefits in using supercritical R134a in CPTES in reference of its storage energy density when comparing it to subcritical energy density, given the increase in the specific heat in supercritical regime. However, in the constant volume regime, the isocoric specific heat is followed by a reduction of the storage volumetric capacity, resulting in the author's conclusion that there are no visible advantages in working with supercritical fluids in isocoric system. It is expectad that the tendencies observed in the results obtained by Furst et al. (2013) with R134a can be applied to other supercritical working fluids because of the correspondent stated principle.

More recently, Hobold & da Silva (2017) obtained similar tendencies for CPTES with supercritical fluids, showing that CPTES possess higher energy density compared to CVTES. The authors also discuss that for constant pressure regime, with pressures close to

P_c, the characteristic peak in specific heat is very narrow, getting larger the more distant the pressure is from the critical. This may have some relation to the optimal conditions of pressure and temperature variation for energy density the authors found in CPTES systems. It is suggested the use of carbon dioxide in supercritical TES systems, where the carbon dioxide can still be potentially coupled with a refrigeration cycle as thermal energy storage fluid at high pressures. The authors also corroborate the discussion from Section 2.1 about the broad range of applications of supercritical fluids for TES. This is shown in Figure 2.9 which presents the energy density of several fluids evaluated at their critical temperature, for a temperature variation of 50 °C, and varying the operating pressures. The fluids analysed present critical temperatures that range from -200 to 600 °C and the operational pressures range from 0 to 500 bar.

Figure 2.9 – Energy density of CPTES for several fluids, classified by their critical temperature for a temperature variations of 50 °C. Reprinted from (HOBOLD; da Silva, 2017) with permission from Elsevier

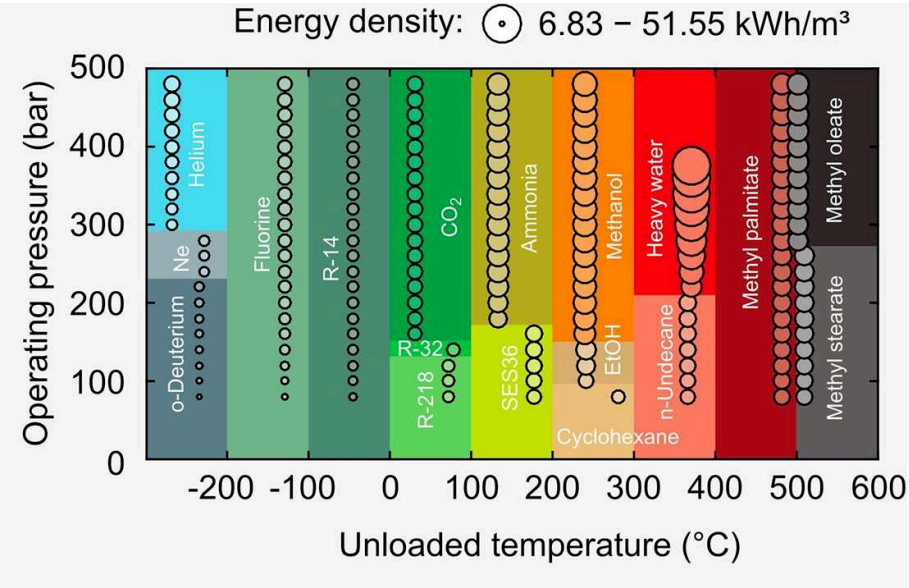

In the following study, Hobold & da Silva (2018) used a correlation for natural convection on a heated plate to analyse the heat transfer coefficient using s-CO_2. A thermodynamical analysis is developed to study the s-CO_2 thermal energy storage density for a CPTES system. The authors verified optimal operating conditions for the heat transfer phenomena concerning the bulk temperature, the pressure and the temperature difference between the surface and the fluid. The pressure that maximizes the heat transfer is nearly the same that maximizes the energy density of the system, and these optimal conditions are usually connected to the conditions in which the properties of the fluid vary the most. Another possibility would be to use s-CO_2 directly for power generation on Brayton cycles, as studied by Dostal et al. (2004), which states that for the same temperature and pressure applications, the s-CO_2 presents higher efficiencies when compared to Helium cycles.

Despite all these numerical works considering supercritical fluids for TES, few experimental studies involving supercritical TES were found. Tse et al. (2014) executed experiments to evaluate the durability of several fluids under different temperatures, intending to verify if the organic fluids analysed (naftalene, 1-methylnaftalene, orto-xylene, mete-xylene, para-xylene, decane, byfenil, Tert-buthylbenzene) presented the desirable characteristics to be used as TES storage fluids at supercritical conditions. Nonetheless, the authors do not study the actual behaviour of such fluids in a Supercritical Thermal Energy Storage (s-TES) system.

Still discussing experimental studies with s-TES, Ganapathi et al. (2013) executed a test with a 5 kWht storage tank with naphtalene in supercritical conditions as storage fluid. Temperatures of 500 °C and 6.9 MPa were reached during this experiment. The apparatus design was made through the concept of a shell and tube heat exchanger, as shown in Figure 2.10, with tubes filled with naphtalene being the heat storage medium and air working as the heat transfer fluid flowing around those tubes to add or remove energy. The system was instrumented in a manner that would make it possible to obtain the heat stored in the steel of the tank, the heat stored in the naphtalene and the heat lost to the environment. The authors got to the conclusion that the energy density of a single tank with supercritical fluid as storage medium is significantly higher than the energy density presented by a two-tanks storage system with molten salts. This is credited to the high compressibility characteristic of supercritical fluids. Even with a larger cost with the tank walls materials, which must be in accordance with safety requirements, using a single-tank with supercritical fluid as storage media can result beneficial in economical analysis because the savings with fluid costs when compared with two-tank molten-salts systems.

Figure 2.10 – Experimental apparatus developed by Ganapathi et al. (2013). Adapted from Ganapathi et al. (2013)

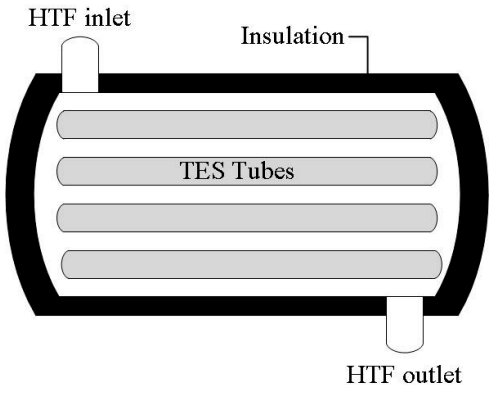

2.4 PROBLEM SPECIFICATION

After reading this chapter it is possible to realize that TES systems are a fundamental part concerning the development and propagation of concentrating solar power plants. The main technologies currently being used in TES systems are latent and sensible heat storage, mostly using PCMs as storage medium. Nonetheless, these materials present a series of undesirable characteristics for TES and industry applications. There are several papers experimenting with PCMs as storage media, testifying about the limitations of such materials, mostly regarding the low heat transfer rate when the phase change is occurring given the materials low conductivity.

In order to try and contribute in this matter, researches considering supercritical fluids as storage medium are being developed. The thermophysical properties variations near the critical point seem to greatly increase the heat transfer coefficient, as shown in experimental works studying natural convection with carbon dioxide at supercritical conditions. Also, many numerical works have been published in recent years presenting supercritical fluids as promising mediuns for TES applications. However, given the difficulties of working experimentally with supercritical fluids, there is a lack of experimental works applying such fluids for TES use.

It is also clear that carbon dioxide seems to be a good fluid for this type of applications, because of its properties variations, the fact that it is already widely used in industry and the fact that it is not a toxic, polluting gas, since it can be captured from the atmosphere and released to it again after its use. Thus, as shown in Figure 2.11, the focus of this work will be to evaluate, both in a numerical and experimental approach, carbon dioxide at supercritical conditions as a storage medium for TES applications in concentrating power plants.

Figure 2.11 – Where the current research fits in the literature

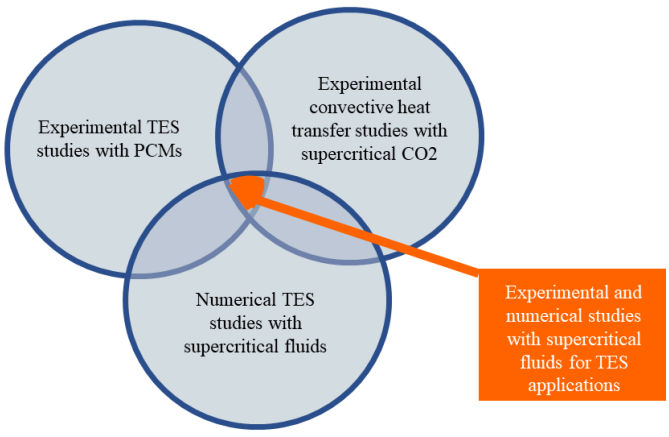

3 EXPERIMENTAL METHODOLOGY

This Chapter describes the experimental apparatus in Section 3.1 and the approach followed to run the experiments with s-CO_2 in Section 3.2. Section 3.3 presents the parameters tested, the equations to calculate these parameters through the measurements made, and the uncertainty analysis of the measurements. The validation of the experimental apparatus using air as the working fluid is shown in Section 3.4.

3.1 EXPERIMENTAL SETUP

The experimental apparatus consists of a cylindrical pressure vessel made out of galvanized carbon steel, with a height of 30 cm and internal diameter of 15 cm. A bottom horizontal lid, also made out of carbon steel, is weld on the cylinder while the top horizontal lid is bolted to it; between the lid and the cylinder, an o-ring is used to prevent leakage of the working fluid. The top lid, which allows access to the pressure vessel, is attached to two 20 cm long copper electrodes; these are separated 10 cm from each other. Between the electrodes, a nichrome wire of 0.45 mm diameter dissipates power inside the vessel, which will be filled with carbon dioxide.

Five type T thermocouples, all attached to the top lid by a feed, at different heights, are used to measure the vertical temperature gradient inside the vessel. The thermocouples' tips were positioned 12.0, 14.5, 15.5, 19.5 and 22.5 cm from the lower surface of the lid and separated from each other by a distance of 3 cm. One type E thermocouple which tip was welded in a 2 mm external diameter tube was used to measure directly the temperature of the wire, as represented by Figure 3.1, where it is possible to see two electrodes, the wire between being involved by a tube. The thermocouple is welded in the tube, which is welded in the wire to ensure full contact between the tube's internal surface and the wire. Figure 3.2 shows pictures of the vessel and of its lid with the electrodes and the thermocouples attached.

Figure 3.1 – Measurement of the wire's temperature through a thermocouple welded in a capillary tube, involving part of the wire

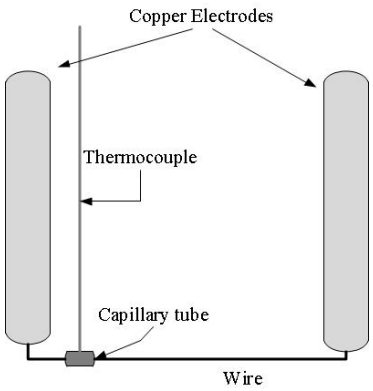

The wire used for the experiment was made of nichrome 80/20. The initial concept imagined for this experiment was to measure the temperature of the wire through its resistance variation, as done in the experiments presented in Section 2.2. Nonetheless, as it can be seen in Figure A.1 presented in the Appendix A, the wire's resistance varies only 1.6% from 20 to 93 °C, indicating that the limitation of the electrical resistance of the wire with the temperature would be smaller than the uncertainty of the measurement. Such a small variation made it difficult to obtain repeatability when trying to calibrate the resistance with temperature curve of the wire. Besides, the resistance curve with the wire's temperature is not linear, presenting an increase in the resistance until 538 °C and oscillating for higher temperatures. The power dissipated through the wire was provided by a power source which supplies DC voltages from 0 to 80 V and currents between 0 and 60 A, with a control of 0.001 V and 0.001 A.

Figure 3.2 – Pressure vessel and the lid with the electrodes

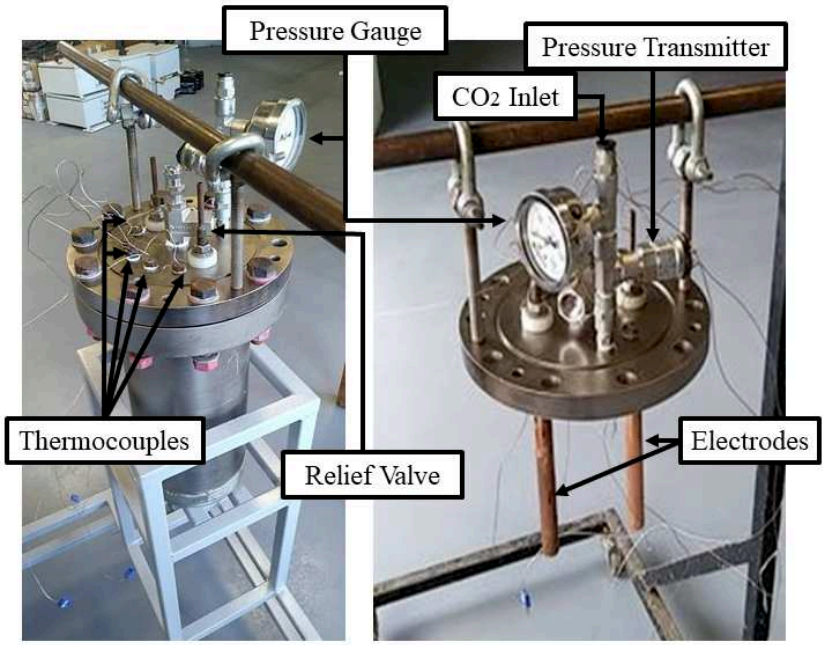

Also on the top lid of the vessel, a pressure transmitter measured the pressure inside of it. The pressure transmitter was fed by a 12 V power source and connected to the data acquisition current module. The electrical resistance of the transmitter varies with the pressure it measures. Hence, the current passing through the pressure transmitter varies linearly from 4 to 20 mA with the pressure it measures going from 0 to 20 MPa.

Besides this, a pneumatic ball valve, which was actuated remotely, was partially opened when the pressure inside the vessel needed to be reduced, discharging CO_2 to the atmosphere. This guaranteed both the pressure control and the safety of the operations of this experimental apparatus. An electrovalve connected an air compressor with the pneumatic ball valve and was used to control the pneumatic valve. It opened to release the air flow from the compressor in order to partially open the ball valve, and closed to

restrain the air flow, closing the ball valve. The pneumatic valve was also partially opened to feed CO_2 to the vessel. Nevertheless, before this procedure, vacuum was made into the system using a vacuum pump to ensure the vessel would be filled only with carbon dioxide and without any residual air from the atmosphere. In this sense, a carbon dioxide circuit was built to feed the CO_2 into the pressure vessel safely, using valves and connections from Swagelock™. Figure 3.3 presents a picture taken of the valves board built next to the experiment, indicating each connection and valve. This circuitry and its operation will be described in details in Subsection 3.2.1.

Figure 3.3 – Valves board of the carbon dioxide circuitry

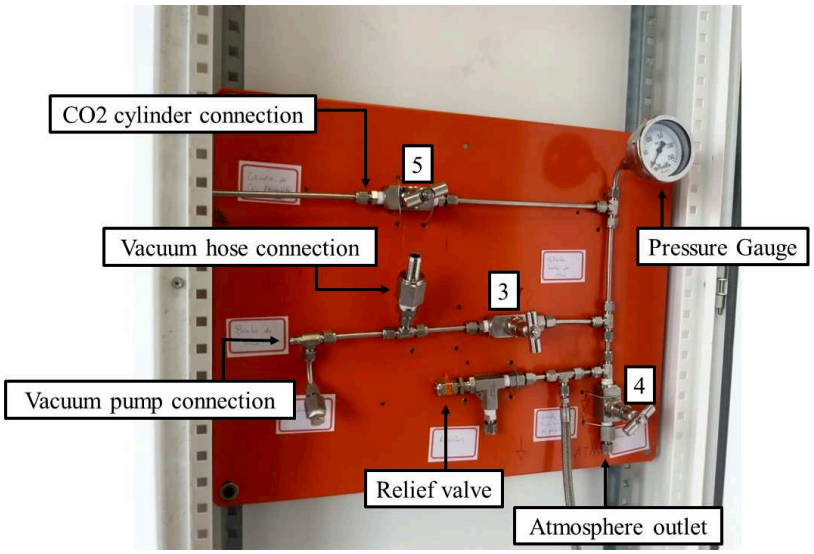

Before being able to fill the vessel with CO_2, two mechanical tests were performed to ensure the safety of the experiments and proper sealing of the vessel, which was built to resist pressures of 15.0 MPa. Therefore, a mechanical test was executed using air at pressure of 0.8 MPa. This test ensured the vessel's integrity and proper sealing through the connection between the top lid and the cylinder, and the connections in the top lid. Afterwards, a hydrostastic test was performed, which reached the pressure of 15.0 MPa. Once again, mechanical integrity of the system was ensured with this test.

Focusing now on the temperature control of the experimental apparatus, the vessel was surrounded by a polyvinyl chloride container filled with a mixture of water and ethilenoglycol. This container was connected to an ultrathermostatic bath, with a tank volume of 11 L and operating temperatures between -20 °C and 120 °C. The ultrathermostatic bath was capable of pumping water to the container, however it was not capable of pumping it back from it. To solve this problem, the container, with the vessel inside it, was elevated 55 cm from the ground level, so the water would return to the bath by gravity. Figure 3.4 presents a picture of the ultrathermostatic bath and the hoses connecting it to the PVC container inside of a metallic structure in which the experimental apparatus was set. This ultrathermostatic bath was used to control the temperature inside the vessel.

Figure 3.4 – Thermostatic bath and metal structure of the experimental setup

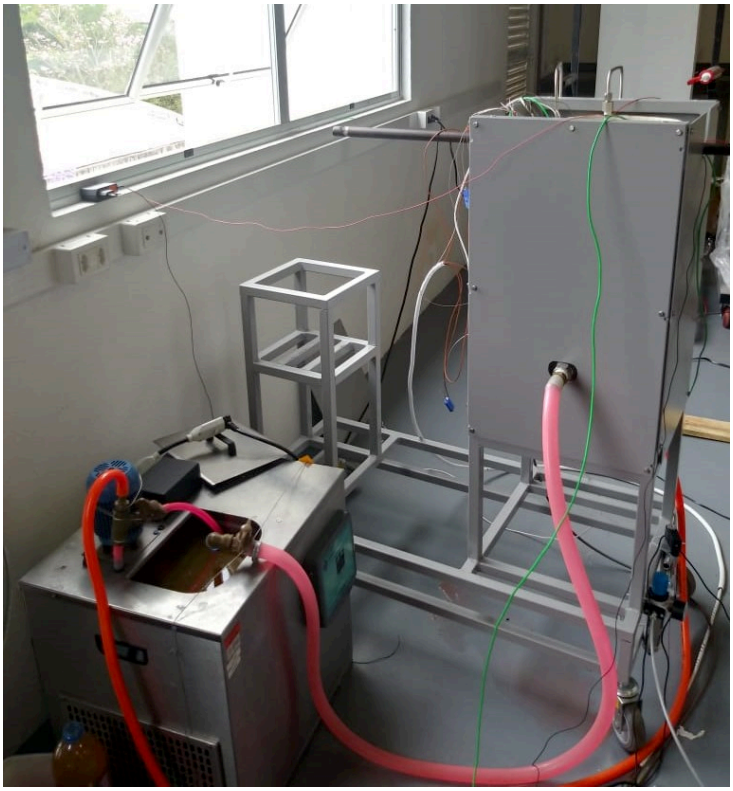

It still remains to be explained about the data of the experiments, which were acquired by the Data Aquisition System (DAQ) from National Instruments™, Figure 3.5 presents the schematics of the experimental apparatus, showing all the components described in this Section and how they are connected. The water circuitry, which is composed by the ultrathermostatic bath and the polyvinyl chloride container; the power circuitry is assembled by the power source connected to the electrodes, which dissipates power through the wire; the data acquisition circuitry, which stores the temperature, voltage, current, and pressure data; and the CO_2 circuitry, which contains the valves and connections between the CO_2 cylinder, the vacuum pump, and the vessel. For safety during the operations, the tests were run remotely. The next Section describes the experimental approach followed through them.

3.2 EXPERIMENTAL PROCEDURES

The experimental procedure is divided into two main steps: (a) feeding the carbon dioxide into the pressure vessel and reaching the desired pressure and temperature levels to run the tests; (b) actually running the tests, measuring the power released through the wire, in order to evaluate the convective heat transfer coefficient and calculate the thermal energy stored. Both steps will be explained in the following subsections.

Figure 3.5 – Schematics of the experimental setup

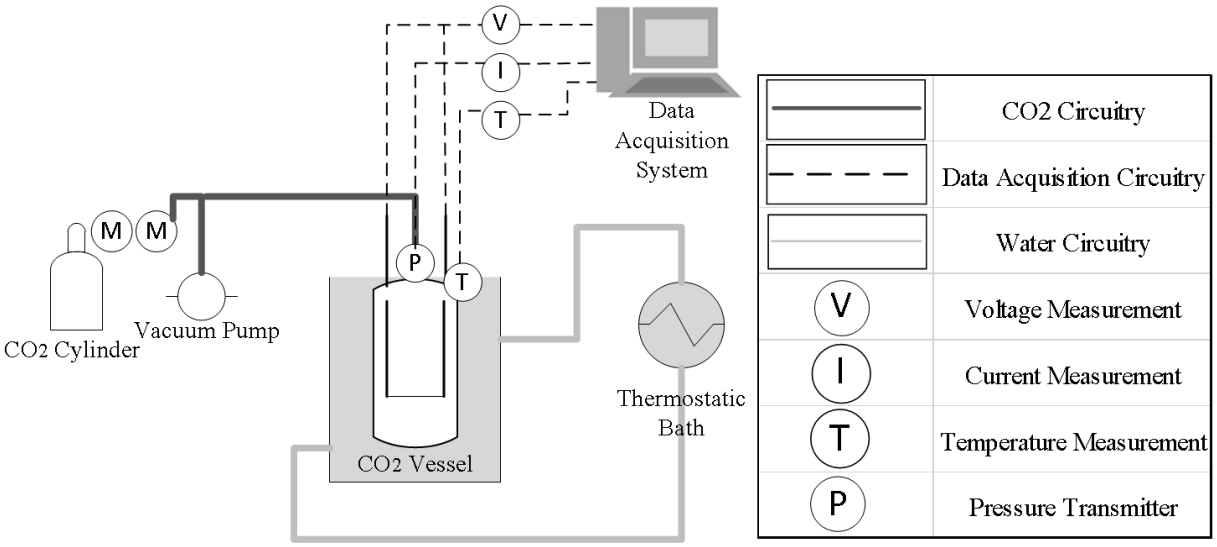

3.2.1 CO_2 Circuit Operation

There was a limitation concerning the initial pressure of CO_2 to be fed to the vessel, since the CO_2 cylinder presents a maximum pressure of 5.8 MPa while the pressure regulator guarantees an output pressure of 5.3 MPa for this input, which was the maximum initial pressure of the vessel. Because of this, before opening the carbon dioxide feeding valve the temperature of the vessel was lowered using the ultrathermostatic bath. During this procedure, the vacuum pump worked to make vacuum in the vessel. Once at a lower temperature, a higher amount of CO_2 compared to the amount fed at higher temperatures was fed to the vase in the output pressure of the pressure regulator. Then, when increasing its temperature to the desired operating temperature, the pressure inside the vessel also increased until reaching the desired supercritical values. This entire process took between five and six hours to be completed. As already mentioned, if the pressure of the vessel needed to be reduced, the pneumatic ball valve was partially opened to release CO_2 to the atmosphere. Figure 3.6 presents a schematic of the carbon dioxide circuit, with all the connections and valves used. The rectangle containing most of the connections and valves is a representation of the valves board shown previously in Figure 3.3.

Besides the pneumatic valve already discussed, the CO_2 circuitry presented other four valves, all numbered in Figure 3.6, being 1) the pneumatic ball valve. The other valves could open and shut the paths to 2) a hoose that shortened the path between the vacuum pump and the vessel, opened when the vacuum pump was operating; 3) the CO_2 circuitry, the vessel and the vacuum pump, also opened when the vacuum pump was operating; 4) the CO_2 circuitry, the vessel and the atmosphere, opened when in need to release CO_2 from the vessel or from the circuitry; and 5) the circuitry and the CO_2 cylinder, opened only when feeding CO_2 to the vessel. The operation of the systems goes

Figure 3.6 – Schematics of the CO_2 circuitry

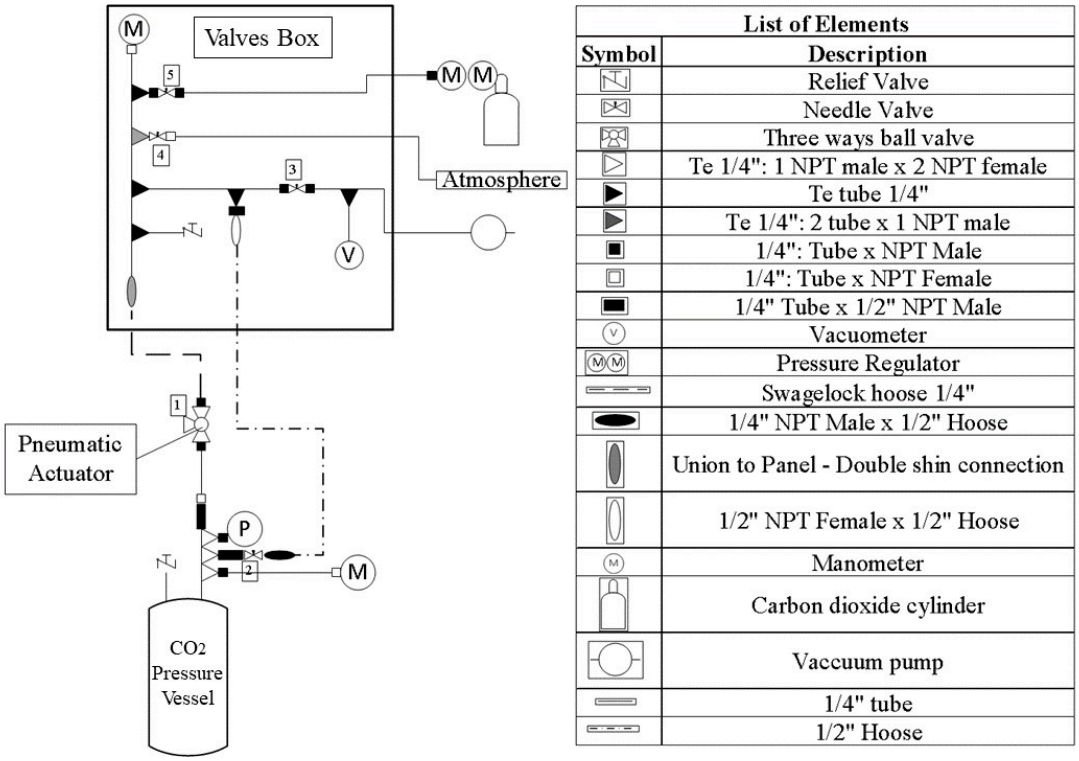

as summarized on Table 3.1, showing which valves are opened and closed and when to operate them in each step of the experimental procedure. After the CO_2 feeding and reached the desired conditions of temperature and pressure the tests could be executed. These will be described in the following Subsection.

3.2.2 Testing Procedure

The execution of the tests consisted on dissipating power through the wire and measuring both the voltage and current passing through it, its temperature and the temperature and pressure of the s-CO_2. A scheme of the power circuitry of the experiment is presented in Figure 3.7. The two electrodes were connected to the wire and to the power supply. The voltage drop of the wire was measured directly by the voltage module of the DAQ system, being the differential voltage between the two electrodes. However, the voltage module only measures voltages up to 10 V in each channel, and the maximum voltage desired to be given by the power source was 30 V. In order to enable the assessment of the voltage applied into the electrodes in any operating condition, a voltage divisor consisting of three 180 kΩ resistors in series was connected in parallel with the electrodes. Hence, the voltage divisor and the electrodes were both in the same voltage potential. The voltage drop in each of the resistors was evaluated separately, being the voltage applied in the electrodes the sum of the three voltages measured, ensuring that even for 30 V the voltage drop in each resistor would not be higher than 10 V.

Another important aspect to measure the power dissipated by the wire is to assess

Table 3.1 – Valves operation for CO_2 charging and discharging on/off vessel during the experiment. Source: Developed by the author

	Valve 1	**Valve 2**	**Valve 3**	**Valve 4**	**Valve 5**
Start Procedure	Closed	Closed	Closed	Closed	Closed
Open vacuum pump valves	Open	Open	Open	Closed	Closed
Turn on vacuum pump	Opened	Opened	Opened	Closed	Closed
Turn off vacuum pump when vacuum condition is reached	Opened	Opened	Opened	Closed	Closed
Turn off vacuum pump valves	Close	Close	Close	Closed	Closed
Lower temperature of vessel with thermostatic bath until desired CO_2 loading temperature	Closed	Closed	Closed	Closed	Closed
Open CO_2 valves	Open	Closed	Closed	Closed	Open
Turn on CO_2 pressure regulator in the desired loading pressure	Opened	Closed	Closed	Closed	Opened
Wait for pressure of the vessel to estabilize	Opened	Closed	Closed	Closed	Opened
Close pressure regulator and CO_2 valves	Close	Closed	Closed	Closed	Close
Increase temperature of the vessel with thermostatic bath to desired mixture temperature to run the experiment	Closed	Closed	Closed	Closed	Closed
To unload the CO_2, or to release pressure, open valves to atmosphere	Open	Closed	Closed	Open	Closed

the current passing through it. In this sense, a shunt resistor of 0.02 Ω was used to measure the current of the system through its voltage drop, also measured by a differential connection in the data acquisition system, using Ohm's Law, (Equation 3.1), where I_{wire} is the current passing through the wire, V_{shunt} is the voltage drop of the shunt resistor and R_{shunt} is the shunt's resistance. The equivalent resistance of the three resistors in parallel with the electrodes, which was used to measure the voltage applied into them, is so elevated compared to the branch of the circuitry of the electrodes and the wire that it is acceptable to assume that the current passing through the voltage divisor is nearly zero. Thus, it is safe to consider that the current passing through the wire is the same

Figure 3.7 – Schematics of the power circuitry of the experimental apparatus.

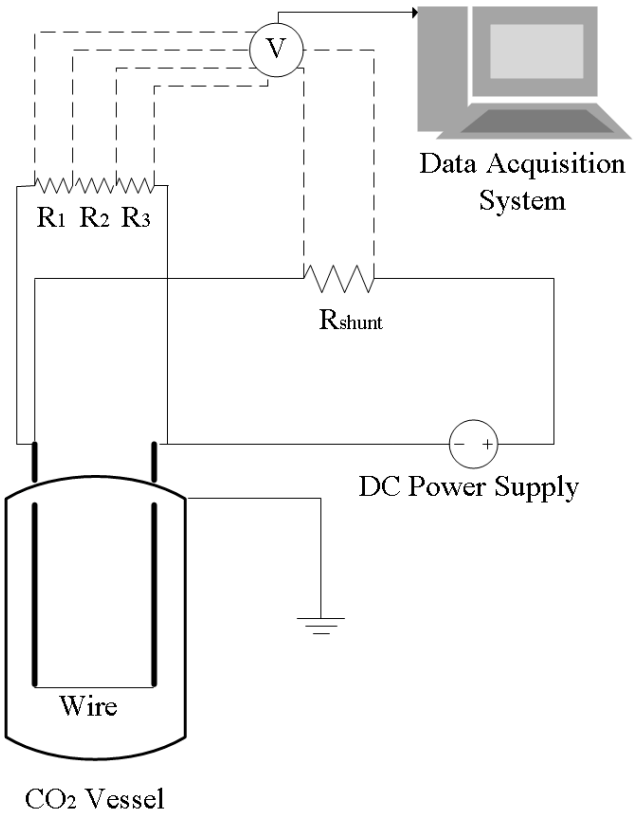

measured by the shunt resistor.

$$I_{\text{wire}} = \frac{V_{\text{shunt}}}{R_{\text{shunt}}} \tag{3.1}$$

Three current levels were set in the power source during the experiments: 1.5 A, 7.7 A and 10.0 A. These currents were chosen trying to ensure that the wire would not present temperatures much above 100 °C, because the thermocouples calibration, presented in Appendix B, was performed only until 90 °C. Hence, after this temperature the uncertainty in the temperatures measurements could increase. Table 3.2 presents the uncertainty analysis of the current measurements for the three current levels used in the experiments, following the methodology proposed by JCGM et al. (2008), as explained in Appendix C. The resistance of the shunt resistor was chosen to ensure that, for a current of 0.1 A, the voltage drop through it was 2 mV, equal to the uncertainty of the voltage module. Consequently, it was acceptable to work with currents higher than 0.1 A concerning the uncertainty measurement of the current. For higher currents, lower uncertainties related to the shunt voltage measurement are achieved.

After assessing the voltage drop through the wire and the current passing through it, the power dissipated by the wire, and its heat rate, q_{wire}, is calculated through Equation 3.2. The test was run dissipating three different heat fluxes through the wire (i.e, 1.2 W, 30.5 W and 53.0 W). Experimentally, it is easier to maintain the heat flux constant than

Table 3.2 – Uncertainty analysis for current measurement

Uncertainty	Source	1.5 A	7.7 A	10.0 A
Type A	Repeatability	0.01 %	0.003 %	0.002 %
Type B	Shunt Voltage	0.11 %	0.003 %	0.001 %
	Shunt Resistance		0.5 %	
u_{comb}		0.51 %	0.50 %	0.50 %
U		1.02 %	1.00 %	1.00 %

the temperature of the wire, which is the reason for the tests had been run maintaining the currents and the fluxes constant. A higher heat flux means a higher temperature difference between the wire and the fluid, since the wire's temperature increases with the current. Table 3.3 presents the uncertainty analysis for the three power levels dissipated by the wire, showing the influence of the voltage and current uncertainties for each level of power dissipated.

$$q_{\text{wire}} = V_{\text{wire}} \times I_{\text{wire}} \tag{3.2}$$

Table 3.3 – Uncertainty analysis for power measurement

	Source	1.2 W	30.5 W	53.0 W
Type A	Repeatability	0.0005 %	0.0008 %	0.0005 %
Type B	Wire Voltage	0.128%	0.05 %	0.05 %
	Wire Current	1.02 %	1.00 %	1.00 %
u_{comb}		0.28 %	0.06 %	0.05 %
U		0.57 %	0.11 %	0.10 %

The stationary condition for the experiments was reached when the thermocouples' temperature measurement stopped increasing. After acquiring data for the heat flux of 53.0 W for one hour, which was the flux with longer transient, and realizing that the system reached stationary condition, after 20 minutes for this flux, the data acquisition for each power dissipated was taken as shown in Table 3.4. This ensured that the transient data would be stored for the TES study, and that at least 10 minutes of data in stationary condition would be taken for the heat transfer coefficient evaluation. Once the data was acquired for the three fluxes and three repeatability tests were run for each flux in a given temperature and pressure condition, the CO_2 valve was activated to release an amount of gas to the atmosphere, decreasing the pressure inside the vessel so the test could be repeated for the same temperature, but at a lower pressure condition.

3.3 PARAMETERS EVALUATED

The parameters that were evaluated with the experiments were the convective heat transfer coefficient for natural convection and the energy density of s-CO_2, because these

Table 3.4 – Approximated time to reach stationary conditions in each test and duration of tests for each current used

Power [W]	Time to reach stationary condition	Time in which data was acquired
1.2	30 seconds	15 minutes
30.5	7 minutes	20 minutes
53.0	20 minutes	30 minutes

are two key parameters to evaluate a material as TES medium. The process to evaluate them will be discussed in the following subsections.

3.3.1 Convective Heat Transfer Coefficient

Assuming all the power that goes through the wire is dissipated in the form of thermal energy, it is possible to calculate the heat transfer coefficient using Equation 3.3, where A_s is the superficial area of the wire, measured manually before each experiment. The tests were run for two different temperatures, i.e., $1.05 \times T_c = 32.6$ °C and $1.1 \times T_c = 34.2$ °C. The pressures used for each temperature were chosen based on the c_v behavior in Figure 2.1, trying to reach pressures where the c_v was both increasing and decreasing and verifying its effect on the heat transfer coefficient. Table 3.5 presents the tests run and the conditions of each experiment.

$$h = \frac{q_{\text{wire}}}{A_s(T_{\text{wire}} - T_{\text{bulk}})} \tag{3.3}$$

Table 3.5 – Conditions of temperatures and pressures for each test run

Temperature [°C]	1.2 W	30.5 W	53.0 W
	Pressures tested [MPa]		
32.60	7.45	8.20	8.20
	7.54	8.01	8.00
	7.59	7.86	7.92
	7.67	7.81	7.80
	7.79	7.63	7.62
	7.89	7.52	7.60
	8.02	7.50	7.54
	8.21		
34.20	7.74	7.75	7.79
	7.80	7.81	7.87
	8.01	8.04	8.09
	8.18	8.25	8.30
	8.34	8.45	8.47
	8.62	8.68	8.85

Tables 3.6 and 3.7 present the uncertainty analysis for the convective heat transfer coefficient in the conditions the experiments were executed. The uncertainty of the

temperature measurement depends on the temperature difference between the wire and the fluid; the higher the temperature difference is, smaller is the uncertainty. Because the experiments were run maintaining the heat fluxes constant, h variation was acknowledged by the variation of ΔT, which means that the uncertainty analysis of h must be assessed for each value of ΔT obtained in each test run, as seen in the before mentioned tables.

Figure 3.8 presents a flowchart showing the procedures for the tests execution.

Figure 3.8 – Flowchart of the experimental procedure

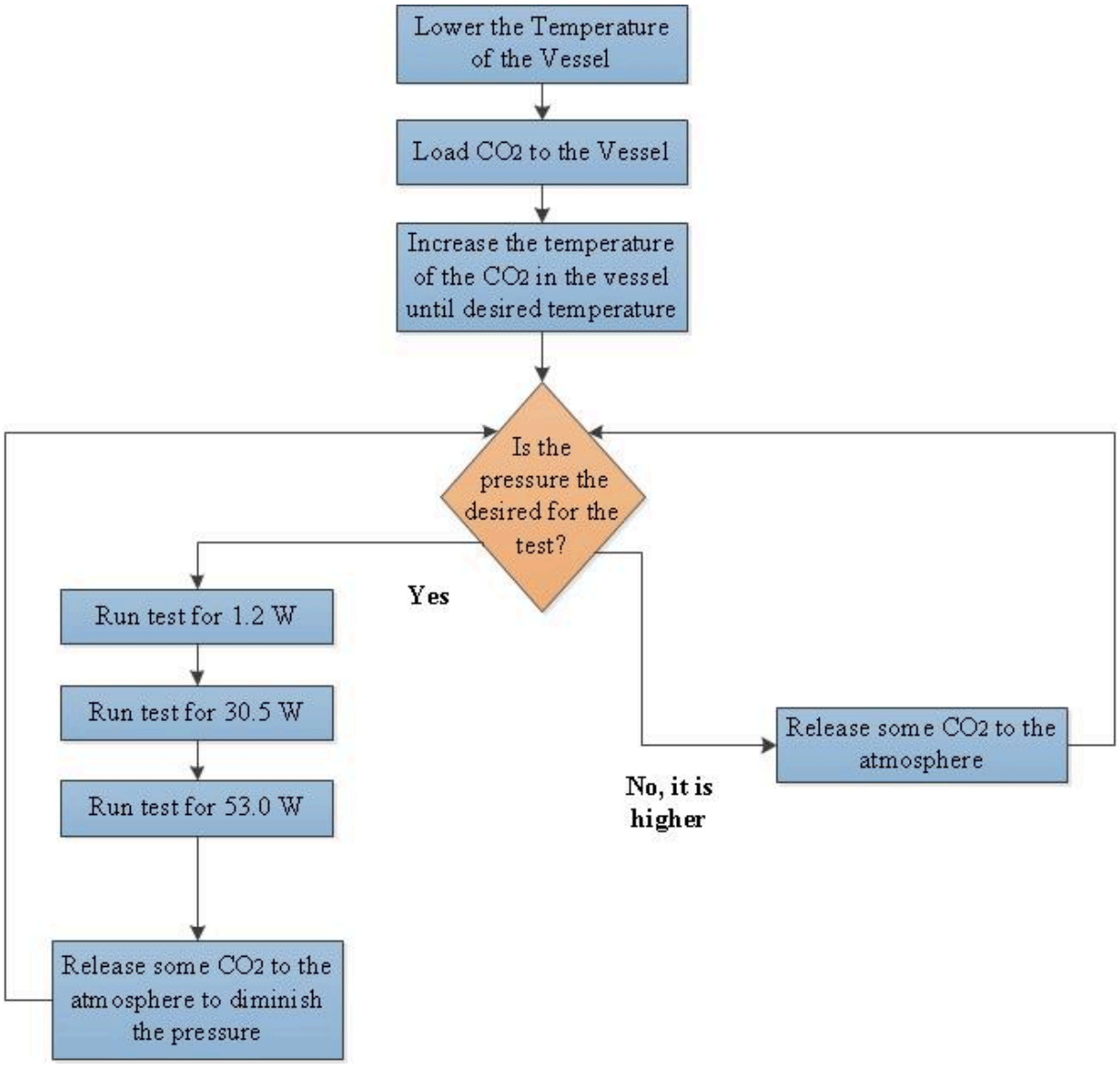

As seen in Figure 3.8, for each bulk temperature evaluated, the procedure was to reach the maximum pressure tested, run the experiments for each power levels, then release an amount of CO_2 to the atmosphere in order to decrease the pressure of the vessel. Once in a lower pressure, run the tests for the three power levels chosen and repeat the procedure for all pressures tested. This was the procedure for both the convective heat transfer study and for the energy density. The three power levels were chosen because

the two smaller of 1.2 W and 30.5W presented temperature differences between the wire and the bulk temperature of the fluid that were in the range of calibrated temperatures, which was important for the convective heat transfer study. In this manner, two fluxes could be compared for the studies concerning the convective heat transfer phenomena with supercritical fluids. The larger flux studied of 53.0 W presented a wire temperature much above the calibration limits, so it was not advisable to use these results for the convective heat transfer coefficient study. However, the flux of 1.2 W did not present enough bulk temperature variation as to use these results for the energy stored study. Hence, using these three fluxes it was possible to use two of them for each study: 1.2 and 30.5 W to the convective heat transfer study, and 30.5 and 53.0 W to the energy density stored study.

Table 3.6 – Uncertainty analysis for convective heat transfer coefficient for T_{bulk}=32.6 °C and q = 1.2, 30.5 and 53.0 W

T_{bulk} 32.6 °C, q = 1.2 W									
Uncertainty Type		**Source**	**ΔT [°C]**						
			1.49	**1.41**	**1.10**	**0.96**	**0.57**	**0.52**	**0.84**	**1.54**
A	h	[W/m²/K]	6.20	14.75	30.10	18.67	67.31	94.55	211.91	54.83
B	T	[°C]	0.02							
	q	[%]	0.57							
$\mathbf{u}_{\text{comb}}$		**[%]**	1.47	1.60	2.05	2.19	3.66	4.04	4.83	2.34
U		**[%]**	2.95	3.19	4.09	4.39	7.32	8.09	9.66	4.67
T_{bulk} 32.6 °C, q = 30.5 W									
Uncertainty Type		**Source**	**ΔT [°C]**						
			24.78	**42.27**	**42.81**	**45.19**	**54.06**	**52.07**	**68.50**	
A	h	[W/m²/K]	72.51	11.67	1.49	14.53	5.78	26.61	72.80	
B	T	[°C]	0.02							
	q	[%]	0.11							
$\mathbf{u}_{\text{comb}}$		**[%]**	0.014	0.002	0.0003	0.003	0.001	0.005	0.013	
U		**[%]**	0.029	0.004	0.001	0.005	0.002	0.010	0.027	
T_{bulk} 32.6 °C, q = 53.0 W									
Uncertainty Type		**Source**	**ΔT [°C]**						
			36.87	**81.94**	**105.17**	**103.27**	**105.17**	**94.78**	**136.95**	
A	h	[W/m²/K]	11.28	52.91	19.54	33.71	7.11	18.41	89.60	
B	T	[°C]	0.02							
	q	[%]	0.10							
$\mathbf{u}_{\text{comb}}$		**[%]**	0.77	2.86	0.94	1.65	0.33	0.77	1.78	
U		**[%]**	1.54	5.73	1.88	3.31	0.65	1.54	3.55	

Table 3.7 – Uncertainty analysis for convective heat transfer coefficient for T_{bulk}=34.2 °C and q = 1.2, 30.5 and 53.0 W

T_{bulk} 34.2 °C, q = 1.2 W								
Uncertainty Type		**Source**	**ΔT [°C]**					
			1.29	**1.14**	**0.95**	**1.22**	**1.43**	**1.69**
A	h	[W/m²/K]	28.08	58.20	75.58	44.86	64.42	16.41
B	T	[°C]	0.02					
	q	[%]	0.57					
$\mathbf{u}_{\text{comb}}$		**[%]**	1.84	2.32	2.71	2.10	2.53	1.45
U		**[%]**	3.67	4.65	5.43	4.21	5.06	2.89
T_{bulk} 34.2 °C, q = 30.5 W								
Uncertainty Type		**Source**	**ΔT [°C]**					
			72.29	**64.19**	**49.14**	**44.38**	**40.21**	**35.15**
A	h	[W/m²/K]	46.25	2.20	0.84	35.60	46.43	19.14
B	T	[°C]	0.02					
	q	[%]	0.11					
$\mathbf{u}_{\text{comb}}$		**[%]**	2.63	0.12	0.05	1.28	1.53	0.56
U		**[%]**	5.26	0.23	0.11	2.56	3.07	1.12
T_{bulk} 34.2 °C, q = 53.0 W								
Uncertainty Type		**Source**	**ΔT [°C]**					
			131.88	**118.94**	**96.68**	**94.58**	**93.05**	**88.02**
A	h	[W/m²/K]	102.84	65.76	31.98	61.37	3.73	26.23
B	T	[°C]	0.02					
	q	[%]	0.10					
$\mathbf{u}_{\text{comb}}$		**[%]**	6.43	3.70	1.45	2.73	0.20	1.10
U		**[%]**	12.87	7.40	2.89	5.46	0.39	2.19

3.3.2 Energy Density

As already mentioned, the energy density is an important characteristic of the material considered to be used as TES medium. The energy provided to the carbon dioxide, Q_{wire} is given by Equation 3.4, where the power dissipated through the wire is multiplied by the time of the test (Δt) and divided by the volume of CO_2, (V_o). Tables 3.8 and 3.9 present the uncertainty analysis made for the measurements of the energy dissipated by the wire with the two bulk temperatures studied in the experiments. Again, this assessment had to be done for each ΔT achieved in each test.

$$Q_{\text{wire}} = \frac{\sum V_{\text{wire}} I_{\text{wire}} \Delta t}{V_o} \tag{3.4}$$

Table 3.8 – Uncertainty analysis for the measurement of the thermal energy dissipated by the wire at bulk temperature of 32.6 °C.

T_{bulk} **32.6 °C,** q **= 30.5 W**									
Uncertainty Type	**Source**		**ΔT [°C]**						
			0.41	**0.38**	**0.60**	**0.50**	**0.50**	**0.49**	**0.56**
A	Q_{wire}	[J/m³]	482.62	535.13	475.39	1216.33	319.89	32.39	78.80
B	T	[°C]				0.02			
	q	[%]				0.11			
$\mathbf{u}_{\text{comb}}$		**[%]**	12.53	9.31	9.12	7.53	6.61	6.55	5.34
U		**[%]**	25.06	18.62	18.24	15.07	13.22	13.10	10.69
T_{bulk} **32.6 °C,** q **= 53.0 W**									
Uncertainty Type	**Source**		**ΔT [°C]**						
			0.84	**0.79**	**0.69**	**1.15**	**0.94**	**1.00**	**0.94**
A	Q_{wire}	[J/m³]	121.66	1115.91	145.67	499.39	98.54	1314.73	2277.18
B	T	[°C]				0.02			
	q	[%]				0.10			
$\mathbf{u}_{\text{comb}}$		**[%]**	7.22	5.22	4.66	3.08	3.43	3.76	5.01
U		**[%]**	14.44	10.44	9.31	6.17	6.85	7.53	10.02

Table 3.9 – Uncertainty analysis for the measurement of the thermal energy dissipated by the wire at bulk temperature of 34.2 °C.

T_{bulk} 34.2 °C, q = 30.5 W								
Uncertainty Type	**Source**		**ΔT [°C]**					
			0.41	**0.46**	**0.59**	**0.68**	**0.73**	**0.61**
A	Q_{wire}	[J/m³]	401.67	826.80	25.71	21.03	35.46	347.86
B	T	[°C]	0.02					
	q	[%]	0.11					
$\mathbf{u}_{\text{comb}}$		**[%]**	11.71	8.37	6.03	4.99	4.44	5.06
U		**[%]**	23.41	16.73	12.05	9.97	8.88	10.13
T_{bulk} 34.2 °C, q = 53.0 W								
Uncertainty Type	**Source**		**ΔT [°C]**					
			0.91	**0.79**	**1.02**	**1.09**	**0.98**	**1.35**
A	Q_{wire}	[J/m³]	345.48	244.19	179.53	580.24	105.13	12.99
B	T	[°C]	0.02					
	q	[%]	0.10					
$\mathbf{u}_{\text{comb}}$		**[%]**	5.74	5.21	3.57	3.04	3.26	2.31
U		**[%]**	11.49	10.42	7.14	6.08	6.52	4.62

The initial idea was to measure energy lost, Q_{lost} as it is measured and calculated in the experimental works from Subsection 2.3.2. Afterwards an energy balance would be performed, as shown in Equation 3.5, to calculate the energy stored Q_{stored}, comparing it with the theoretical stored energy for the initial and final conditions reached in the experiment. However, the power dissipated by the wire is so small and the temperature variation reached in the experiments was so modest that the options considered to evaluate the density of thermal energy lost would present an uncertainty much higher than the value measured.

$$Q_{\text{stored}} = Q_{\text{wire}} - Q_{\text{lost}} \tag{3.5}$$

Along these lines, the measurements of temperature and pressure of the CO_2 are more reliable than the assessment of the thermal energy lost in the conditions the experiments were executed. Because of this, it was preferred to use these data and use CoolProp, (BELL et al., 2014) to evaluate the density, (ρ), and the internal energy, (e), of the fluid at initial and final conditions to calculate the density of stored thermal energy using Equation 3.6. After evaluating Q_{stored}, the density of thermal energy lost can be assessed by Equation 3.5, as $Q_{\text{lost}} = Q_{\text{wire}} - Q_{\text{stored}}$. The uncertainty analysis for the thermal energy stored measurements are presented in Tables 3.10 and 3.11. These analyses were determined considering the uncertainties present in the temperature and pressure measurement, which would entail in uncertainties in the thermophysical properties from Equation 3.6 evaluated with CoolProp.

$$Q_{\text{stored}} = \rho_{\text{initial}}(e_{\text{final}} - e_{\text{initial}}) \tag{3.6}$$

Table 3.10 – Uncertainty analysis for the measurement of the thermal energy stored by the s-CO_2 at bulk temperature of 32.6 °C.

T_{bulk} 32.6 °C, q = 30.5 W									
Uncertainty Type	**Source**		**ΔT [°C]**						
			0.41	**0.38**	**0.60**	**0.50**	**0.50**	**0.49**	**0.56**
A	Q_{stored}	[J/m³]	54.65	134.64	122.06	50.09	67.54	45.05	45.08
B	T	[°C]	0.02						
	q	[%]	0.11						
$\mathbf{u_{comb}}$		**[%]**	14.32	17.47	13.68	6.22	7.97	7.26	6.00
U		**[%]**	28.65	34.93	27.36	12.44	15.94	14.52	11.99
T_{bulk} 32.6 °C, q = 53.0 W									
Uncertainty Type	**Source**		**ΔT [°C]**						
			0.84	**0.79**	**0.69**	**1.15**	**0.94**	**1.00**	**0.94**
A	Q_{stored}	[J/m³]	140.02	87.23	362.32	105.58	33.21	52.84	29.91
B	T	[°C]	0.02						
	q	[%]	0.10						
$\mathbf{u_{comb}}$		**[%]**	11.90	6.70	20.01	4.78	3.56	3.59	3.43
U		**[%]**	23.80	13.41	40.02	9.56	7.11	7.18	6.86

Table 3.11 – Uncertainty analysis for the measurement of the thermal energy stored by the s-CO_2 at bulk temperature of 34.2 °C.

T_{bulk} 34.2 °C, q = 30.5 W								
Uncertainty Type	**Source**		**ΔT [°C]**					
			0.41	**0.46**	**0.59**	**0.68**	**0.73**	**0.49**
A	Q_{stored}	[J/m³]	19.05	106.56	85.43	75.80	83.84	177.33
B	T	[°C]	0.02					
	q	[%]	0.11					
$\mathbf{u_{comb}}$		**[%]**	11.92	13.52	7.95	6.35	5.96	11.20
U		**[%]**	23.85	27.03	15.90	12.71	11.93	22.40
T_{bulk} 34.2 °C, q = 53.0 W								
Uncertainty Type	**Source**		**ΔT [°C]**					
			0.91	**0.79**	**1.02**	**1.09**	**0.98**	**1.35**
A	Q_{stored}	[J/m³]	85.81	198.45	54.31	469.12	24.82	72.37
B	T	[°C]	0.02					
	q	[%]	0.10					
$\mathbf{u_{comb}}$		**[%]**	7.48	11.55	4.02	15.32	3.37	2.96
U		**[%]**	14.96	23.10	8.05	30.64	6.74	5.91

3.4 VALIDATION OF THE EXPERIMENTAL APPARATUS

To validate the experimental apparatus, the experiment was run using air at atmospheric pressure as working fluid. The experiment was performed at a bulk temperature of T_{bulk} = 20.0 °C. Increasing the power dissipated through the wire and, consequently, its

temperature, it was possible to compare the heat transfer coefficient obtained experimentally with experimental correlations found in the literature. The first correlation was the one proposed by Morgan (1975), which is presented in Equation 3.7 and uses coefficient C = 1.02 and n = 0.148 for Rayleighs in the order of 10^{-2} to 10^{2}. This correlation was chosen because for the conditions tested in air, the Rayleighs found were on the order of 10^{-1} to 10^{0}, depending on the ΔTs tested, so the correlation proposed by Morgan (1975) fits well in the range of Rayleighs found.

$$\overline{Nu_{\mathrm{D}}} = \quad CRa_{\mathrm{D}}^{n} \tag{3.7}$$

The second correlation was proposed by (CHAND; VIR, 1979 apud BOSWORTH, 1944) and is presented by Equation 3.8, which is valid for both laminar and turbulent Rayleighs. The correlations provide the average Nusselt number. From Equation 2.1 it is possible to calculate the heat transfer coefficient and compare it to the experimental results.

$$\overline{Nu_{\mathrm{D}}}^{0.5} = 0.63 + 0.35(Gr.Pr)^{1/6} \tag{3.8}$$

In both correlations the diameter dimension is used in the Nu_{D} calculation and in the calculation of the superficial area of heat transfer for the experimental convective heat transfer coefficient. In the calculation of the superficial area, both the superficial area of the tube with the thermocouple and of the wire were taken into account. For the diameter used in the correlations, an effective heat transfer coefficient, h_{average}, was used as a weighted average between the wire diameter and its length and the tube diameter and the length it covers the wire, represented by Figure 3.9. In this image it is possible to verify that the diameters of the wire and of the tube are different and to see how their lengths were evaluated for the calculation of Equation 3.9, showing how the average coefficient was calculated. In Equation 3.9, L_{wire} is the total length of the wire and L_{tube} is the length of the wire covered by the tube, h_{Dwire} is the convective heat transfer coefficient calculated using the wire diameter and h_{Dtube} is the coefficient calculated using the tube diameter. To guarantee that there was repeatability in the results, the tests with air were executed five times for the conditions presented on Table 3.12.

$$\overline{h}_{\mathrm{average}} = \left(\frac{L_{\mathrm{wire}} - L_{\mathrm{tube}}}{L_{\mathrm{wire}}}\right) h_{\mathrm{Dwire}} + \left(\frac{L_{\mathrm{tube}}}{L_{\mathrm{wire}}}\right) h_{\mathrm{Dtube}} \tag{3.9}$$

The results of the tests and their comparison with the correlations are presented in Figure 3.10. The colored circles present the experimental results obtained during these tests, while the black and grey circles present the results obtained for the same conditions using the correlations of Morgan (1975) and Chand & Vir (1979), respectively. The continuous black line and the dashed line present the quadratic integration of the values for the correlations, showing the trend these values display. It is noticeable in Figure 3.10

Figure 3.9 – Scheme of the wire and of the tube lengths used for the convective heat trasnfer coefficient calculation

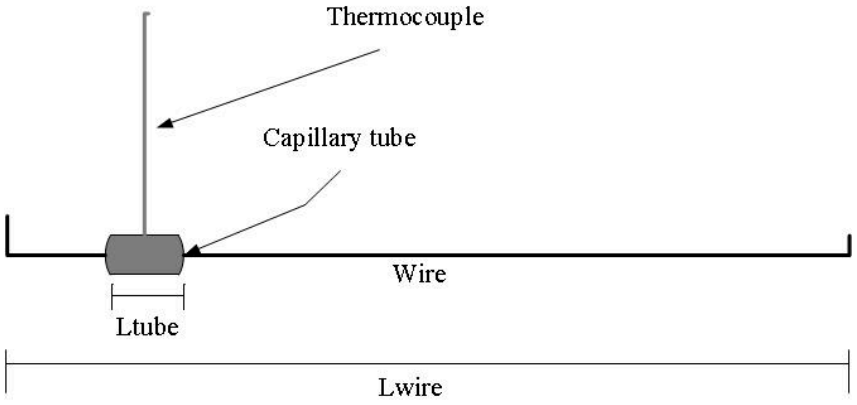

Table 3.12 – Experimental conditions for validation tests using air.

i [A]	v [V]	T_{bulk} [°C]	T_{wire} [°C]
0.305	0.225	20.02	24.67
0.600	0.443	20.02	36.02
0.900	0.664	20.02	52.22
1.200	0.888	20.02	72.33
1.501	1.112	20.03	95.56
1.800	1.336	20.03	121.32
2.100	1.561	20.03	149.06

that there is repeatability in the results between the tests, being the standard deviation between the five measurements of the convective heat transfer coefficient for each ΔT presented in Table 3.13. Another aspect that can be noticed is that the trends presented by the correlations are noticeable in the tests results, where the convective heat transfer coefficient increases with the rise of the temperature difference between the wire and the fluid. However, for smaller temperature differences, the experimental results are closer to the trends presented by the correlations. One possible explanation for this behavior is that the thermocouples calibration was made until 90 °C, as it is highlighted in Figure 3.10. Hence, for higher temperatures differences, when the wire temperature is above this maximum value, the uncertainty in the wire's temperature measurement can be increased. Table 3.14 presents the uncertainty analysis for each measurement of the convective heat transfer coefficient in this validation experiment with air.

Table 3.15 present the comparisons between the results from the experiment and the correlations. It can be seen that for values where the wire temperature is under 90 °C, which was the highest temperature calibrated, the difference between the experimental result and the correlations is for the most part under 15%, which is in the uncertainty range for the correlations, validating these results. For wire temperatures over this upper limit of 90 °C, the difference goes a little higher, remaining under 20% for Morgan (1975) correlation, which can still be accepted as a good result. What can be noticed from both

Figure 3.10 – Comparison of tests using air with the correlations for natural convection around heated cylinders.

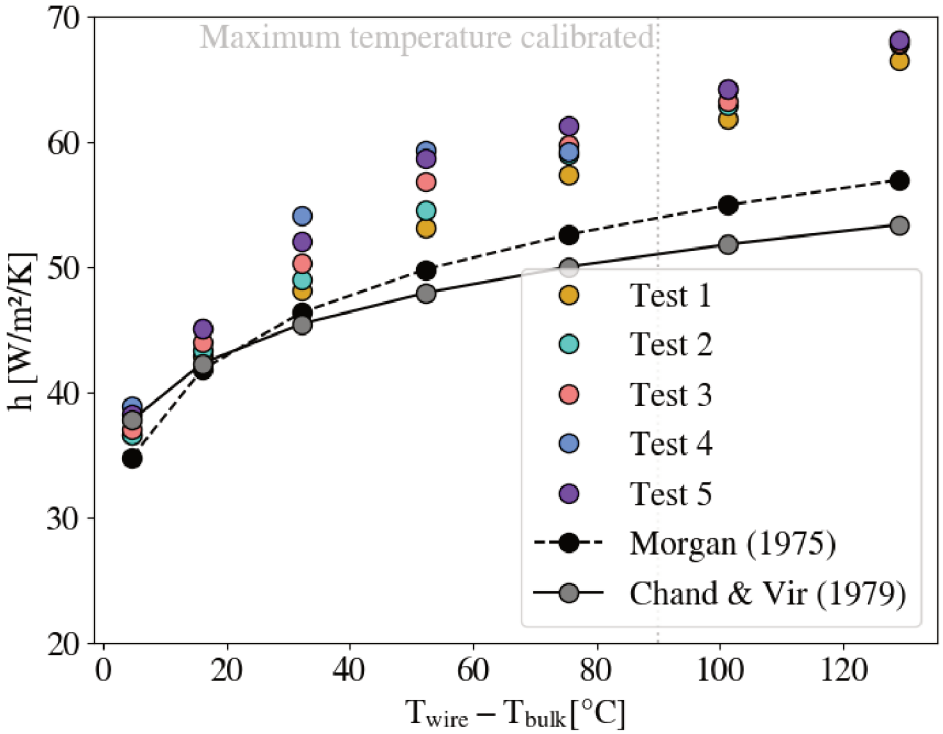

Table 3.13 – Standard deviation of tests with air at 20 °C and atmospheric pressure

ΔT [°C]	Standart Deviation [°C]	$h_{average}$ [W/m²/K]	Standart Deviation [W/m²/K]
4.67	0.04	37.49	1.06
16.02	0.03	44.09	1.00
32.22	0.06	50.72	2.40
52.33	0.03	56.49	2.63
75.56	0.05	59.33	1.42
101.32	0.03	63.29	0.99
129.06	0.03	67.70	0.67

Table 3.14 – Uncertainty analysis of convective heat transfer coefficient measurements in air

Uncertainty Type	Source	ΔT [°C]						
		4.67	16.02	32.22	52.33	75.56	101.32	129.06
A	h [W/m²/K]	0.11	0.10	0.24	0.26	0.14	0.10	0.07
B	T [°C]	0.02						
	q [%]	1.00	1.00	2.00	2.00	3.00	4.00	4.00
u_{comb} [%]		1.01	1.01	2.01	2.02	3.00	4.00	4.00
U [%]		2.02	2.02	4.02	4.02	6.00	8.00	8.00

Tables 3.13 and 3.15 is that both for the experimental results as for the the results obtained from the correlations, the value of the convective heat transfer coefficient increases with the rising of the temperature differences values. In fact, with the increase of the temperature differences between the wire and the bulk temperature of the fluid, the Rayleigh increases as well, passing for Rayleigh's in the order of 10^{-1} for ΔT of 4 °C to 10 °C for ΔT of 100 °C. This increase in the Rayleigh means the buoyancy effects are stronger for higher temperature differences, boosting the convective heat transfer phenomena.

Table 3.15 – Comparison between experimental results and correlations by Morgan (1975) and (CHAND; VIR, 1979 apud BOSWORTH, 1944)

ΔT [°C]	h_{average} [W/m²/K]	h_{Morgan} [W/m²/K]	Difference [%]	h_{Chand} [W/m²/K]	Difference [%]
4.67	37.49	34.84	-7.59	37.79	0.81
16.02	44.09	41.82	-5.43	42.32	-4.18
32.22	50.72	46.38	-9.36	45.47	-11.55
52.33	56.49	49.83	-13.37	47.95	-17.81
75.56	59.33	52.61	-12.78	50.03	-18.60
101.32	63.29	54.95	-15.17	51.81	-22.15
129.06	67.70	56.95	-18.87	53.38	-26.82

4 NUMERICAL METHODOLOGY

A steady-state study was developed computationally using COMSOL *Multiphysics*®, (COMSOL Inc, 2017), to evaluate the convective heat transfer coefficient of carbon dioxide at supercritical conditions, and will be described in Section 4.1, which presents the geometry, the governing equations of the physics of the problem, the boundary conditions and the mesh used in the simulation. Section 4.2 shows the mesh independence study. Section 4.3 presents the model validation and is followed by Section 4.4, which discusses some considerations about the model. At last, Section 4.5 shows the method followed to compare s-CO_2 with other fluids as TES mediums.

4.1 MODEL AND GEOMETRY

The steady-state model was developed to evaluate the natural convective heat transfer coefficient for several conditions using carbon dioxide at supercritical pressures and temperatures. A two-dimensional cut of the pressure vessel with a heated wire inside of it was modelled. The computational domain is presented in Figure 4.1. The domain consists on a horizontal heated wire fixed in a rectangular cavity full of carbon dioxide. The cavity is rectangular to represent a vertical cut in the real cylindrical pressure vessel of the experiment described in Chapter 3. Only half of the domain was modelled, due to symmetry conditions. A two-dimentional model was chosen because the length of the wire is immense compared to the wire's diameter. This makes the assumption of infinite length possible, justifying the 2D approach.

Figure 4.1 – Computational domain built in COMSOL

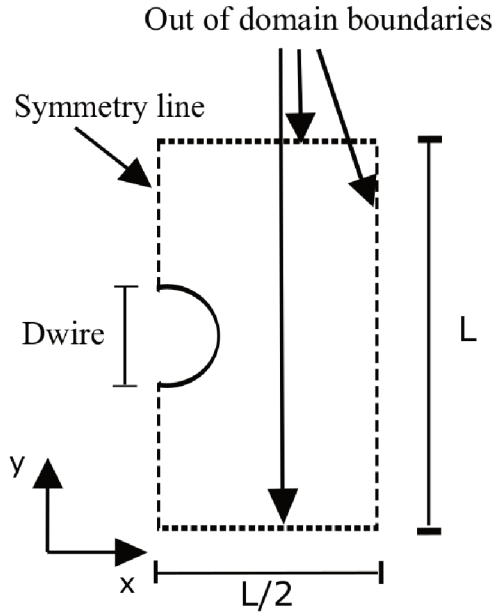

The assumptions made for this computational model were:

- Cartesian coordenates in two dimensions;
- Steady-state study;
- Fluid circulation caused by natural convection;
- Uniform temperatures distributed in the walls;
- Vertical cut in the middle of the wire and the vessel, symmetry between the two sides;
- Thermophysical properties of carbon dioxide as function of temperature evaluated with CoolProp, (BELL et al., 2014), for a given pressure.

Under the assumptions presented, the mass conservation equation, the Navier-Stokes or the momentum equation and the Energy Equation can be written as shown in Equations 4.1, 4.2 and 4.3 respectively, where $\mathbf{u}$ is the velocity field, $\mathbf{F}$ represent the tensional forces, μ is the dynamic viscosity, $\mathbf{I}$ is an unitary vector and $\boldsymbol{g}$ is the gravitational force. These governing equations are solved by COMSOL *Multiphysics*® using Finite Element Method (FEM).

$$\nabla \cdot (\rho \mathbf{u}) = 0 \tag{4.1}$$

$$\rho(\mathbf{u} \cdot \nabla \mathbf{u}) = \nabla \cdot \left[-\rho \mathbf{I} + \mu \left(\nabla \mathbf{u} + (\nabla \mathbf{u})^T \right) - \frac{2}{3} \mu \left(\nabla \cdot \mathbf{u} \right) \mathbf{I} \right] + \mathbf{F} + \rho \mathbf{g} \tag{4.2}$$

$$\rho c_p \mathbf{u} \cdot \nabla T + \nabla \cdot (-k \nabla T) = 0 \tag{4.3}$$

The boundary conditions defined for the model were as described. u and v are the velocities in the x and y directions; D_{wire} is the wire diameter and $\boldsymbol{q}$ is the heat flux.

Vertical axis (x = 0, 0≤y≤L):
$\boldsymbol{u}\cdot\mathbf{n}$=0 (Symmetry condition)
-$\mathbf{n}\cdot\boldsymbol{q}$=0 (Symmetry condition)
Inner radius (x, y = D_{wire}/2):
$v = u = 0$ (wall),
$T = T_{\text{wire}}$ (constant temperature)
The wall of the pressure vessel (0 ≤ x ≤ L/2, 0 ≤ y ≤ L):
$v = u = 0$
$T = T_{\text{bulk}}$
The point (x = L/2, y = L):
$P = P_o$

The initial conditions for the problem were defined as follow:

$v = u = 0$

$T = T_{\text{bulk}}$

$P = P_o$

A study to verify the influence of the length of the wall in comparison to the wire diameter was made in order to have a cavity big enough so the presence of the wall with boundary condition of T=T_{bulk} would not influence the heat transfer on the wire. The results for this investigation are shown in Figure 4.2, using carbon dioxide at 4.0 MPa and 31 °C, which is the value simulated with the smaller Rayleigh number. This condition was chosen for this analysis because of the study developed by Kuehn & Goldstein (1980), which shows that higher Rayleigh numbers result in the appearance of smaller free convection plumes. Because the thermal plumes are the region where the temperature of the fluid vary the most in natural convection, smaller plumes mean smaller wall lengths required to ensure there would be no influence of the wall in the natural convection phenomena. It can be observed in Figure 4.2 that the ratio between the length of the wall and the wire diameter for which the Nusselt number stops varying with the increase of the wall is 300. Nonetheless, it was too demanding of the computational resources available at the time to reach convergence using $L/D_{\text{wire}} = 300$. Since the difference between the Nusselt number using a wall 200 and 300 times the value of the wire diameter was 2%, as seen in Figure 4.2, and this was the condition with smaller Rayleigh number, which means the condition that demanded a larger wall length, the simulations were performed using a wall 200 times the wire diameter for all simulations of this work using CO_2. It is worth mentioning that the heat transfer equation used during this analysis to calculate the average Nusselt number is given by Equation 2.1 and the heat transfer coefficient is calculated by Equation 3.3, where the characteristical length D is D_{wire}.

After defining the length of the wall in the geometry built in the model, a mesh was created to perform the simulations. In this work, a triangular mesh was used, with finer elements very close to the heated cylinder and of the region where the thermal plume of natural convection is expected to occur. The thermal plume, according to Hernández (2015), is a pattern formed by the fluid, caused because of the heat source that increases the temperature of the fluid and consequently its buoyancy. The refinement of the mesh in this region was made to help in the convergence of the simulation since a higher gradient of temperature is expected, making this region the one with the most intense properties variation. The region of fluid further from the cylinder presents larger elements, since this is not the region of interest. An example of the used mesh is shown in Figure 4.3. The convergence study for the mesh and its convergence criteria will be presented in the following Section. However before this discussion it is still important to deliberate about the materials' thermophysical properties evaluation and the conditions of temperature and pressure for which the simulations were run.

Figure 4.2 – Influence of the length of the wall on Nusselt number

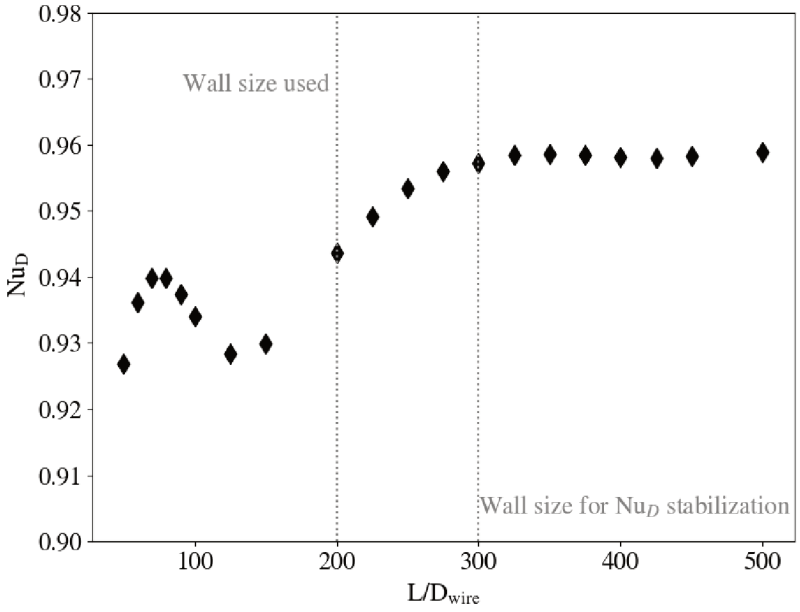

In this context, the evaluations of the thermophysical properties of the material were taken for carbon dioxide and were imported from CoolProp, (BELL et al., 2014), in tables for constant pressure P_o and temperatures varying from 16.85 °C to 476.85 °C in steps of 0.05°C. Interpolation of the properties were made for any temperature between two values set in the table. The properties imported were the dynamic viscosity μ, the ratio of specific heats γ, specific heat at constant pressure c_p, density ρ and thermal conductivity k. When linking the software with MATLAB™, the properties from CoolProp were imported automatically every time a new pressure for the simulation was evaluated.

Initially, the simulations were executed for conditions near the critical point of CO_2, from 26.85 °C until 76.85 °C, in steps of 5 °C, evaluating pressures from 8.0 to 35.0 MPa in ranges of 0.1 MPa. In all simulations the temperature differences were made for a first value of $\Delta Ts = T_{wire} - T_{bulk} = 0.5$ °C and then from of 5 to 60 ° C, in steps of 5 °C. Because these temperature values are low for CSP applications, simulations with higher bulk temperatures were executed. Temperatures from 226.85 °C to 426.85 °C were evaluated, in a steps of 25 °C. The same pressure and ΔTs conditions were applied in these simulations.

4.2 MESH INDEPENDENCE STUDY

After defining the parameters for the geometry and wall length, a mesh independence study was performed for the lowest ΔT studied, 0.5 °C, and for the highest analysed, 60 °C because these are the extreme cases concerning the temperature differences between the wire and the fluid. The pressures analysed were 4.0, 5.5, 7.0, 8.5 and 10.0 MPa and

Figure 4.3 – Example of the configuration of mesh used

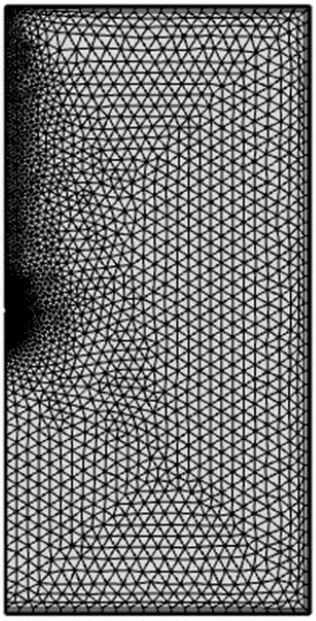

T_{bulk} of 31°C. This study was made by verifying the Nusselt number results obtained with different numbers of elements on the mesh. A mesh is considered refined enough when the difference between the Nusselt number obtained with it and a mesh with the double of elements is under 1% (ROUSSELET et al., 2013b). Figure 4.4 shows the Nusselt number obtained for each mesh size, at each pressure tested and ΔT of 0.5 °C at the top image. In the image below the difference in percentage between the results with a mesh and the previous mesh analysed. It is noticeable that for all pressures studied, when reaching a number of elements of 47,446, the number of elements is sufficient to provide a consistent result.

The same analysis was made for a temperature difference between the wire and the fluid of 60 °C, which was the maximum ΔT used in the simulations. The results are presented in Figure 4.5 and are very similar to the ones of Figure 4.4 for the smaller ΔT studied. The main difference, besides the values found for Nu_{D}, is that for 7.0, 7.5 and 10.0 MPa for sparser meshes no convergence was found, probably caused by the intense property variation at such conditions. However, once reaching convergence, the mesh already presented results with less than 1% compared to a mesh with the double of elements.

When observing Figures 4.4 and 4.5 it is noticeable that the mesh independence is reached already for a mesh with 47,446 elements, which is highlighted in both mentioned figures. Using this mesh entailed in convergence issues when working with conditions of temperature and pressure where the thermophysical properties variation were more intense. Because of this, the mesh selected to run the simulations presented 361,366 elements, ensuring convergence in all conditions, so all the simulations would be run with

Figure 4.4 – Mesh validation $\Delta T = 0.5$ °C, $T_{bulk} = 31$ °C in all ranges of pressures simulated and the percentage difference between the mesh with that number of elements and the one with half of that amount

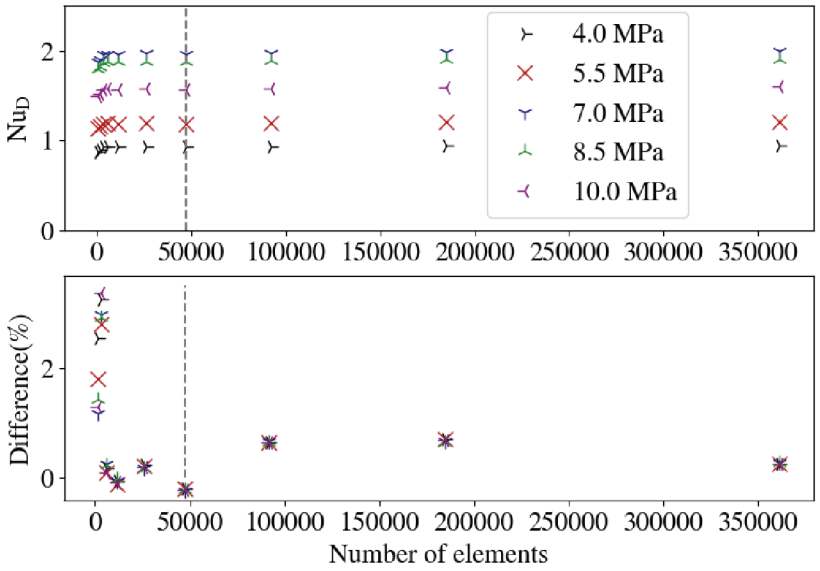

Figure 4.5 – Mesh validation DeltaT = 60 °C, $T_{bulk} = 31$ °C in all ranges of pressures simulated and the percentage difference between the mesh with that number of elements and the one with half of that amount

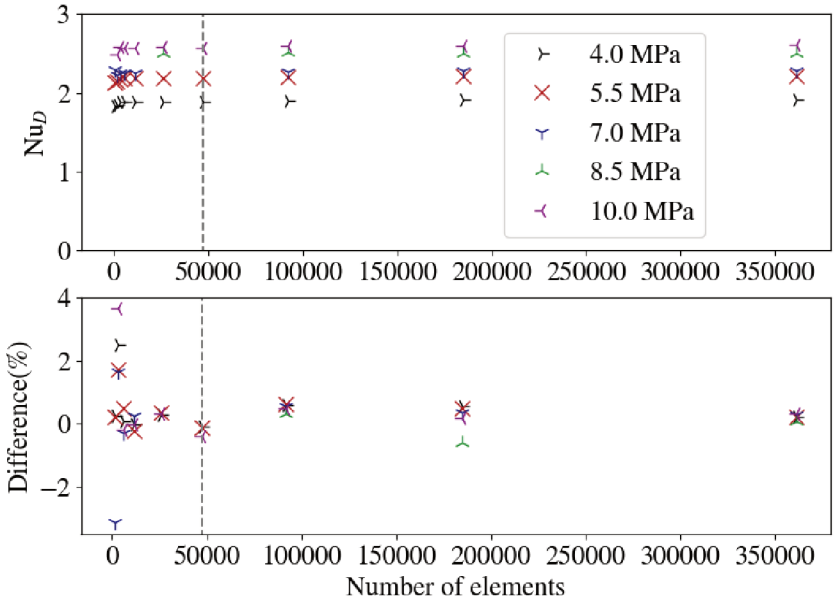

the same mesh and a proper comparison between the results of the simulations could be done.

4.3 MODEL VALIDATION

The model validation was made in two steps: the first was a comparison between the simulation results and the correlations for natural convection around horizontal heated cylinders, using air as the working fluid. The second step was to run the simulations using carbon dioxide and evaluating the thermophysical properties, as already mentioned, using CoolProp (BELL et al., 2014). These results were then compared with the experimental and numerical results published by Rousselet et al. (2013a) and Rousselet et al. (2013b). The approach of validating the simulation with air before using carbon dioxide is because the thermophysical properties of air vary only with the temperature, while for carbon dioxide in the conditions simulated they vary with both the pressure and temperature. Hence it was decided to start validating the model with a simpler condition, where it would show that the equations and boundary conditions set for the model were accurate, and afterwards to add the complexity of the varying thermophysical properties.

In this background, the first validation was made, as already discussed, when the simulation was solved using air as the working fluid. The Nusselt numbers obtained with the simulations were compared with the experimental correlation shown in Equation 4.4 for heated horizontal cylinders developed by Churchill & Chu (1975). This correlation is valid for $Ra_{\mathrm{D}} < 10^{12}$. The Nusselt of the simulation was also compared with the two correlations used in Chapter 3 to validate the experimental apparatus, one proposed by Morgan (1975), Equation 3.7, valid for $10^{-2} < Ra_{\mathrm{D}} < 10^{2}$ and the other by Chand & Vir (1979), Equation 3.8, which is valid for both laminar and turbulent Ra_{D}. In these simulations, the conditions were P_o=0.101 MPa, $T_{\mathrm{bulk}} = 30$ °C, $T_{\mathrm{wire}} = 60$ °C and the wire diameter D_{wire} was changed in order to vary the Rayleigh number and compare the results for different orders of Rayleigh. The results are presented in Table 4.1. It is possible to verify that this model can be applied for Rayleigh numbers in the order of 10^0 to 10^4, being the simulations results in the limits of the uncertainty of the correlation used for comparison.

$$\overline{Nu_{\mathrm{D}}} = \left\{ 0.60 + \frac{0.387 Ra_{\mathrm{D}}^{1/6}}{\left[1 + (0.559/Pr)^{9/16}\right]^{8/27}} \right\}^2 \tag{4.4}$$

On Table 4.1 it is possible to observe that both for the simulation and for the correlations, the Nu_{D} increases for higher Ra_{D}. Besides, the simulation results match very well with the Ra_{D} of the three correlations, being the only exception for Ra_{D} in the order of 10^4 and the correlation of Morgan (1975). In fact, this Ra_{D} is over the valid range of this correlation. Despite this, the results found with the simulation using air as the working fluid match very well with the the three correlation results, validating the model.

After performing the validation with air, the next step was to run the simulation using carbon dioxide as the working fluid, and using the properties imported from CoolProp,

Table 4.1 – Comparison between the Nusselt Number from simulations and from correlation for different orders of Rayleigh

Order of Ra_D	10^0	10^1	10^2	10^3	10^4
Nu_D Churchill & Chu (1975)	0.85	1.15	1.67	2.61	4.37
Nu_D Morgan (1975)	1.02	1.44	2.02	2.84	4.00
Nu_D Chand & Vir (1979)	0.96	1.31	1.92	3.02	5.10
Nu_D Simulation	0.98	1.32	1.96	3.05	4.99
Difference Churchill & Chu (1975) [%]	-15.62	-14.74	-17.18	-16.75	-14.09
Difference Morgan (1975) [%]	4.07	8.54	3.20	7.16	-24.64
Difference Chand & Vir (1979) [%]	-1.91	-0.46	-1.84	-0.88	2.24

(BELL et al., 2014), as explained in Section 4.1. The results in this step were compared both with experimental and numerical results presented by Rousselet et al. (2013a), Rousselet et al. (2013b) for wire diameter of 0.1 mm. In Figure 4.6 the results obtained with the model developed were compared with Rousselet et al. (2013a) experimental results for a bulk temperature of 31 °C and pressure of 8.1 MPa. It can be noticed that for smaller ΔTs the difference between the experimental and the results is higher, which is explained by Rousselet et al. (2013a) themselves with the fact that, for smaller ΔTs the uncertainty of the temperature measurement is higher. Despite that, for higher ΔTs there seems to be a good confluence between the experimental results by Rousselet et al. (2013a) and the numerical ones developed in this work. Figure 4.7 shows that the difference between both numerical models is under 10% for all ΔT evaluated, which also helps in validating this computational model.

Figure 4.6 – Comparison between the experimental results found by Rousselet et al. (2013a) and the computational model developed, for T_{bulk} = 35.25 °C and P_o = 8.1 MPa, and the difference between the results for the same ΔT

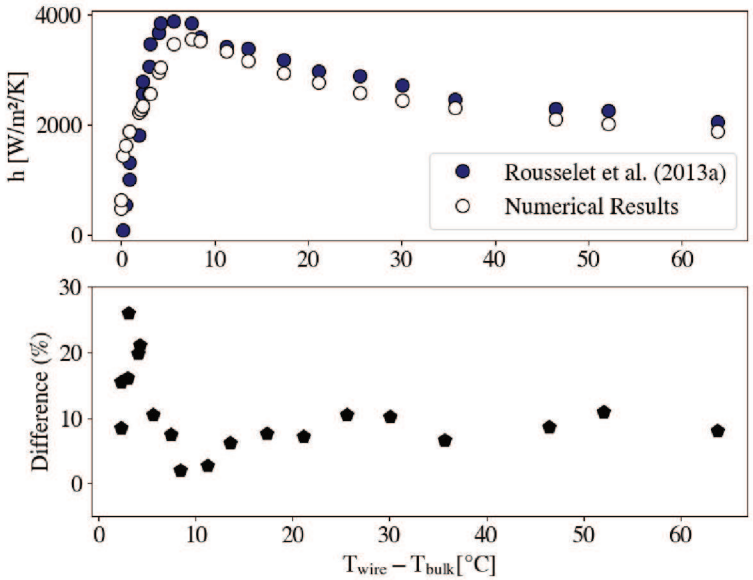

Figure 4.7 – Comparison between the numerical results found by Rousselet et al. (2013b) and the computational model developed, for T_{bulk} = 31.0 °C and P_o = 8.1 MPa, and the difference between the results for the same ΔT

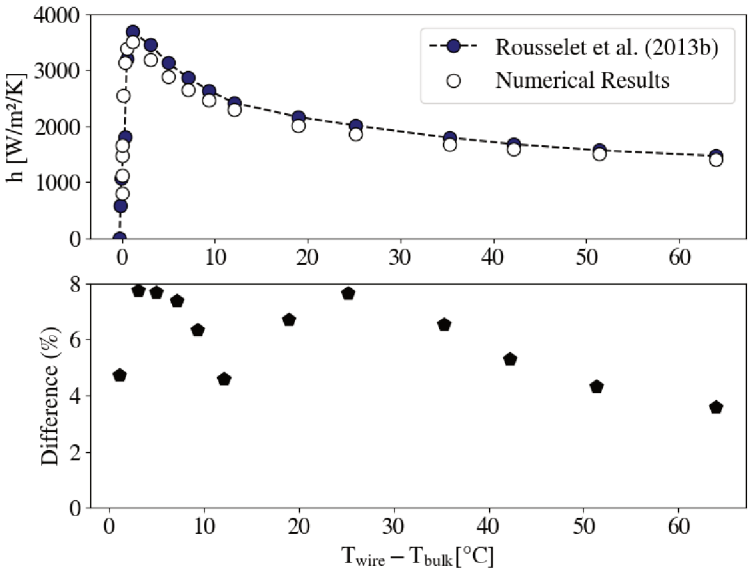

Table 4.2 presents the comparison of the actual results between the experimental tests performed by Rousselet et al. (2013a) and the numerical results of this work, both displayed in Figure 4.6, in order to better visualize the differences in the results. The simulations were executed using a wire diameter of 0.25 mm. This diameter was one of the wires available to perform the experimental tests because the initial idea was to compare the experimental results with the simulation's. However, because of the method used to evaluate the wire temperature in the experiment, as already discussed in Chapter 3, the effective superficial area for the heat transfer could not be evaluated using the wire diameter, which made it impossible to compare the experimental and numerical results of this work.

4.4 CONSIDERATIONS ABOUT THE NUMERICAL MODEL

After presenting the model validation both for air and for carbon dioxide, it is important to discuss two aspects of the numerical model developed in this dissertation. The first is related to how the thermophysical properties of the material are evaluated. The second concerns the difficulties in the development of a transient-study model to assess the thermal energy stored in s-CO_2.

As mentioned, the first discussion about the model concerns the evaluation of the thermophysical properties. COMSOL *Multiphysics*®, (COMSOL Inc, 2017), possess a material library with all the relevant properties for the simulations of a wide list of substances. However, for carbon dioxide the properties are assessed considering variation

Table 4.2 – Comparison between experimental results from Rousselet et al. (2013a) and the numerical results

ΔT [°C]	Rousselet et al. (2013a) [W/m²/K]	Numerical Results [W/m²/K]	Difference [%]
1.94	1813.67	2228.82	-22.89
2.09	2263.62	2274.06	-0.46
2.33	2563.60	2345.78	8.50
2.34	2781.79	2348.76	15.57
3.03	3054.47	2562.38	16.11
3.05	3470.34	2568.94	25.97
4.03	3681.66	2954.10	19.76
4.21	3852.11	3038.85	21.11
5.62	3886.11	3478.27	10.49
7.49	3845.07	3557.33	7.48
8.43	3592.73	3518.45	2.07
11.25	3428.91	3332.21	2.82
13.6	3381.02	3171.12	6.21
17.35	3189.85	2946.80	7.62
21.11	2978.23	2762.85	7.23
25.57	2889.29	2585.08	10.53
30.03	2725.35	2445.16	10.28
35.66	2465.88	2301.74	6.66
46.46	2294.69	2094.90	8.71
52.09	2260.21	2014.08	10.89
63.83	2048.05	1881.35	8.14

only with the temperature of the fluid. When working with supercritical fluids this is not a valid approach since the thermophysical properties of the fluid vary intensely both with the temperature and the pressure. Figure 4.8 presents a comparison of the results for convective heat transfer coefficients obtained with a simulation run for conditions of 8.1 MPa, 47 °C and varying the temperature differences between the wire and the fluid, for the same mesh of 361,366 elements. The first set of results presented as the white markers consists on results obtained with the simulation using the thermophysical properties imported to the simulation from CoolProp, (BELL et al., 2014); the second set of results, represented by the blue markers, show the results obtained using the default properties for carbon dioxide in the materials library of the software. The simulation takes a longer time to run when it imports the properties from CoolProp, approximately 30 minutes for one condition of temperature and pressure, while it takes about 15 minutes using the default properties of the software. Nonetheless, it is clear in Figure 4.8 that using the properties from the material library of the software is not adequate for simulations using supercritical fluids, reaching differences between the results higher than 85% in smaller ΔTs and over 76% for the highest ΔT used in the simulation.

The second consideration about the model concerns a problem faced during the

Figure 4.8 – Comparison between the results of simulations using properties for CO_2 at 8.1 MPa and using ideal gas properties at the same conditions

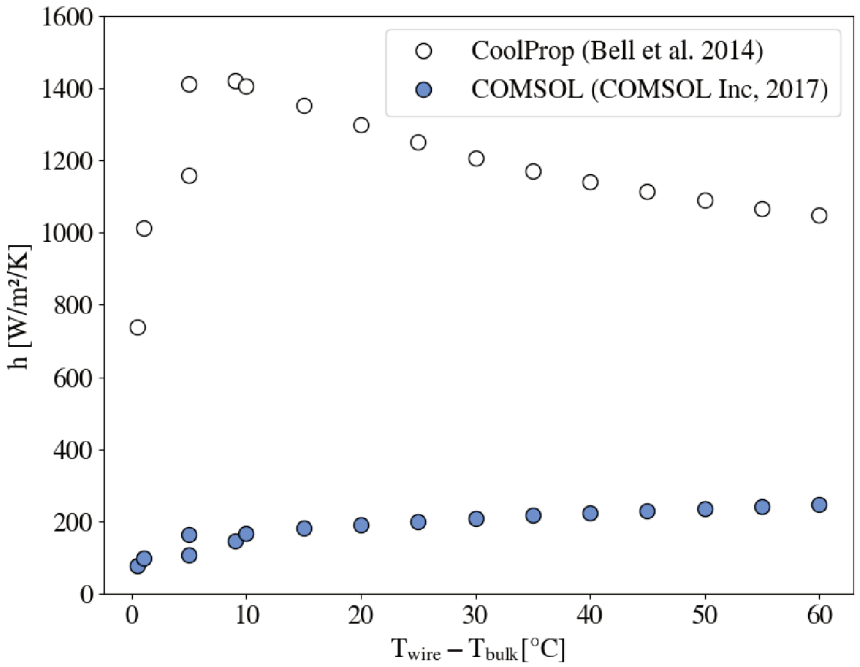

development of the transient study to evaluate the energy density stored in the fluid. It was taking too long to run the simulation with a converged mesh. Because of this, the heat storage capacity of carbon dioxide was evaluated through a thermodynamical approach using the CoolProp, (BELL et al., 2014), properties library.

4.5 COMPARISON WITH OTHER FLUIDS AS TES MEDIUM

To evaluate CO_2 as a TES fluid, it is important to compare it with other working fluids used in industry. It does not seem to be a fair comparison to contrast the fluids in the same temperature and pressure conditions. To simplify the analysis, it was contemplated the use of the storage fluid directly in the power block as working fluid, instead of exchanging heat in a heat exchanger. Figure 1.1 exemplifies well the considerations made in this study.

Studies using Brayton cycles with air, helium, nitrogen (WANG; GU, 2005) and s-CO_2 (MOROZ et al., 2014; DYREBY, 2014) were used to verify the conditions in which the fluid enters and leaves the power block. These conditions were considered as the discharging and charging conditions in which the TES fluid will operate in the TES system. Table 5.1 presents the conditions used in this analysis for each fluid.

These fluids were compared in two aspects: heat transfer rate and stored energy density of the fluid. The convective heat transfer coefficient was calculated using Equation 3.7 for air, helium and nitrogen and Equation 2.3 for s-CO_2. The properties were evaluated

Table 4.3 – Optimized operational conditions for Brayton cycles with s-CO_2, helium, nitrogen and air used for comparison os these fluids as TES medium.

Author	Fluid	P [MPa]	T_{load} [°C]	T_{unload} [°C]
Dyreby (2014), Moroz et al. (2014)	s-CO_2	24.2	263.0	400.0
Wang & Gu (2005)	He	6.83	573.0	900.0
Wang & Gu (2005)	Ni	6.83	573.0	900.0
Wang & Gu (2005)	Air	0.485	571.0	900.0

using CoolProp for all fluids and integrating the properties for s-CO_2 as proposed by Equation 2.2. The temperature difference between the fluid and a heated surface was chosen arbitrarily as $\Delta T = 30$ °C for all fluids, because it is the average value of the ΔT evaluated in the simulations. Before this study, the simulation results were compared with the supercritical fluid correlation given by Equation 2.3, and by a regular correlation of free convection around heated cylinders using constant properties, given by Equation 3.7. This was done in order to evaluate how close the correlations results were from the simulation results, and to verify in which conditions each correlation can be used. These results of the comparisons will be presented in Section 5.1. As mentioned the second comparison between the fluids is the thermal energy storage density, evaluated by Equation 3.6, where the initial time refers to the loading conditions and the final time refers to the unloading conditions.

5 RESULTS AND DISCUSSION

The results of this study are presented in three different sections. Section 5.1 presents the experimental and numerical results about the convective heat transfer coefficient of s-CO_2, discussing about trends found in its behaviour. Section 5.2 shows the analysis about the TES capacity of s-CO_2. The third section, 5.3, discusses the results of the comparison of s-CO_2 with other working fluids, as described in Section 4.5 of Chapter 4.

5.1 CONVECTIVE HEAT TRANSFER COEFFICIENT

This section presents both the experimental and the numerical results for the convective heat transfer coefficient of s-CO_2 around a heated cylinder. The comparison between correlations with constant and integrated properties is also done.

5.1.1 Experimental Results

The experiments were run using two bulk temperatures for the s-CO_2, 32.60 °C and 34.20 °C, for three different heat fluxes. Figure 5.1 shows the heat transfer coefficient curves for the two temperatures evaluated and a power dissipated by the wire of 1.2 W.

Figure 5.1 – Experimental curves of convective heat transfer coefficient behavior for bulk temperatures of 32.6 °C and 34.2 °C with pressure, for power dissipated of 1.2 W and $\Delta T < 2.0$ °C

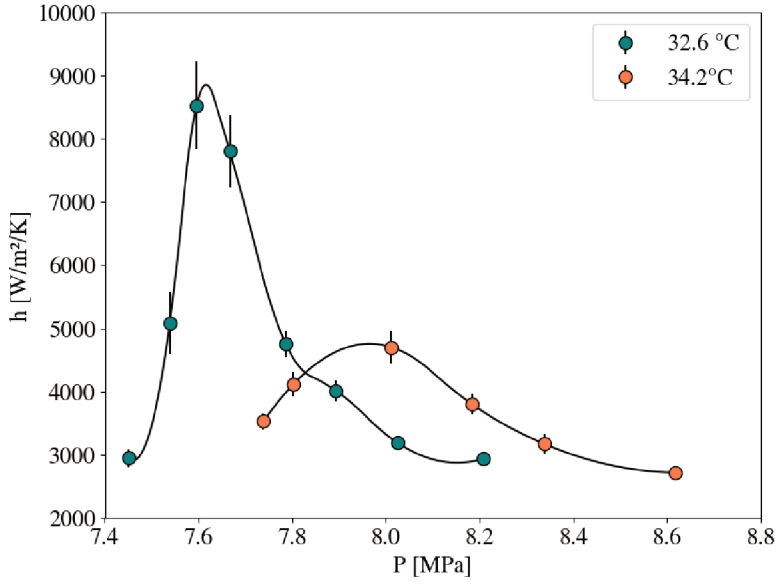

The colored circles in Figure 5.1 are the experimental results obtained, and the black curves present the interpolated tendency of the experimental results, using quadratic

polynomial. The experimental uncertainty for each measurement is also represented as the error line over each circle. It is possible to notice that, the closer the temperature is to T_c, which is 31.10 °C, the higher is the peak in the heat transfer coefficient. In these points evaluated near the peak of the convective heat transfer coefficient, the uncertainty is higher because the temperature difference between the wire and the fluid is smaller than in the other measured points. This occurs because of the enhanced convective heat transfer in such conditions. The pressure where the maximum c_v is obtained is 7.65 MPa for 32.6 °C and 7.9 MPa for 34.2 °C. Hence, one can suppose that the peak in the heat transfer coefficient is related with the peak in the specific heat capacity at constant volume. Besides this, it is noticeable an extremely intense difference between the behaviours of the curves of the two bulk temperatures. This can be justified by the behaviours observed on c_v and c_p presented in Figure 2.1, which vary intensely with the bulk temperature. Besides this, thinking about it in a molecular level, Hall (1971) commented that for temperature increasing, the liquid structure of the molecules gives way to structure of clusters of liquid in a matrix of gas, presenting a high degree of association. Hence with the slight increase of the bulk temperature, the molecules start distancing each other, justifying why the convective heat transfer coefficient is so much lower for slightly higher bulk temperature: because the molecules are further apart.

Running the experiments for the same conditions but for a higher power dissipation of 30.5 W, the same trend of different values of convective heat transfer coefficient for slightly different bulk temperatures are noticed, as seen in Figure 5.2.

Figure 5.2 – Experimental curves of convective heat transfer coefficient behavior for bulk temperatures of 32.6 °C and 34.2 °C with pressure, for power dissipated of 30.5 W and 20.0 °C < ΔT < 50.0 °C

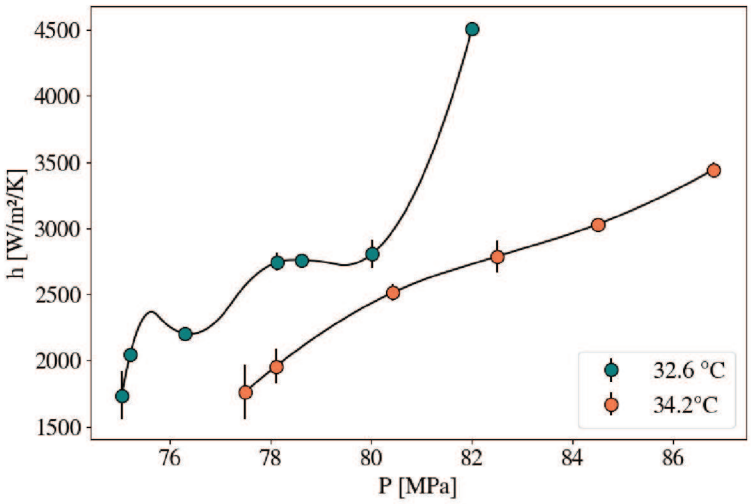

A different behavior was observed in the heat transfer coefficient for each bulk

temperature, as seen in , than the one observed in Figure 5.1, for 1.2 W. In this scenario, it is observed that the convective heat transfer coefficient keeps increasing with the pressure, not presenting its maximum value for the same pressures as it did with a smaller heat flux, as seen in Figure 5.1. To verify if the pressure where the maximum heat transfer coefficient varied with the magnitude of the temperature difference between the wire and the fluid, the heat transfer coefficient was calculated for several ΔTs. For that, the correlation for natural convection with the properties integration, Equation 2.3, was used to evaluate the Nu_D for several ΔT and then calculate h. The result is shown in Figure 5.3, where it is noteworthy that the higher the temperature difference between the wire and the fluid is, the higher is the pressure where the maximum heat transfer coefficient presents itself until reaching a value, in this case ΔT = 50 °C where no optimal pressure is observed in terms of heat transfer coefficient. Hobold & da Silva (2018) had already commented that for higher ΔTs the optimal pressure might be related with the pressure where the maximum thermal expansion coefficient, β, occurs, instead of the maximum c_p. It makes sense since β is an important property when natural convection heat transfer takes place.

Figure 5.3 – Convective heat transfer coefficient calculated through experimental correlation by (KATO et al., 1968) for T_{bulk} = 32.6 °C and different ΔTs

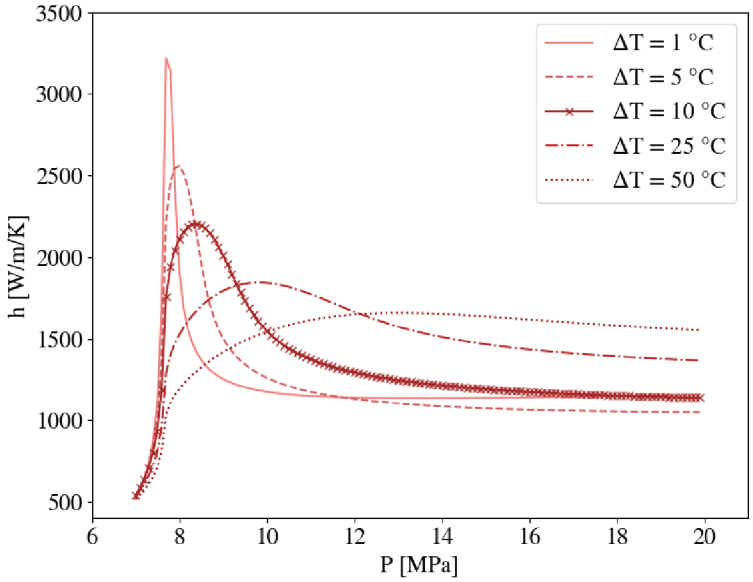

5.1.2 Numerical Results

From the simulations it is possible to observe in Figure 5.4 how the heat transfer coefficient behaves with the bulk temperature for the same pressure of 8.0 MPa. The colored circles are the simulated results and the black lines are the tendencies for the

interpolated results presented, using quadratic polynomial for the interpolation. A pseudocritical point is a condition in which $T_{pc} > T_c$ and $P_{pc} > P_c$ that is characterized as the maximum value of specific heat for that pressure. The closer the temperature is of the pseudocritical temperature for the evaluated pressure, the higher the heat transfer coefficient is, presenting a peak for smaller ΔTs and decreasing its value as ΔT increases. When distancing from T_{pc} for a given pressure, the heat transfer coefficient starts to exhibit lower values, being harder to find a peak for any ΔT.

Figure 5.4 – Convective heat transfer coefficient behavior for several T_{bulk}, ΔTs ranging from 0.5 to 60 °C and for P = 8.0 MPa

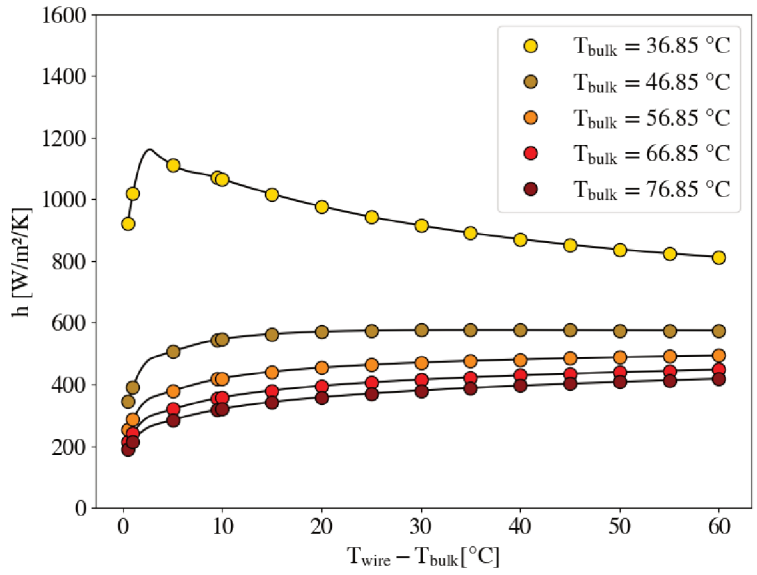

Still discussing about the behavior of the heat transfer coefficient with the operational conditions, in Figure 5.5 it is possible to verify the convective heat transfer coefficient behavior when setting a bulk temperature of the fluid and increasing its pressure. Again, the colored circles are the results obtained with the simulations and the lines are the tendencies exhibited by the results. It is apparent that the increasing of the pressure requires higher ΔTs to reach the maximum heat transfer coefficient value. Besides, the further the pressure is from P_{pc} for a given temperature, smaller is the peak of the heat transfer coefficient, which makes sense when analysing the c_v behavior in Figure 2.1 of this work. The only exception for this behavior is the pressure of 8.0 MPa, which presents heat transfer coefficients much lower than the ones presented by other pressures, mostly compared to 9.0 MPa, which is the pressure that, for smaller ΔTs presents the highest heat transfer coefficient. This occurs because the pressure at which c_v is maximized for 36.85 °C is 8.35 MPa, so at 8.0 MPa the the s-CO_2 has not yet reached P_{pc} for this temperature condition, presenting smaller heat transfer coefficient.

Figure 5.5 – Convective heat transfer coefficient behavior with pressure for T_{bulk} = 36.85 °C and ΔTs from 0.5 to 60 °C

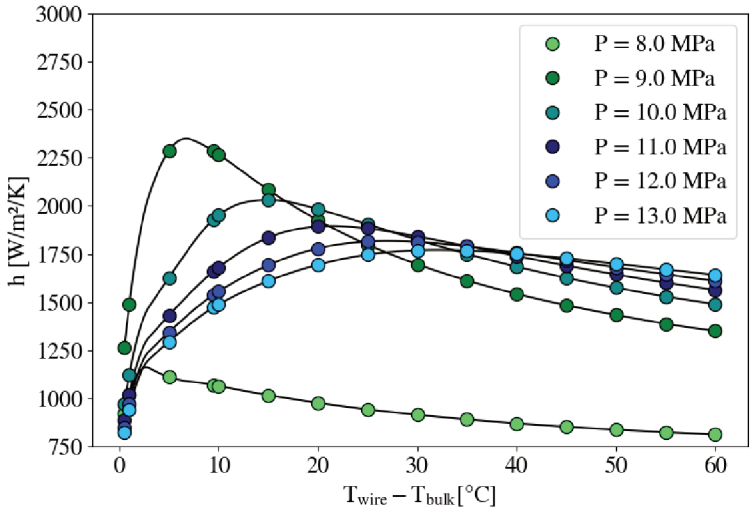

Another fact that can be noticed in Figure 5.4 is that, after ΔT of 20 °C the pressures that become optimal for the heat transfer are different as ΔTs keep increasing. This fact can be attested by Figure 5.6, where the results for the simulations were all mapped in one image, showing the optimal pressure for every bulk temperature and ΔT simulated.

Figure 5.6 – Optimal pressures for each bulk temperature and ΔTs for s-CO_2

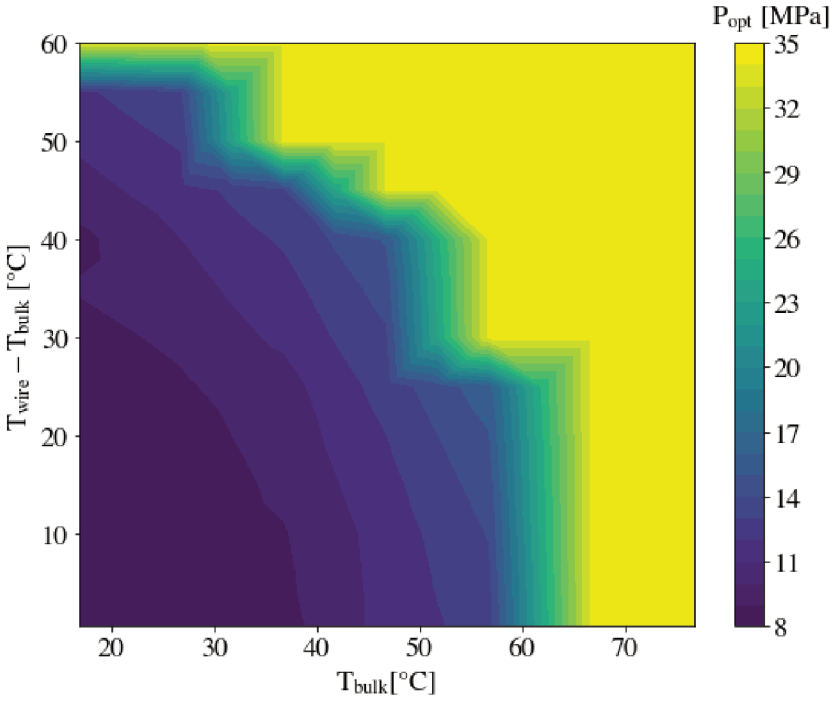

These results presented in Figure 5.6 are not smooth in certain regions, probably

because of the simulated conditions, which could be smoother if more conditions of pressure, bulk temperature and temperature difference between the wire and the fluid were analysed. Despite this, a very clear tendency that there is indeed an optimal operating pressure to enhance the heat transfer depending on the operational conditions until a certain condition is seen. The optimal pressure increases with the bulk temperature until about 56.85 °C and ΔTs of 50 °C , after these conditions the optimal pressure will be the highest pressure analyzed. This behavior is probably connected to the conditions of temperature and pressure where the thermophysical properties vary the most, presenting optimal values for heat transfer coefficient when the properties variation is very intense and no optimal is found for conditions in which the variation is not as extreme.

Precisely, in some experimental works presented in Section 2.2, when discussing about the properties integration for supercritical fluids to make proper use of the Nu_{D} correlations, some authors discussed that after reaching conditions of temperature and pressure elevated enough there would be no need to integrate the properties, so the supercritical fluid could be treated as an ideal gas, with constant properties. This can be confirmed in Figure 5.7, where the simulation results are compared with both correlation with integrated properties for supercritical fluids, Equation 2.3, and with constant properties correlations for natural convection, Equation 3.7. The temperatures analysed were a temperature close to T_{c}, 36.85 °C, and the highest temperature simulated, 426.85 °C. These temperatures were paired with the lowest and the highest pressure simulated, 8.0 MPa and 35.0 MPa.

In this context, it is very clear that the supercritical correlation fits almost perfectly with the heat transfer coefficient behavior found with the simulations conditions near the critical point, as seen in Figure 5.7a being this result very different from the one expected using constant properties correlation. For the same pressure but a higher temperature, Figure 5.7c shows that the results are closer to the ones obtained with constant properties correlation. When using these temperatures but enhancing the pressure to 35.0 MPa, the results fit well with both correlations, in some cases closer to the supercritical and in other closer to the constant properties, but still in the uncertainty range for both correlations. In this case, maybe it would be simpler to use the constant properties correlation.

Despite stating that after a certain condition of temperature and pressure the constant properties correlations could be used for supercritical fluids, it was not found in the literature so far a parameter to determine when it is acceptable to use this simpler correlation instead of going to the trouble of integrating the properties and requiring more computational work to solve a natural convective heat transfer problem. Figure 5.8 is presented trying to find a parameter that helps in this sense, comparing the conditions of temperature and pressure for which the correlation with constant properties present differences compared to the simulation that are above 15%, the conditions for which β and c_p vary the most.

Figure 5.7 – Comparison between the simulation results, results using constant properties correlation and results using integrated properties

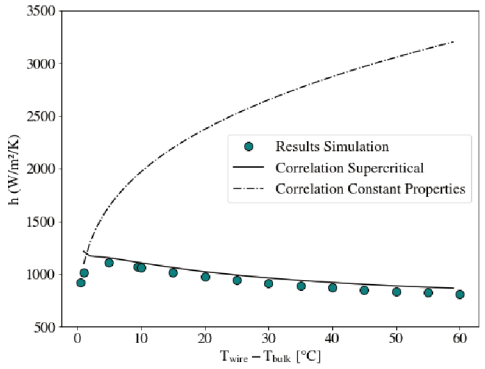

(a) $T_{\text{bulk}} = 36.85$ °C and $P = 8.0$ MPa

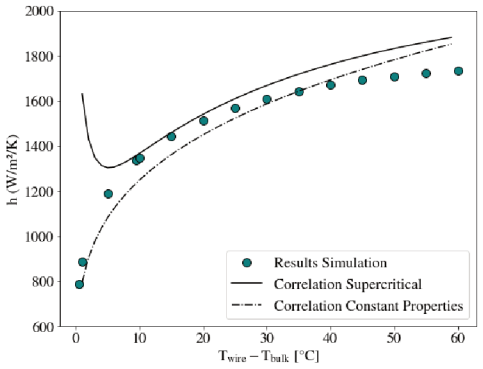

(b) $T_{\text{bulk}} = 36.85$ °C and $P = 35.0$ MPa

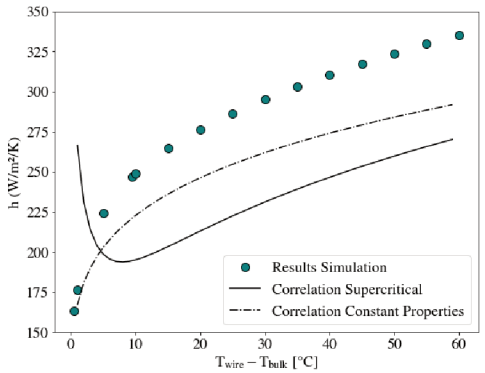

(c) $T_{\text{bulk}} = 426.85$ °C and $P = 8.0$ MPa

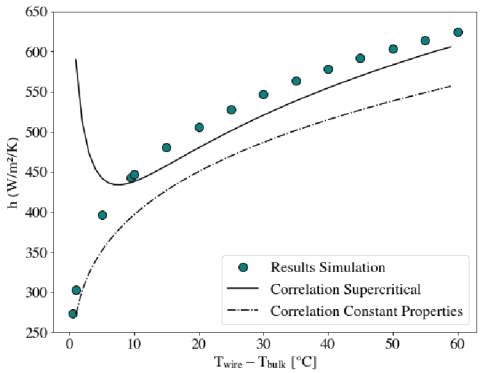

(d) $T_{\text{bulk}} = 426.85$ °C and $P = 35.0$ MPa

As mentioned, in Figure 5.8a it can be observed the conditions of temperature and pressure for which the constant properties exhibit a difference with the results that are over than 15 % in green, with values 1 on the graph. The blue region, for values 0, represents all conditions for temperature and pressure for which the constant properties correlation presents a results which differences compared to the simulation are under 15%. Hence, this means that in the green region of the image it is not acceptable to use the constant properties approach, which is the region near the critical point of CO_2. At the same time, Figure 5.8b shows how c_p varies with the temperature and pressure, comparing its value at bulk temperature and at the bulk temperature minus 1 °C. c_p is evaluated because it is already attested it is an important thermophysical property for the heat transfer in supercritical fluids. It is perceptible that c_p variation occurs intensely for all range of temperatures and pressures evaluated. Hence, to use c_p variation as a parameter to define whether or not to use integrated properties correlation does not seem to be valid idea, even if it is the first instinct one might have after studying about supercritical fluids and the importance of c_p in the heat transfer phenomena in these fluids.

It is Figure 5.8c the one that seems to bring a solution to this problem, showing that the conditions for which the coefficient of thermal expansion β of the fluid varies the most

are almost a perfect fit to the regions where the difference between the simulations results and the constant properties correlation are over the uncertainty limits of this correlation. It actually makes sense that the β has a higher importance concerning the evaluation of properties than c_p when discussing natural convective heat transfer, which is a phenomena that is dictated by the variation of density of the fluid and β is directly related to that.

This conclusion can also aid to justify why in Figure 5.6, after a certain condition, the optimal pressure is the highest pressure tested. In the conditions where the variations of c_p and c_v are more intense, the optimal pressure is related to the conditions that maximize the specific heat. However, c_v and c_p decrease with the increase of the pressure for the same temperature. The density of the fluid, however, always increases with the pressure. Hence, maybe after a certain temperature and pressure, the density of the fluid becomes more relevant for the heat transfer than the specific heat, in a manner that after this condition the optimal pressure for the convective heat transfer is dependent of ρ. Then, if ρ keeps increasing with the pressure, the optimal pressure increases too.

Figure 5.8 – Comparison between the conditions where constant properties correlation can be used with s-CO_2 and the variation of c_p and β

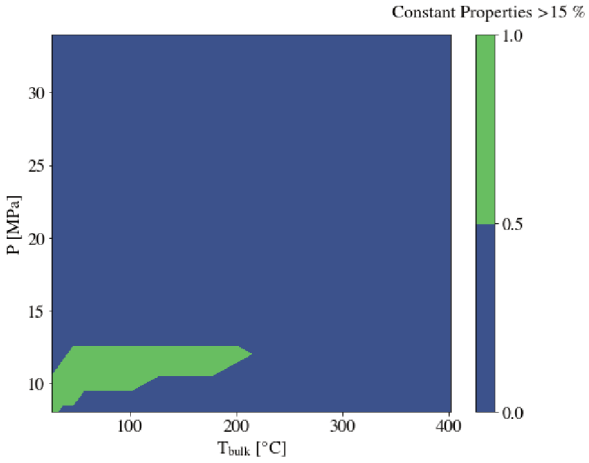

(a) Temperature and Pressure conditions where the difference between the constant properties correlation and the simulation is above 15%.

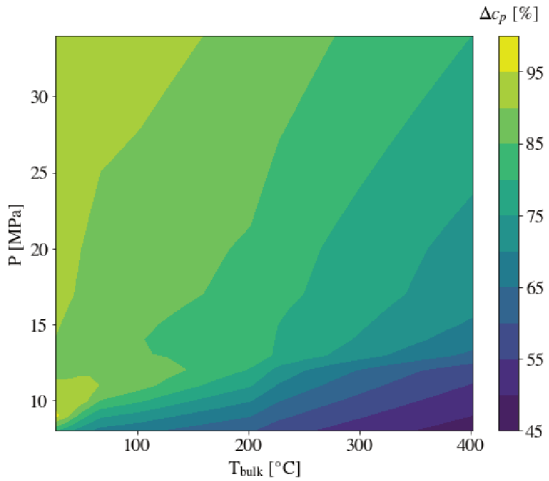

(b) Conditions of Temperature and Pressure where c_p varies

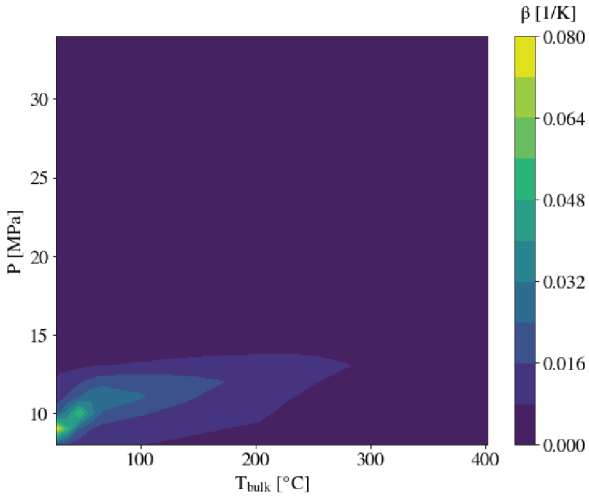

(c) Conditions of Temperature and Pressure where β varies

5.2 THERMAL ENERGY STORAGE CAPACITY

The data relevant to evaluate the storage energy capacity is the transient regime of the experiments. Figure 5.9 displays the temperature measurements during one hour for: the four the s-CO_2 thermocouples, in Figure 5.9a; the average temperature of the carbon dioxide T_{bulk}, in Figure 5.9b and the wire temperature T_{wire}, in Figure 5.9c.

Figure 5.9 – Transient measurements of the thermocouples during 1 hour dissipating 53.5 W in the wire

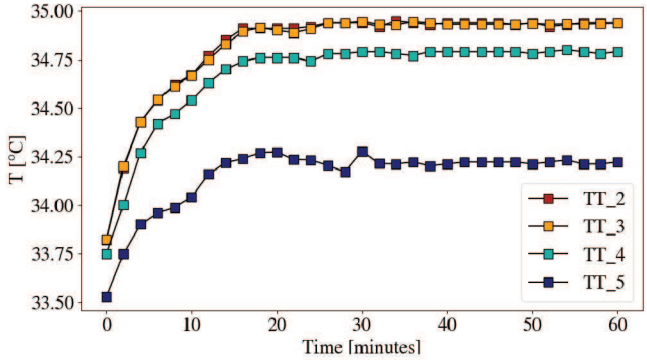

(a) One hour measurement of the s-CO_2 thermocouples

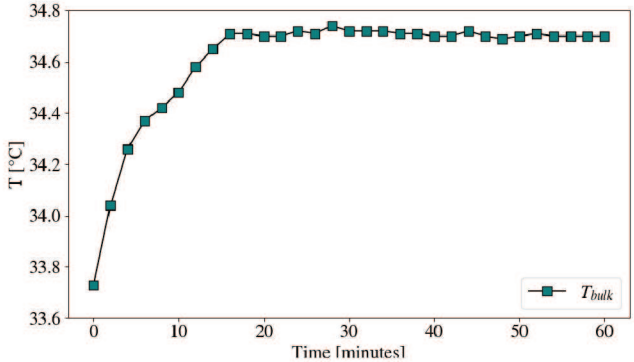

(b) One hour measurement of the average temperature measured by the s-CO_2 thermocouples, T_{bulk}

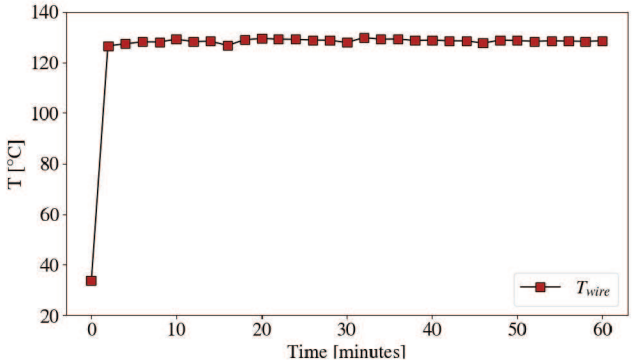

(c) One hour measurement of the wire temperature

These data from Figure 5.9 were saved for an experiment dissipating 53.5 W, the

highest power dissipated during the tests performed in this work, which was the power that took longer for the fluid to reach stationary condition. It is noticeable that after 20 minutes, the temperature reaches stationary conditions. As mentioned in Chapter 3, 30 minutes of data were acquired for this power level, 20 minutes for 30.5 W and 15 minutes for 1.2 W, ensuring both transient and steady state conditions data would be recorded. The transient data was used for TES study and steady-state data for heat transfer coefficient study. Besides, for TES study, only the powers 53.5 W and 30.5 W will be considered, because those are the conditions in which the fluid's temperature and pressure suffer a significant change because of the heating.

Figure 5.10 presents the values of dissipated heat by the wire, the thermal energy stored and the thermal energy lost with a power dissipation of 30.5 W, both for 32.6 °C, on Figure 5.10a and 34.2 °C, on Figure 5.10b.

Figure 5.10 – Thermal energy analysis dissipating 30.5 W through the wire for 32.6 °C and 34.2 °C

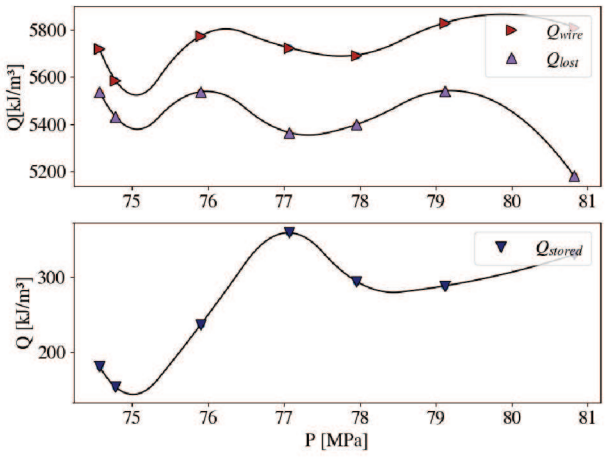

(a) Thermal energy balance for 32.6 °C

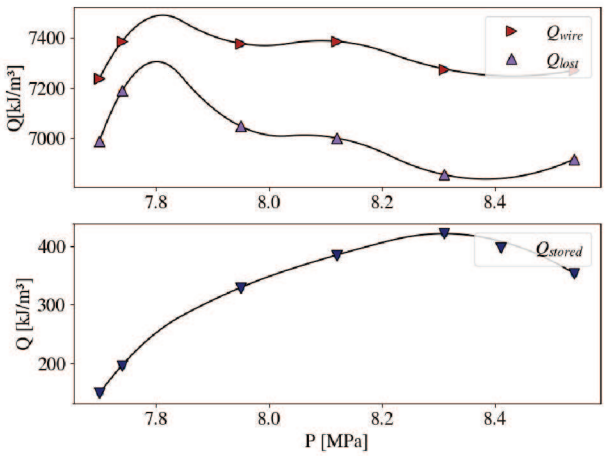

(b) Thermal energy balance for 34.2 °C

The same analysis was executed for the power dissipated of 53.5 W in Figure 5.11.

Figure 5.11 – Thermal energy analysis dissipating 53.5 W through the wire for 32.6 °C and 34.2 °C

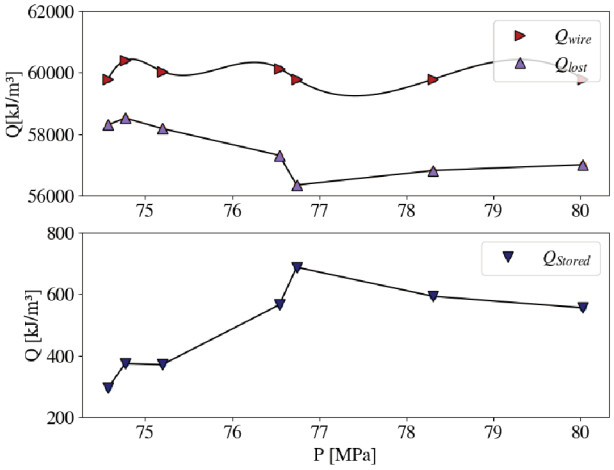

(a) Thermal energy balance for 32.6 °C

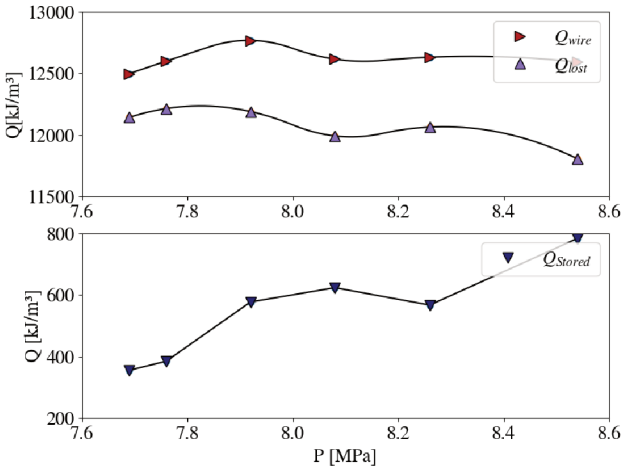

(b) Thermal energy balance for 34.2 °C

It is notorious from Figures 5.10 and 5.11 that most of the energy dissipated by the wire was lost to the water from the thermostatic bath. This experimental setup, although very good to analyse the convective heat transfer coefficient, is not perfectly fit to study thermal energy storage, because it does not possess insulation and only the charging cycle of the system could be evaluated since the system can only be heated by the wire but not cooled by it. Despite that, two main preliminary and interesting results can be noticed in Figures 5.10 and 5.11 about the TES behaviour of s-CO_2. The first is that the thermal energy stored tends to be higher the more elevated the pressure is, exhibiting an increase in the distance between the energy dissipated and the energy lost as the pressure increases. Another curious aspect is that, for both powers dissipated, the higher temperature showed

a greater amount of thermal energy stored.

When expanding these results for other pressures with a thermodynamic approach, which is shown in Figure 5.12, there seems to be an optimal operating pressure for thermal storage for initial temperature 34.2 °C and temperature variation of 30 °C. However these optimal operating pressures seem to be a little higher than the optimal for the heat transfer coefficient, which justifies why no optimal seems to have been reached by the storage thermal energy experimental results for 34.2 °C (Figures 5.10b and 5.11b). For the results with 32 °C, there seems to be an optimal in both cases closer to 7.7 MPa, however to be certain of this it would be interesting tho run testes for more pressure points.

Figure 5.12 – Behavior of storage energy density with pressure for T_{bulk}= 34.2 °C and temperature variation of 30 °C

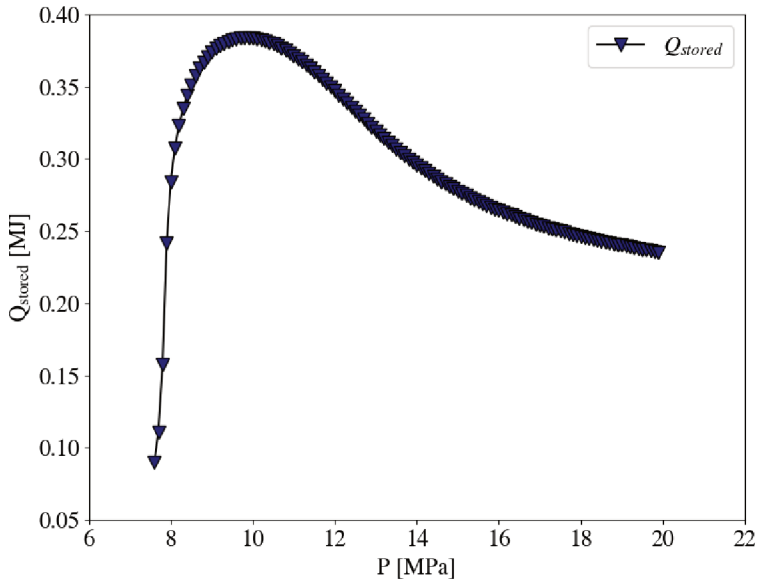

When comparing the thermal energy stored with the density of the fluid, in Figure 5.13, it is clear that the TES, for constant volume operation, increases with the density. This explains why for more elevated pressures and temperatures in Figures 5.10 and 5.11 the TES was also higher, because constant volume at higher pressures and temperatures means higher density and mass of the fluid in the vessel.

5.3 SUPERCRITICAL CARBON DIOXIDE AS TES MEDIUM

What can be concluded from the results discussed until this point is that s-CO_2 seems to be a good fluid in terms of presenting enhanced heat transfer coefficient and TES density, both desirable characteristics for a thermal energy storage medium, as already mentioned. Hobold & da Silva (2017) have already discussed the advantages of TES systems using supercritical fluids in comparison to other TES technologies, as

Figure 5.13 – Stored energy density variation with the fluid's density for bulk temperature of 34.2 °C

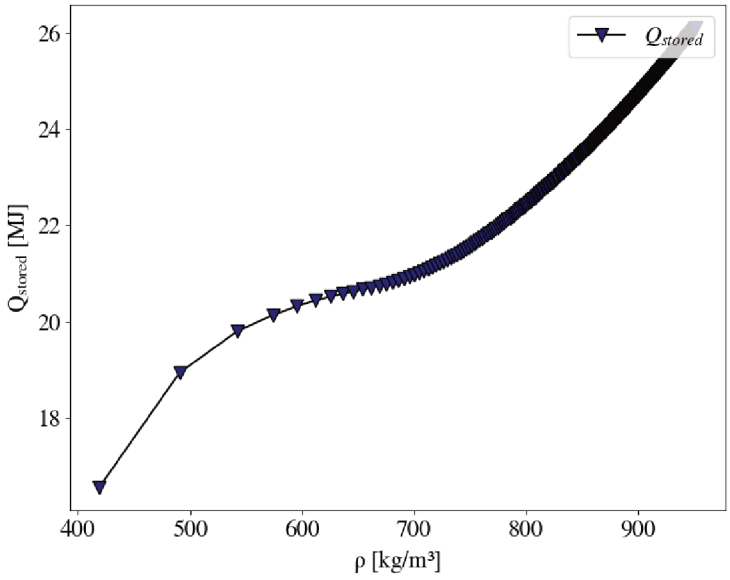

discussed in Sections 2.3.2 and 2.3.3, and in Figure 2.8. However, these characteristics are prominent near the critical point. Other supercritical fluids, with critical point closer to the operational conditions of a TES system for power generation in CSP application, for example, can be used.

Nonetheless, since there are works researching the use of s-CO_2 and other fluids to enhance the power generation in Brayton cycles for CSP applications, it is interesting to compare s-CO_2 in such conditions, which are much above its critical point, as TES medium with some of these other fluids studied. Hence, to be coherent when evaluating s-CO_2 as thermal energy storage medium, it is important to compare its performance with other fluids used in power cycles, in the conditions these fluids and the s-CO_2 would actually be used in the power block. In this context, Figure 5.14 presents a comparison between the convective heat transfer coefficient of s-CO_2 and three other fluids, helium, air and nitrogen, in the conditions these fluids are used to optimize a Brayton Bycle. The conditions are presented in Table 5.1, which was already presented in the end of Chapter 4.

Figure 5.15 shows a comparison between these fluids for thermal energy storage, where Θ presents a ratio between the actual loading and unloading temperatures of the TES system and the desired loading and unloading temperatures presented on Table 5.1. Hence, $\Theta = (T_{\text{load}} - T_{\text{unload}})_{\text{actual}}/(T_{\text{load}} - T_{\text{unload}})_{\text{Brayton}}$.

When evaluating the heat transfer coefficient in power generation application conditions, helium is the only fluid that possesses a higher coefficient than s-CO_2. On the other hand, s-CO_2 presents a much higher energy density than the other three fluids,

Table 5.1 – Optimized operational conditions for Brayton cycles with s-CO_2, helium, nitrogen and air used for comparison os these fluids as TES medium.

Author	Fluid	P [MPa]	T_{load} [°C]	T_{unload} [°C]
Dyreby (2014), Moroz et al. (2014)	s-CO_2	24.2	263.0	400.0
Wang & Gu (2005)	He	6.83	573.0	900.0
Wang & Gu (2005)	Ni	6.83	573.0	900.0
Wang & Gu (2005)	Air	0.485	571.0	900.0

Figure 5.14 – Convective heat transfer coefficient for the loading temperature of each fluid and $T_{\text{wire}} - T_{\text{bulk}} = 30°\text{C}$

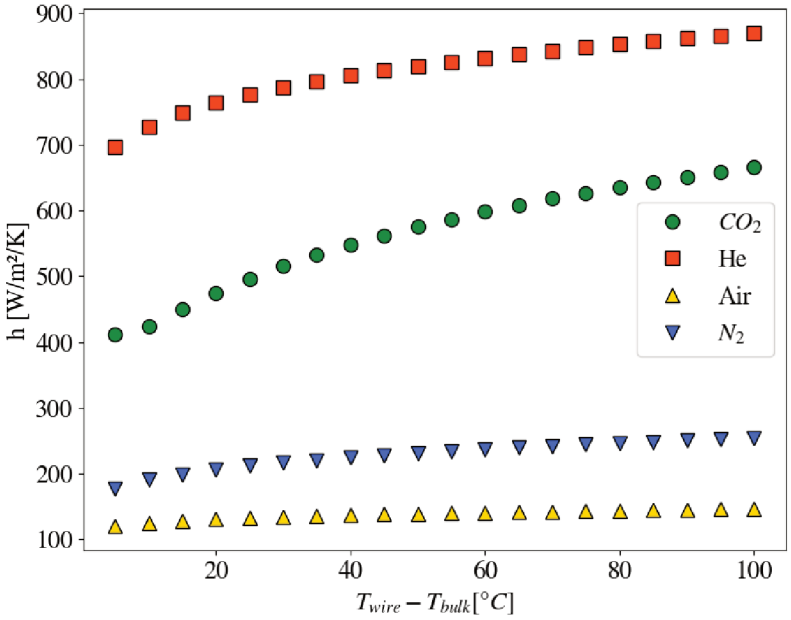

meaning it can store a higher amount of energy in a smaller volume. Given that helium is a very limited fluid in the atmosphere, even if it presents a heat transfer coefficient higher than s-CO_2, it is more interesting to use this second more abundant fluid as TES medium. Besides, Dostal et al. (2004) discussed that higher turbine efficiencies can be reached using s-CO_2 instead of helium. Hence, even for conditions way beyond the critical point, sCO_2 seems to be a promising TES medium.

Figure 5.15 – Energy density comparison of the fluids in relation to the ratio of the temperature variation over the maximum temperature variation required in the power cycle of each fluid

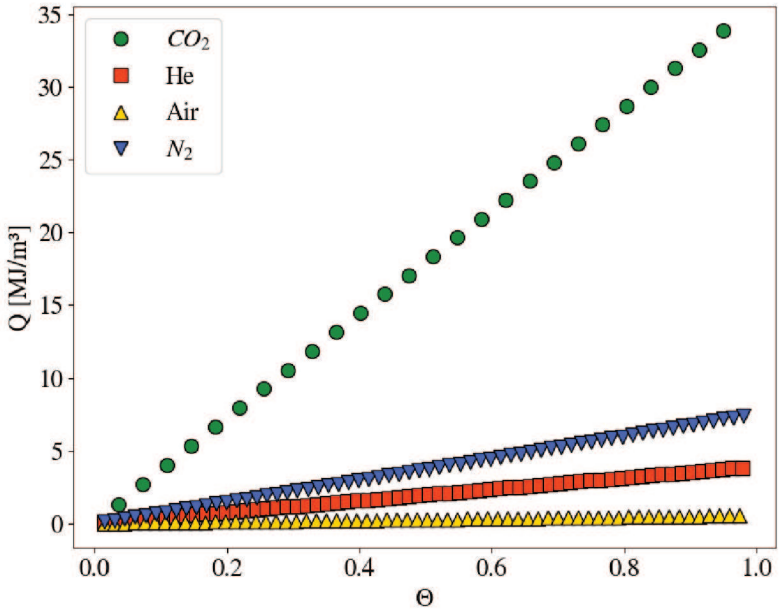

6 CONCLUSIONS

6.1 THERMAL ENERGY STORAGE WITH S-CO_2

The results showed that the convective heat transfer coefficient depends on the operational conditions, which are the bulk temperature, the pressure of the system and the difference of temperature between the wire and the fluid, ΔT. Until certain conditions of bulk temperatures and ΔTs, optimal operational pressures are found. These optimal conditions are usually closer to the critical point, where the properties variation are intense and the specific heat is maximized. After a certain bulk temperature, the optimal pressure found was the maximum pressure analysed. This may have some relation with the increasing density of the fluid with pressure, but further investigation is required to affirm this. When comparing the numerical results with correlations using integrated or constant properties evaluation it was found that for conditions of temperatures and pressures where the isothermal coefficient of expansion, β, of the carbon dioxide does not vary, it is possible to use the constant properties correlations. This result was found only for carbon dioxide, but it is expected to find similar results using other supercritical fluids, because, as before mentioned, the thermophysical characteristics of supercritical fluids behave the same for all fluids near their critical points.

The experimental results for energy density of s-CO_2 in operation at constant volume require more and better tests and analyses. However, thermodynamic analyses showed that for higher pressures and temperatures the energy density stored was higher. This occurs because in these conditions, the fluid exhibited a higher density in the pressure vessel, which presents direct relation with the energy stored. Expanding this result for conditions of pressure higher than the ones achieved experimentally show that there seems to be an optimal pressure for thermal energy storage. It would be interesting to verify this experimentally in the future.

The literature review of this work has already discussed the fact that supercritical fluids present better results as TES mediums than other technologies of TES. In fact, the main advantage of using supercritical fluids is the enhanced heat transfer rate in comparison to the other technologies existent, and this was verified by the experimental results of the convective heat transfer coefficient in this work. For TES applications that require higher temperatures and pressures, other fluids with critical points closer to the desired operational conditions can be used, taking advantage of the intense thermophysical properties variation near the critical point and enhancing the heat transfer coefficient and the energy density stored. However, it is also interesting to imagine a direct application of s-CO_2 in TEs systems connected to power cycles for CSP application, which is only an application example of TES systems. When comparing the convective heat transfer coefficient of s-CO_2 with Helium, Nitrogen and Air in conditions they are used in these before mentioned power cycles, the convective heat transfer of the carbon dioxide lost only

for Helium, presenting, however, higher energy density than all fluids for all conditions analysed. This means that s-CO_2 seems to be a good alternative as storage media even in conditions of temperature and pressure much above the critical point.

6.2 SUGGESTIONS FOR FUTURE WORKS

Certain modifications on the experimental apparatus are suggested for future works to impros the TES analyses.

- Release more power through the wire, or substitute the wire for a resistance, allowing more power dissipation to the fluid; this would cause a higher temperature variation of the s-CO_2. For a higher power dissipated and temperature variation, the temperature of the water circulating around the pressure vessel can change enough, making it possible to measure with small enough uncertainty the energy lost by the CO_2 to the water, by measuring the inlet and outlet temperatures of the water and its mass flow rate.
- Further modify the experimental apparatus to be able to study charging and discharging cycles of s-CO_2 as TES medium; instead of a resistance dissipating power, use a coil connected to a second thermostatic bath. By the same method of measuring the inlet and outlet temperatures of the water in the coil passing through the pressure vessel containing s-CO_2, and its mass flow rate, it is possible to evaluate the energy released or absorbed to/from the s-CO_2, depending if this water temperature is higher or below the temperature of the s-CO_2. In this manner, it would be possible to study charging and discharging cycles for s-CO_2, which are relevant studies for TES applications.

REFERENCES

ALAPTEKIN, E.; EZAN, M. A. Performance investigations on a sensible heat thermal energy storage tankwith a solar collector under variable climatic conditions. *Applied Thermal Engineering*, ELSEVIER, v. 164, 2020.

AVCI, M.; YAZICI, Y. Experimental study of thermal energy storage characteristics of a paraffin in a horizontal tube-in-shell storage unit. *Energy Conversion Management*, Elsevier, v. 73, p. 271–277, 2016.

BATAINEH, K.; GHARAIBEH, A. Optimal design for sensible thermal energy storage tank using natural solid materials for a parabolic trough power plant. *Solar Energy*, ELSEVIER, v. 171, p. 519–525, 2018.

BEJAN, A. *Advanced Engineering Thermodynamics*. [S.l.]: Wiley, 1988.

BELL, I. H. et al. Pure and pseudo-pure fluid thermophysical property evaluation and the open-source thermophysical property library coolprop. *Industrial & Engineering Chemistry Research*, v. 53, n. 6, p. 2498–2508, 2014. Disponível em: <http://pubs.acs.org/doi/abs/10.1021/ie4033999>.

BERGMAN, T. L. et al. *Fundamentos de transferência de calor e massa*. [S.l.]: LTC, 2016. v. 7.

BOSWORTH, R. *J. Roy. Soc*, NSW, v. 78, n. 220, 1944.

CABEZA, L. F. et al. Supercritical co_2 as heat transfer fluid: A review. *Applied Thermal Engineering*, Elsevier, v. 125, p. 799–810, 2017.

CECCINATO, L.; CORRADI, M. Transcritical carbon dioxide small commercial cooling applications analysis. *International Journal of Refrigeration*, ELSEVIER, v. 31, p. 50–62, 2011.

CHAND, J.; VIR, D. Natural convection heat transfer from horizontal cylinders. *Journal of chemical engineering of Japan*, NSW, v. 12, n. 3, p. 242–247, 1979.

CHURCHILL, S.; CHU, H. Correlating equations for laminar and turbulent free convection from a horizontal cylinder. *International Journal of Heat and Mass Transfer*, Pergamon Press, v. 18, n. 11, p. 1049–1053, 1975.

COMSOL Inc. *COMSOL Multiphysics*. 2017. Disponível em: <https://br.comsol.com/>.

DINKER, A.; AGARWAL, M.; AGARWAL, G. D. Experimental assessment on thermal storage performance of beeswax in a helical tube embedded storage unit. *Applied Thermal Energy*, Elsevier, v. 111, p. 358–368, 2017.

DOSTAL, V.; DRISCOLL, M.; HEJZLAR, P. *A Supercritical Carbon Dioxide Cycle for Next Generation Nuclear Reactors*. Tese (Doutorado) — Massachussets Institute of Technology, 2004.

DUBROVINA, E. N.; SKRIPOV, V. P. Convection and heat transfer near the critical point of carbon dioxide. *Zhurnal prikladnoi mekhaniki i tekhnicheskoi fiziki*, v. 1, n. 2, p. 115–119, 1965.

DYREBY, J. J. *Modeling the Supercritical Carbon Dioxide Brayton Cycle with Recompression*. Tese (Doutorado) — Massachussets Institute of Technology, 2014.

EL-KADDADI, L. et al. Experimental study of sensible heat storage/retrieval in/from a nanofluid enclosed between concentric annular tubes. *Energy Procedia*, Elsevier, v. 139, p. 73–78, 2017.

FLEMING, E. et al. Experimental and theoretical analysis of an aluminum foam enhanced phase change thermal storage unit. *, International Journal of Heat and Mass*, ELSEVIER, v. 82, n. 273–281, 2015.

FURST, B. I. et al. Isobaric, isochoris and supercritical thermal energy storage in r134a. *Proceedings of the ASME 2013 Mechanical Engineering Congress and Exposition*, ASME, v. 7, n. 4, p. 1–7, 2013.

GANAPATHI, G. B. et al. A 5 kwht lab-scale demonstration of a novel thermal energy storage concept with supercritical fluids. *Proceedings of the ASME 2013 7th International Conference on Energy Sustainability*, ASME, v. 7, n. 6, p. 1–9, 2013.

GANAPATHI, G. B.; WIRZ, R. High density thermal energy storage with supercritical fluids. *Proceedings of the ASME 2012 6th International Conference on Energy Sustainability*, ASME, v. 6, n. 2, p. 1–9, 2012.

GIL, A. et al. State of the art on high temperature thermal energy storage for power generation. part 1 - concepts, materials and modellization. *Renewable and Sustainable Energy Reviews*, Elsevier, v. 14, n. 7, p. 31–55, 2010.

GOLDSTEIN, R. J.; AUNG, W. Heat transfer by free convection from a horizontal wire e to carbon dioxide in its critical region. *Journal of Heat Transfer*, v. 90, n. 2, p. 51–55, 1968.

HALL, W. Heat transfer near the critical point. *Advances in Heat Transfer*, v. 7, n. 1, p. 1–86, 1971.

HERNáNDEZ, R. Natural convection in thermal plumes emerging from a single heat source. *International Journal of Thermal Sciences*, ELSEVIER, v. 98, p. 81–89, 2015.

HOBOLD, G. M.; da Silva, A. K. Critical phenomena and their effect on thermal energy storage in supercritical fluids. *Applied Energy*, Elsevier, xx, n. 2, p. xxx–xxx, 2017.

HOBOLD, G. M.; da Silva, A. K. Optimal operating pressures for supercritical heat transfer during natural convection. *Proceedings of the 16th International Heat Transfer Conference, IHTC-16*, IHCT-16, p. 1–8, 2018.

JCGM, J. et al. Evaluation of measurement data—guide to the expression of uncertainty in measurement. *Int. Organ. Stand. Geneva ISBN*, v. 5, p. 134, 2008.

KABBARA, M.; GROULX, D.; JOSEPH, A. Experimental investigations of a latent heat energy storage unit using finned tubes. *Applied Thermal Energy*, Elsevier, v. 101, p. 601–611, 2016.

KATO, H.; NISHIWAKI, N.; HIRATA, M. Studies on the head transfer of fluids at a supercritical pressure. *Bulletin of Japan Society of Mechanical Engineering*, JSME, v. 11, n. 46, p. 654–663, 1968.

KNAPP, K. K.; SABERSKY, R. H. Free convection heat transfer to carbon dioxide near the critical point. *Int. J. Mass Transfer*, Pergamon Press, v. 9, p. 41–51, 1966.

KUEHN, T.; GOLDSTEIN, R. Numerical solution to the navier-stokes equations for laminar natural convection about horizontal isothermal circular cylinder. *Int. J. Heat and Mass Transfer*, Pergamon Press Ltd, v. 23, p. 971–979, 1980.

LAKEH, R. B. et al. Effect of natural convection on thermal energy storage in supercritical fluids. *Proceedings of the ASME 2013, 7th International Conference on Energy Sustainability*, ASME, p. 1–9, 2013.

LI, G. Sensible heat thermal storage energy and exergy performance evaluations. *Renewable and Sustainable Energy*, ELSEVIER, v. 53, p. 897–923, 2016.

LIU, C.; GROULX, D. Experimental study of the phase change heat transfer inside a horizontal cylindrical latent heat energy storage system. *International Journal of Thermal Sciences*, Elsevier, v. 82, p. 100–110, 2014.

LIU, M. et al. Design of sensible and latent heat thermal energy storage systems for concentrated solar power plants: Thermal performance analysis. *Renewable Energy*, Elsevier, xx, n. xxxx, p. 1–12, 2019.

LIU, M.; SAMAN, W.; FRANK, B. Review on storage materials and thermal performance enchancement techniques for high temperatura phase thermal storage systems. *Renewable and Sustainable Energy*, Elsevier, v. 16, n. 3, p. 2118–2132, 2012.

LIU, M. et al. Review on concentrating solar power plants and new developments in high temperature thermal energy storage technologies. *Renewable and Sustainable Energy Reviews*, Elsevier, v. 53, n. 8, p. 1411–1432, 2016.

LIU, Z.; WANG, Z.; MA, C. An experimental study on heat transfer characteristics of heat pipe heat exchanger with latent heat storage. part i: Charging only and discharging only modes. *Energy Conversion Management*, Elsevier, v. 47, p. 944–966, 2006.

LUGOLOLE, R. et al. Experimental analyses of sensible heat thermal energy storage systemsduring discharging. *Sustainable Energy Technologies and Assessments*, ELSEVIER, v. 35, p. 117–130, 2019.

MORGAN, V. The overall convective heat transfer from smooth circular cylinders. *Advances in Heat Transfer*, Academic Press, v. 11, p. 199–264, 1975.

MOROZ, D. L. et al. Turbomachinery flowpath design and performance analysis for supercritical co2. In: *Proceedings of ASME Turbo Expo 2014: Turbine Technical Conference and Exposition*. [S.l.: s.n.], 2014.

NEUMANNT, R. J.; HAHNE, E. W. Free convective heat transfer to supercritical carbon dioxide. *Int. J. Heat Mass Transfer*, Pergamon Press Ltd, v. 23, p. 1643–1652, 1980.

NORDBECK, J.; BAUER, S.; BEYER, C. Experimental characterization of a lab-scale cement based thermal energy storage system. *Applied Energy*, ELSEVIER, v. 256, 2019.

NUSSELT, W. Das grundgesetz des wärmeübergangs. *Gesundheits-Ingenieur*, v. 42, p. 477–482, 1915.

OMEGA, E. *Resistance Heating Wire, Nickel-Chromium Alloy, 80% Nickel/20% Chromium*. 2020. Disponível em: <https://www.omega.com/en-us/wire-and-cable/heating-wire/p/NI80>.

PALOMBA, V.; BRACANATO, V.; FRAZZICA, A. Experimental investigation of a latent heat storage for solar cooling applications. *Applied Thermal Energy*, Elsevier, v. 199, p. 347–358, 2017.

PIGANI, L.; BOSCOLO, M.; PAGAN, N. P. Marine refrigeration plants for passenger ships:low-gwp refrigerants and strategies to reduce environmental impact. *International Journal of Refrigeration*, ELSEVIER, v. 64, p. 80–92, 2016.

PéREZ-GARCíA, V. et al. Comparative study of transcritical vapor compression configurations using co2 as refrigeration mode base on simulation. *Applied Thermal Engineering*, ELSEVIER, v. 51, p. 1038–1046, 2013.

ROUSSELET, Y.; WARRIER, G. R.; DHIR, V. K. An experimental study of heat transfer from small horizontal cylinders at near-critical pressures. *Proceedings of the ASME/JSME 2011 8th Thermal Engineering Joint Conference*, AJTEC2011, p. 1–16, 2011.

ROUSSELET, Y.; WARRIER, G. R.; DHIR, V. K. Natural convection from horizontal cylinders at near-critical pressures - part 1: Experimental study. *Journal of Heat Transfer*, v. 135, n. 1, p. 1–10, 2013.

ROUSSELET, Y.; WARRIER, G. R.; DHIR, V. K. Natural convection from horizontal cylinders at near-critical pressures - part 2: Numerical study. *Journal of Heat Transfer*, v. 135, n. 1, p. 1–10, 2013.

ROWLINSON, J. Singularities in the thermodynamic and transport properties of a fluid at its critical point. *Sum. Heat Transfer and Fluid Dynamics of Near Critical Fluids*, Proc. Inst. Mech. Eng, v. 128, n. Part 31, p. 23–26, 1967.

TSE, L. et al. System modeling for a supercritical thermal energy storage system. *Proceedings of the ASME 2012, 6th International Conference on Energy Sustainability*, ASME, p. 1–8, 2013.

TSE, L. A. et al. Spatial and temporal modeling of sub- and supercritical thermal energy storage. *Solar Energy*, Elsevier, v. 103, n. 4, p. 402–410, 2014.

TSE, L. A. et al. Exergetic optimization and performance evaluation of multi-phase thermal energy storage systems. *Solar Energy*, Elsevier, v. 122, p. 396–408, 2015.

WANG, J.; GU, Y. Parametric studies on different gas turbine cycles for a high temperature gas-cooled reactor. *Nuclear Engineering and Design*, ELSEVIER, v. 235, p. 1761–1772, 2005.

WANG, Y.; YU, K.; LING, X. Experimental and modeling study on thermal performance of hydrated salt latent heat thermal energy storage system. *Energy Conversion and Management*, Elsevier, v. 198, p. 1–10, 2019.

ZIJNEN, B. V. d. H. Modified correlation formulae for the heat transfer by natural and by forced convection from horizontal cylinders. *Appl. Scient. Res*, v. 6A, p. 129–140, 1963.

ZONDAG, H. et al. Development of industrial pcm heat storage lab prototype. *Energy Procedia*, Elsevier, v. 135, p. 115–125, 2017.

APPENDIX A – TECHNICAL INFORMATION

A.1 NICHROME WIRE 80/20

Figure A.1 presents the information about how the nichrome wire 's 80/20 resistance varies with its temperature, which is informed by Omega (2020).

Resistance Heating Wire
Nickel-Chromium Alloy
80% Nickel/20% Chromium

OMEGA™

- **Withstands High Temperatures up to 1150°C (2100°F)**
- **Quick Heating, Long Life**
- **Corrosion Resistant**
- **Used to Make Straight or Helical Coil Resistance Heaters**
- **Convenient 15 m (50') and 60 m (200') Spools Available**

OMEGA™ NIC80 wire is a resistance heating wire comprised of 80% Nickel and 20% Chromium. NIC80 wire is commonly used as a resistor at elevated temperatures. NI/CR-80/20 is essential for resistor elements in high temperature applications such as electric furnaces, electric ranges and radiant heaters operating at temperatures up to 1150°C (2100°F).

In addition to these qualities and standard uses, it has found wide application in technical applications due to its combination of high electrical resistance and its temperature coefficient of resistance much less than that of Nickel-Chrome 60.

Specifications

Composition: 80% Ni, 20% Cr

Specific Resistance: 650 Ω per circular mil-foot at 20°C (68°F). See table below for multiplication factors to obtain resistance at other temperatures.

Specific Gravity: 8.41

Density: 0.304 lb/in^3

Melting Point: Approx 1400°C (2550°F)

Nominal Coefficient of Linear Expansion: 0.000017 (10 to 1000°C)

Tensile Strength (lb/in^2) at 20°C (68°F):
Soft Annealed: 100,000

Nominal Temperature Coefficient of Resistance: 0.00011 Ω/Ω/°C (20 to 500°C)

Factor by Which Resistance at Room Temperature Is to Be Multiplied to Obtain Resistance at Indicated Temperatures
(These figures are given as a basis for engineering calculations and represent average material as supplied.)

Temp °C	20	93	204	315	427	538	649	760	871	982	1093°C
Temp °F	68	200	400	600	800	1000	1200	1400	1600	1800	2000°F
Factor	1.000	1.016	1.037	1.054	1.066	1.070	1.064	1.062	1.066	1.072	1.078

To Order

AWG	Dia. mm (1")	Ω per ft @ 20°C (68°F)	Current Temperature Characteristics* °C (°F) 425 (800)	550 (1000)	650 (1200)	750 (1400)	875 (1600)	1100 (2000)	Model No.
18	1.0 (0.040)	0.4062	8.32	10.17	12.48	15.11	18.06	24.03	**NI80-040-(†)**
20	0.81 (0.032)	0.6348	6.17	7.56	9.24	11.13	13.23	17.57	**NI80-032-(†)**
22	0.64 (0.0253)	1.015	4.62	5.62	6.85	8.20	9.69	12.85	**NI80-025-(†)**
24	0.51 (0.0201)	1.609	3.46	4.18	5.06	6.04	7.10	9.40	**NI80-020-(†)**
26	0.40 (0.0159)	2.571	2.62	3.12	3.76	4.49	5.27	6.90	**NI80-015-(†)**
28	0.32 (0.0126)	4.094	1.98	2.38	2.84	3.37	3.93	5.09	**NI80-012-(†)**
30	0.25 (0.010)	6.50	1.50	1.81	2.14	2.53	2.93	3.75	**NI80-010-(†)**

** Showing approximate amperes necessary to produce a given temperature, applying only to a straight wire stretched horizontally in free air.*
*† Specify desired length in feet: "**50**" or "**200**". **Note:** This wire is **not** intended for use in making thermocouple elements.*
***Ordering Example: NI80-032-50** is a 15 m (50') spool of 20 gage bare wire.*

Note: Published prices are based on market value at time of printing and are subject to change due to Nickel surcharges, Chromium and precious-metal market fluctuations.

1

Figure A.1 – Data sheet of the nichrome wire 80/20. Obtained from (OMEGA, 2020)

APPENDIX B – THERMOCOUPLES CALIBRATION

The calibration of the five thermocouples type T used to measure the mixture temeprature of the fluid and the thermocouple type E used to measure the wire temperature were made using the same procedure. A reference temperature measured by a calibrated thermometer TESTO 735-2 was used for the calibration.

B.1 THERMOCOUPLES TYPE T

A total of 100 measurements were made for each reference temperature, taken from 5 to 5 °C.The calibration curve of all type T thermocouples is presented in Figure B.1.

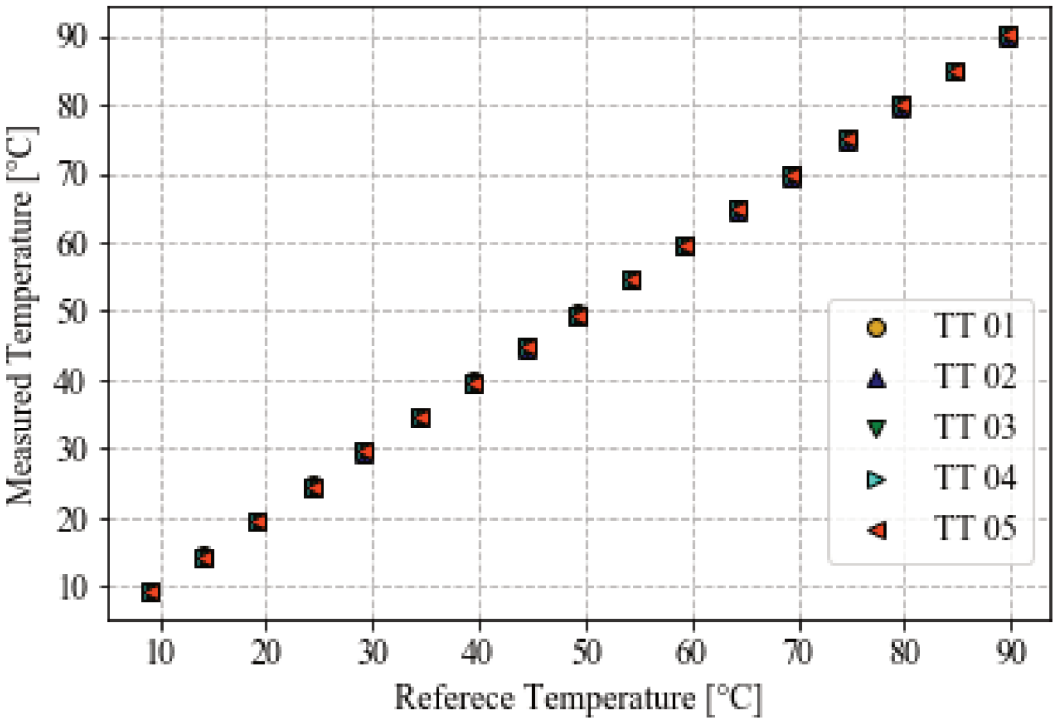

Figure B.1 – Calibration curves for type T thermocouples.

Table B.1 presents the caracteristic equations for each type T thermocouple.

Table B.1 – Caracteristic equations of thermocouples type T.

Thermocouple	Caracteristic Equation
TT 01	Y = 0.99637X - 0.22011
TT 02	Y = 0.99950X - 0.15672
TT 03	Y = 0.99628X - 0.17468
TT 04	Y = 0.99659X - 0.17045
TT 05	Y = 0.99640X - 0.15929

The average value of these measurements for each temperature are presented in Table B.2.

Table B.2 – Average measured temperatures for each type T thermocouple compared with reference temperature.

Reference [°C]	**TT 01 [°C]**	**TT 02 [°C]**	**TT 03 [°C]**	**TT 04 [°C]**	**TT 05 [°C]**
9.180	9.432	9.346	9.364	9.360	9.369
14.175	14.438	14.322	14.386	14.380	14.377
19.225	19.513	19.388	19.470	19.464	19.457
24.345	24.646	24.512	24.616	24.601	24.591
29.285	29.608	29.464	29.577	29.562	29.553
34.365	34.711	34.540	34.677	34.657	34.642
39.425	39.791	39.600	39.749	39.738	39.731
44.380	44.767	44.557	44.729	44.712	44.705
49.190	49.601	49.376	49.565	49.544	49.539
54.375	54.808	54.573	54.767	54.742	54.731
59.330	59.785	59.533	59.747	59.719	59.708
64.335	64.802	64.532	64.760	64.730	64.728
69.335	69.817	69.537	69.778	69.745	69.747
74.510	74.997	74.702	74.956	74.940	74.941
79.510	80.019	79.710	79.983	79.956	79.964
84.565	85.082	84.751	85.031	85.003	85.023
89.620	90.149	89.807	90.111	90.079	90.091

The standard deviation for each reference temperature and each thermocouple measurement is presented in Table B.3.

B.2 THERMOCOUPLE TYPE E

Just as it was made for the type T thermocouples, a total of 100 measurements for each reference temperature were taken fot the type E thermocouple.The calibration curve of the type E thermocouple is presented in Figure B.2.

The caracteristic equation of this thermocouple is presented in Table B.4.

The average of the measurements and the standard deviation are presented in Table B.5.

Table B.3 – Standard deviation of thermocouples type T for each reference temperature

Reference [°C]	TT 01 [°C]	TT 02 [°C]	TT 03 [°C]	TT 04 [°C]	TT 05 [°C]
9.180	0.012	0.010	0.015	0.024	0.012
14.175	0.013	0.014	0.012	0.012	0.015
19.225	0.012	0.019	0.013	0.011	0.012
24.345	0.011	0.012	0.009	0.009	0.010
29.285	0.016	0.014	0.011	0.013	0.014
34.365	0.012	0.013	0.009	0.010	0.012
39.425	0.012	0.015	0.015	0.012	0.016
44.380	0.012	0.014	0.012	0.012	0.014
49.190	0.010	0.011	0.011	0.012	0.013
54.375	0.009	0.010	0.008	0.009	0.010
59.330	0.010	0.010	0.010	0.010	0.009
64.335	0.010	0.012	0.010	0.011	0.011
69.335	0.011	0.012	0.011	0.010	0.011
74.510	0.011	0.010	0.010	0.010	0.010
79.510	0.016	0.015	0.015	0.016	0.014
84.565	0.015	0.014	0.016	0.014	0.013
89.620	0.015	0.013	0.010	0.011	0.011

Table B.4 – Type E caracteristic equation.

Thermocouple	Caracteristic Equation
TE 01	Y = 1.00454X - 3.27670

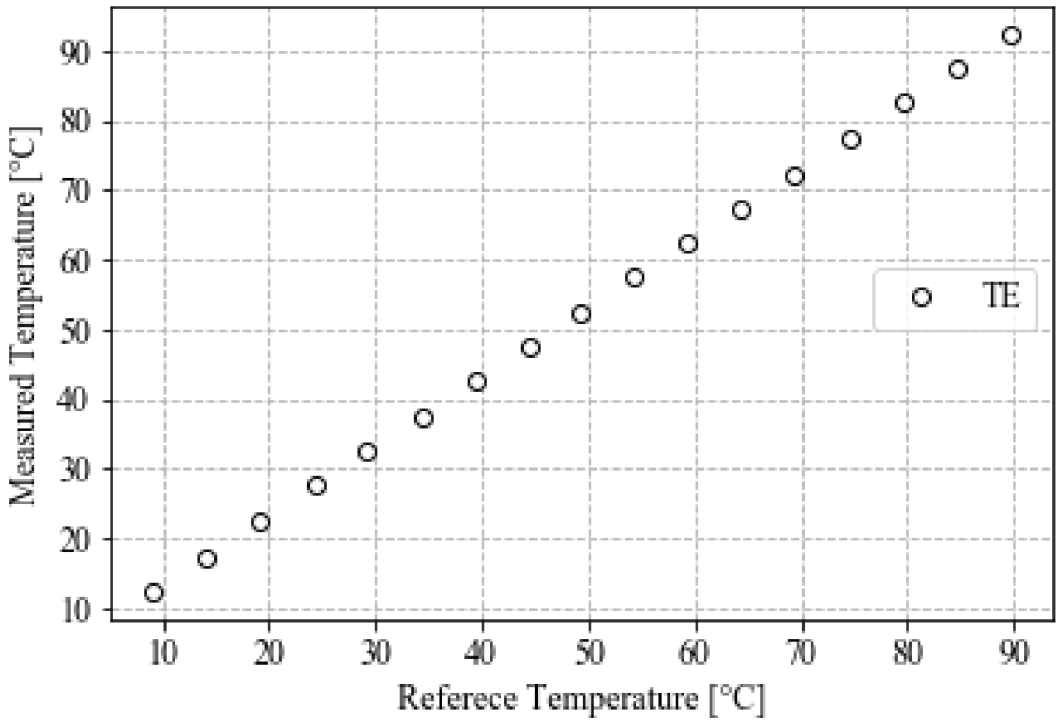

Figure B.2 – Calibration curve for type E thermocouplee.

Table B.5 – Average temperatures and standard deviation of thermocouple type E for each reference temperature.

Reference [°C]	**Temperature TE 01 [°C]**	**Standard Deviation TE 01 [°C]**
9.180	12.363	0.009
14.175	17.350	0.010
19.225	22.389	0.010
24.345	27.494	0.007
29.285	32.414	0.009
34.365	37.457	0.009
39.425	42.522	0.014
44.380	47.454	0.011
49.190	52.266	0.008
54.375	57.413	0.006
59.330	62.343	0.010
64.335	67.309	0.011
69.335	72.304	0.019
74.510	77.376	0.067
79.510	82.731	0.072
84.565	87.396	0.108
89.620	92.228	0.047

APPENDIX C – UNCERTAINTY ANALYSIS

The main objective of determining the uncertainty of a measurement is to evaluate qualitatively how good the measurements are. To determine the uncertainty makes it possible to compare the results amongst them, and comparing them with the results found in the literature. The method adopted in this dissertation follow the methodology presented in the norm JCGM et al. (2008).

The uncertainty contained in a measurement can be divided into two categories that are caused by different mechanisms. These two categories are:

- **Type A uncertainty:** Are determined through statistical analysis of a series of observations.

- **Type B uncertainty:** Are determined through other means, for example from catalogs and calibration certificates.

The type A uncertainty can be calculated through the dispersion of the measured values in relation with the average value of all the measurements. For a generic case, it is desired to evaluate the uncertainty of a variable x_l measured from n independent measurements of $x_{l,m}$ of x_l obtained under the same conditions. In this case the average value of the variable $x_{l,m}$ is determined by Equation C.1:

$$\overline{x_{l,m}} = \frac{1}{n}\sum_{m=1}^{n} x_{l,m} \tag{C.1}$$

The standard deviation is given by Equation C.2:

$$\alpha(x_l) = \sqrt{\frac{1}{(n-1)}\sum_{1}^{n}\left(x_{l,m} - \overline{x_l}\right)^2} \tag{C.2}$$

Finally, the uncertainty is given by Equation C.3

$$u(x_l) = \frac{\alpha(x_l)}{\sqrt{n}} \tag{C.3}$$

As mentioned, the type B uncertainties are given from catalogs and calibration certificates, previous experiments, amongst others.

The combinations of several sources of uncertainties can be determined through the combined uncertainty given by Equation C.4:

$$u_{comb} = \sqrt{u_1^2 + u_2^2 + ... + u_n^2} \tag{C.4}$$

However, to use Equation C.4, the variables must be in the same measurement units. That is why Equation C.4 becomes Equation C.5:

$$u_{comb} = \sqrt{\left(\frac{\delta f}{\delta x}u(x_1)\right)^2 + \quad ... \quad + \left(\frac{\delta f}{\delta x}u(x_n)\right)^2} \tag{C.5}$$

where $\frac{\delta f}{\delta x}$ is called the sensibility coefficient and *u(x)* are the uncertainties of the input quantities.

Finally, one multiplies the combined uncertainty u_{comb} by an coverage factor λ so it is possible to calculate the expanded uncertainty *(U)*, given by Equation C.6.

$$U = u_{comb}\lambda \tag{C.6}$$

C.1 UNCERTAINTY OF THERMOCOUPLES

The uncertainty analysis of the thermocouples calibrations is presented in Table C.1, showing the Type A and Type B uncertanties, the combined uncertainty u_comb and the expanded uncertainty *U*.

Table C.1 – Uncertainty analysis of thermocouples calibration

	Uncertainty [°C]			
Thermocouple	**Type A**	**Type B**	$\mathbf{u}_{\mathrm{comb}}$	**U**
TT 01	0.001	0.005	0.005	0.01
TT 02	0.001	0.005	0.005	0.01
TT 03	0.001	0.005	0.005	0.01
TT 04	0.001	0.005	0.005	0.01
TT 05	0.001	0.005	0.005	0.01
TE 01	0.002	0.005	0.005	0.01